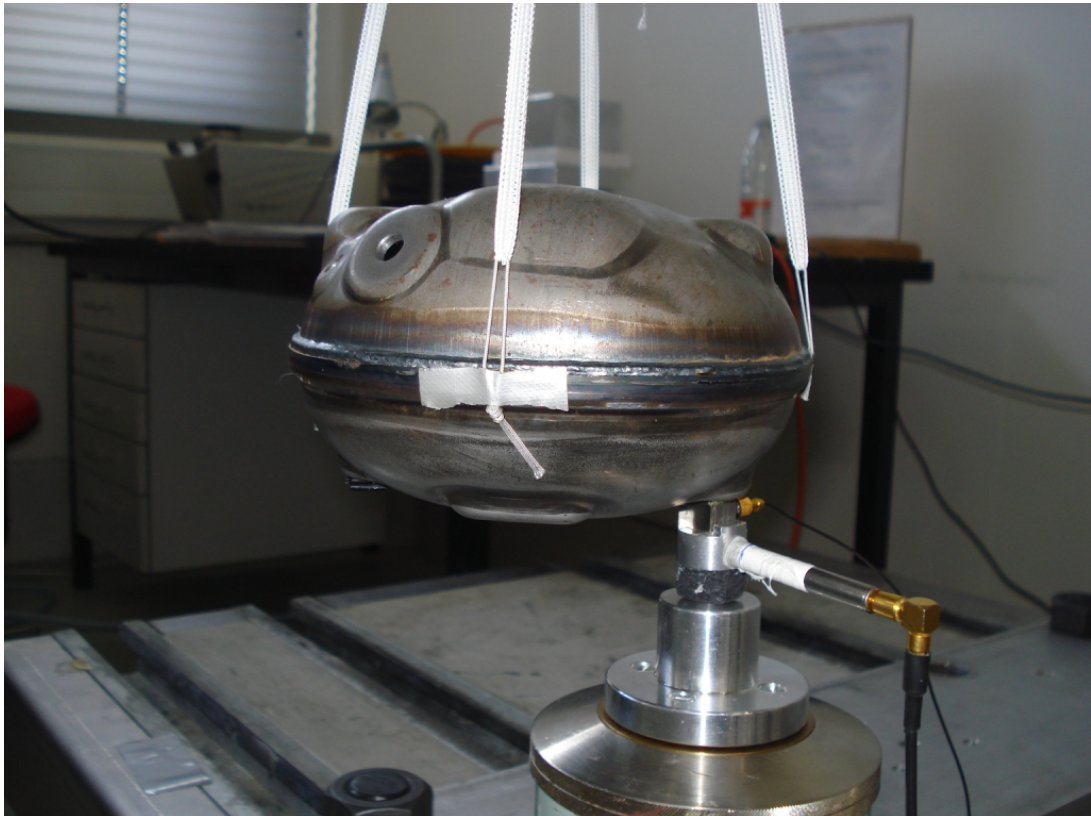


# *Theoretical and experimental comparison of point mobility measurement methods*

---



**AALBORG UNIVERSITET**

DMYTRO SHABALIN  
DESIGN OF MECHANICAL SYSTEMS, 3D AND 4TH SEMESTER  
AALBORG UNIVERSITY  
4TH OF JUNE 2013





## Synopsis:

**Title:** Theoretical and experimental comparison of point mobility measurement methods

**Semester:** 3d and 4th semesters DMS

**Semester theme:** Master thesis project

**Project period:** 1. sep. 2012 - 4. jun. 2013

**ECTS:** 60 point

**Supervisor:** Sergey Sorokin

**Document elaborated by:** Dmytro Shabalin

---

Dmytro Shabalin

**Number printed:** 3

**Pages:** 64

**Appendix:** a-1 to a-30

The main purpose of the project is to examine strengths and weaknesses of the point mobility measurement methods. The investigation involves both analytical analysis, numerical simulations and experimental work. With main focus on the robustness and usability, device denoted as 'adaptor m#3' for acoustic excitation set-up is suggested. The method with use of adaptor m#3 along with the conventional 'shaker via stinger' excitation is applied to a cantilever structure. The results of both methods are compared to analytical solution, and in general are in agreement. The method with use of adaptor m#3 is found to be more robust, and accuracy of the results are estimated as good. Proved to be usable adaptor m#3 is applied to the vibration analysis of compressor housing shell structure. Investigation of the properties of compressor housing is also performed numerically by means of FEM simulations. Finally it is concluded that simplified numerical model for certain points can not provide users with correct results, and the solution obtained by measurements is more accurate and reliable.

Adaptor m#3 is concluded to be usable robust device for measurement of dynamical properties of mechanical systems. The design of adaptor m#3 can serve as the prototype, which can be developed further.



**AALBORG UNIVERSITET**

**Studienævnet for Industri og Global Forretningsudvikling**

Fibigerstræde 16

DK 9220 Aalborg Øst

Tel +45 99 40 93 09 Fax +45 98 15 16 75

swe@me.aau.dk <http://www.industri.aau.dk/>



# Abstract

---

Denne rapport dokumenterer et specialeprojekt, der er udført teoretisk og eksperimentel til undersøgelse af punkt-mobilitetsmålemetoder. Hovedformålet med projektet er at undersøge fordele og ulemper ved en ny metode benytter sig af en lokaliseret akustisk eksitation af en struktur. Denne metode er et alternativ til den almindeligt anvendte “shaker via stinger” eksitationsmetode. Undersøgelsen involverer både analytiske undersøgelser, numeriske simuleringer og eksperimentelt arbejde.

Den teoretiske undersøgelse omfatter studier og anvendelse af den relevante teori, som danner grundlaget for tokenals FFT-analyse. Teorien omfatter grundlæggende akustik, vibrationsanalyse af en bjælke ved brug af Bernoulli-Euler bjælketheori, FEM modal og harmonisk superpositionsanalyse med anvendelsen på skalstrukturer.

Projektet omfatter tre hoveddele: (i) analyse og udvikling af akustisk eksitationsprøvestand med fokus på robusthed og nøjagtighed af de opnåede resultater, (ii) godkendelse af den nye målemetode, der blev anvendt en bjælke, og en efterfølgende sammenligning af resultaterne med den analytiske løsning og den konventionelle målemetode, (iii) anvendelsen af den nye metode til vibrationsanalyse af en skalstruktur.

Med hovedfokus på robusthed og brugervenlighed er flere ændringer af indretningen til den akustiske eksitationsprøvestand blevet foreslået. Den ene eksitationsprøvestand betegnes som “adapter m#3” og det konkluderes, at den er bedst egnede. Det primære koncept med enheden er, at den inkluderer to transducere i én stiv beholder. Denne konfiguration har mange fordele, som bl.a. gør den mere robust og præcis i forhold til alternative konfigurationer.

Den akustiske eksitation af en struktur med adapter m#3 udføres parallelt med den konventionelle “shaker via stinger” eksitation på relativ enkel bjælkestruktur. Resultaterne af begge metoder sammenlignes mellem hinanden og med den analytisk løsning. Metoden der benytter adapter m#3 viser sig at være mere robust, og nøjagtigheden af resultaterne kan forbedres ved yderligere undersøgelse af designet og adapterens egenskaber.

Den bedst anvendelige adapter m#3 benyttes til vibrationsanalyse på en skalstruktur fra et kompressorhus. Undersøgelsen af egenskaberne af kompressorhuset udføres også numerisk ved hjælp af FEM simuleringer. Ved en sammenligning resultaterne konkluderes det, at en forenklet numerisk model for visse eksitationspunkter ikke kan give brugerne korrekte resultater, og at den opnåede opløsning ved hjælp af målinger er mere præcise og pålidelige.

Adapter m#3 konkluderes til at være en brugbar og robust enhed til måling af dynamiske egenskaber af mekaniske systemer. Udformningen af adapter m#3 kan tjene som en prototype, der kan udvikles yderligere til en mere robust og præcis enhed.



# Preface

---

This report is the documentation of the Master Thesis project, that has been conducted in autumn 2012 and spring 2013, during 3rd and 4th semesters of the master program 'Design of Mechanics Systems'(DMS) at Aalborg University. The topic of the report is: 'Theoretical and experimental comparison of point mobility measurement methods'. The project proposal is done in collaboration with two companies: Secop GmbH and Brüel&Kjær. The main focus is on the study of the basic principles of mobility measurements and the comparison of two different approaches. This leads to the design of a robust prototype for measuring point mobility using acoustic excitation.

Special thanks to the industrial co-supervisors: Christian Svendsen, Secop A/S; Dmitri Tcherniak and Andreas Schuhmacher, Brüel&Kjær; for the assistance in both theoretical and practical parts of the project, and for providing materials and equipment for the experiments.

Individual thanks to Radoslav Darula, PhD student from the Department of Mechanical and Industrial Engineering at Aalborg University, for the practical assistance in conducting the experiments, and providing theoretical information and general help during the project.

Through the report, the Harvard method for citation is used [last name, year]. All citations are listed in the Bibliography list in the end of the report with the following information provided: author, year, title, ISBN, edition, and publisher when these were available.

A CD with an electronic version of the report and relevant data included is attached.



# Table of Contents

---

<b>Abstract</b>	<b>v</b>
<b>Preface</b>	<b>vii</b>
<b>Acronyms</b>	<b>xi</b>
<b>Nomenclature</b>	<b>xiii</b>
<b>Chapter 1 Introduction</b>	<b>1</b>
1.1 Presentation of the problem . . . . .	1
1.2 Problem formulation and solution methodology . . . . .	3
<b>Chapter 2 Theoretical basis</b>	<b>7</b>
2.1 Mobility Measurements . . . . .	7
2.2 Basics of acoustics . . . . .	9
2.3 Vibration analysis of a beam . . . . .	14
2.4 FEM, modal and harmonic (mode superposition) analysis . . . . .	17
<b>Chapter 3 Design and analysis of acoustic excitation set up</b>	<b>19</b>
3.1 Analysis and technical improvements of existing design . . . . .	19
3.2 Experimental investigation of the adaptors m#1 and m#3. . . . .	22
3.3 Analytical analysis of the acoustic excitation setup . . . . .	28
3.4 Summary . . . . .	31
<b>Chapter 4 Vibration analysis of a cantilever structure</b>	<b>33</b>
4.1 Specimen and cantilever structure setup . . . . .	33
4.2 Acoustic excitation experiment . . . . .	38
4.3 Analytical vibration analysis. . . . .	42
4.4 'Shaker via stinger' experiment . . . . .	43
4.5 Comparison of the results . . . . .	46
4.6 Summary . . . . .	48
<b>Chapter 5 Vibration analysis of a shell structure</b>	<b>49</b>
5.1 Experimental part . . . . .	49
5.2 FEM analysis and comparison with measurements. . . . .	55
5.3 Summary . . . . .	59
<b>Chapter 6 Conclusion</b>	<b>61</b>
<b>Chapter 7 Discussion</b>	<b>63</b>
<b>Bibliography</b>	<b>65</b>

<b>Appendix</b>	<b>67</b>
<b>Appendix A Blueprints</b>	<b>a-3</b>
<b>Appendix B Mode shapes of cantilever beam s6</b>	<b>a-7</b>
<b>Appendix C Technical characteristics of the devices used in the measurements</b>	<b>a-9</b>
<b>Appendix D Maple calculation for cantilever beam</b>	<b>a-11</b>
<b>Appendix E Maple calculation for acoustic excitation set-up</b>	<b>a-23</b>

# Acronyms

---

BC	Boundary Condition
CAD	Computer Aided Design
DOF	Degrees Of Freedom
EOM	Equation Of Motion
FEM	Finite Element Method
FFT	Fast Fourier Transform
FRF	Frequency Response Function



# Nomenclature

---

$\eta$	Longitudinal wave number	$1/m$
$\gamma$	Coherence function	–
$\lambda$	Wave length	$m$
$\omega$	Angular frequency	$rad/s$
$\rho$	Density	$kg/m^3$
$\varphi$	Velocity potential	–
$\xi_i$	Modal damping ratio	–
$\zeta$	Radial wave number	$1/m$
$A_i$	Coefficients	–
$A$	Area	$m^2$
$B_i$	Coefficients	–
$c$	Speed of sound	$m/s$
$E$	Young's Modulus	$Pa$
$Q$	Force	$N$
$f$	Frequency	$Hz$
$G$	Spectrum	–
$H_t$	Frequency response function	$m/N, m/Ns, m/Ns^2$
$I$	Moment of inertia (area)	$m^4$
$k$	Wave number	$1/m$
$M$	Moment	$N \cdot m$
$m$	Mass	$kg$
$J_y$	Moment of inertia	$kg \cdot m^2$
$p$	Pressure	$Pa$
$Q_s$	Shear Force	$N$

$q$	Distributed load	$N/m$
$r$	Radius	$m$
$T$	Kinetic energy	$J$
$t$	Time	$s$
$U$	External potential energy	$J$
$V$	Internal potential energy	$J$
$v$	Velocity	—
$W$	Vertical displacement	$m$
$X$	System response	$m, m/s, m/s^2$
$Y$	Force input	$N$
$Z$	Specific impedance	—

Mechanical mobility measurements is an important stage of the engineering design process of dynamic mechanical structures. It is an essential part of determining the dynamic characteristics of structures and thereby improve their structural behaviour, including noise and vibration problems. This makes the theoretical and experimental investigation of point mobility measurement methods very important and a relevant subject to examine.

In mechanical and structural engineering, the vibrations measurements represent a distinct part of mechanical vibrations. There are many studies and works done on the investigation and development of different approaches in measurement techniques and use of various equipment. The main applications of the measurements of vibration are listed in e.g. [Rao, 2005, pp. 741 - 742]. The most relevant to the present project are the comparison of the real (measured) characteristics with calculated ones, hence verification of the assumptions used and a validation of approximations done for either analytical or numerical model of a real structure.

The data obtained from vibration measurements, can be used for the determination of the resonances at operational conditions, designing of vibro isolations, and identification of a system in terms of its mass, stiffness, damping and other important informations relevant for different designs.

## 1.1 Presentation of the problem

The present Master Thesis project is carried out in a collaboration with two companies, Secop GmbH and Brüel&Kjær, which jointly made the project proposal presented in the following section. Brüel&Kjær is a manufacturer of sound and vibration measurement equipment with headquarters in Nærum, Denmark. Secop is an international manufacturer of light commercial and household compressors with headquarters in Flensburg, Germany. The idea of the project was initiated by Secop, as the user of Brüel&Kjær equipment for the vibration measurements. They suggested a new method for the mobility measurement technique, which successfully and advantageously has been used by the company for the determining the properties of compressor housing shell structures.

In general, point mobility characteristics proves the dynamical behaviour of a structure and shows its response due to the excitation from a vibration source. There are variety of examples where this characteristic is crucial for the design. For example, in a compressor part design, the mobility of the motor chassis connection points must be determined in order to create a low noise household appliance and avoid resonances at the certain excitation points of compressor. More detailed theoretical background of the mobility measurements is discussed in Chapter 2, Section 2.1. The general definition of mobility can be formulated by means of Frequency Response Function (FRF) as the ratio of measured excitation force applied to the structure and

the corresponding motion of the structure. The motion of the structure can be expressed by means of displacement, velocity or acceleration. According to [Døssing, 1988, p.16 ] the most commonplace motion transducer is an accelerometer, hence the acceleration of a point due to the structure excitation is the most usable characteristic for the measurements, whereas the displacement is more commonly used for the modelling of FRF of a structure. But in general the displacement, velocity and acceleration has a well known algebraic relation, and hence measured data of one of the motion characteristic allows to calculate the other ones.

One of the purposes of the project is to compare two different methods of mobility measurements. One of the methods is commonly used and well known shaker excitation via a stinger. It involves the use a force transducer to measure excitation force applied to a structure and an accelerometer to measure corresponding deflection of the structure in terms of acceleration. An example of such a set-up is shown on Figure 1.1.

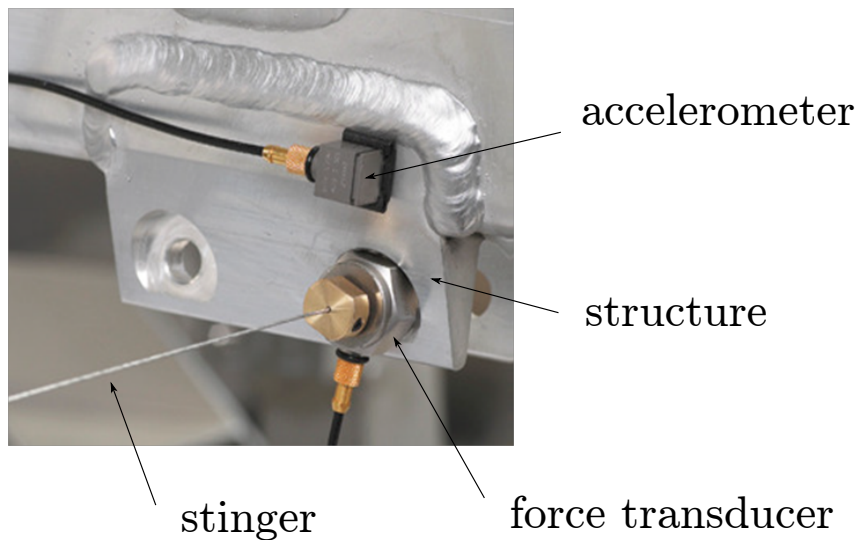


*Figure 1.1: Commonly used shaker excitation via a stinger.*

An alternative method which was suggested by Secop GmbH, was successfully used for the measurements of the point mobility on a compressor housing. It uses an acoustic drive, e.g. a loudspeaker, to excite the structure by acoustic waves; a microphone as the transducer for registration of a reference signal; and an accelerometer for measuring the response of a structure. An example of an experimental set-up with acoustical excitation is shown on Figure 1.2.

The new method has a number of advantages in comparison with shaker via stinger excitation. First of all, it is a non-contact excitation, which means there are no influence on the structure response due to the stinger connection. Secondly, the excitation force and structural deflection are measured at the same point, that is not always possible to do with the shaker via stinger set-up. Thirdly, the stinger has to be initially preloaded to act only in tension condition, that might affect the FRF characteristic of the structure. One more advantage of the acoustic excitation method is the possible quicker way to setting it up and replace, to be able conduct measurements in a different points of the structure in a faster way, as the position of an acoustic duct probably is not required to be precisely aligned with the axis of an accelerometer. There are several more points considering the setting up features, that make the acoustic method more attractive in comparison with classical one.

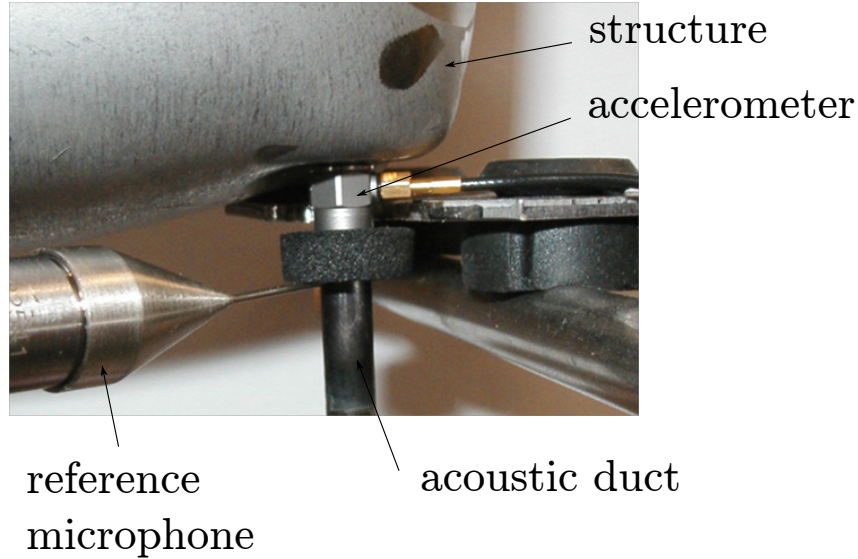


*Figure 1.2: Set-up for the use of localized acoustic excitation.*

The main characteristics of two methods are represented in Table 1.1.

Characteristic	Method 1	Method 2
type of excitation	shaker via stinger	localized acoustic
application of a force	contact	non-contact
ability to apply force and measure motion at the same point	not always possible	essential
pre-loading of the structure	takes place due to stinger pretension requirement	does not take place
robustness	slow, due to specific of set-up	is a design target
usability	in the case of curved surface it is challenging to use	to be verified
accuracy	results might be affected by a stinger influence	to be analysed in experiments

*Table 1.1: Comparison of the characteristics of two methods.*

Thus, to sum up the points of investigation, both the accuracy and the robustness of the methods are to be considered.

## 1.2 Problem formulation and solution methodology

Taking into account the specialisation of the companies products several problems can be formulated within a scope of the project. Firstly, the new method of mobility measurements is supposed to be used for the application on shell structures with complex curved geometry. The compressor housing is an example of such a structure, and the use of the new method for the point mobility measurements is of Secop GmbH interests. Secondly, the investigation of the new method can lead to the development and design of a new device, that can be produced and sold by Brüel&Kjær.

According to the problems considered a solution methodology in three stages is worked out. First stage is the analysis and development of the acoustic excitation set-up, with a focus on both the accuracy and the robustness of the new method. Second stage is the investigation of the both methods by the application to a relatively simple structure, where experimental results can be compared to the analytical ones. A cantilever structure (a beam clamped at one and free at the other) is to be considered as a simple structure, with respect to obtaining an analytical solution. Third stage is the application of the acoustic excitation set-up on flexible shell structure, e.g. compressor housing, and comparison of the results with numerical ones. The main steps of the project are summed up in the form of a diagram, see Figure 1.3.

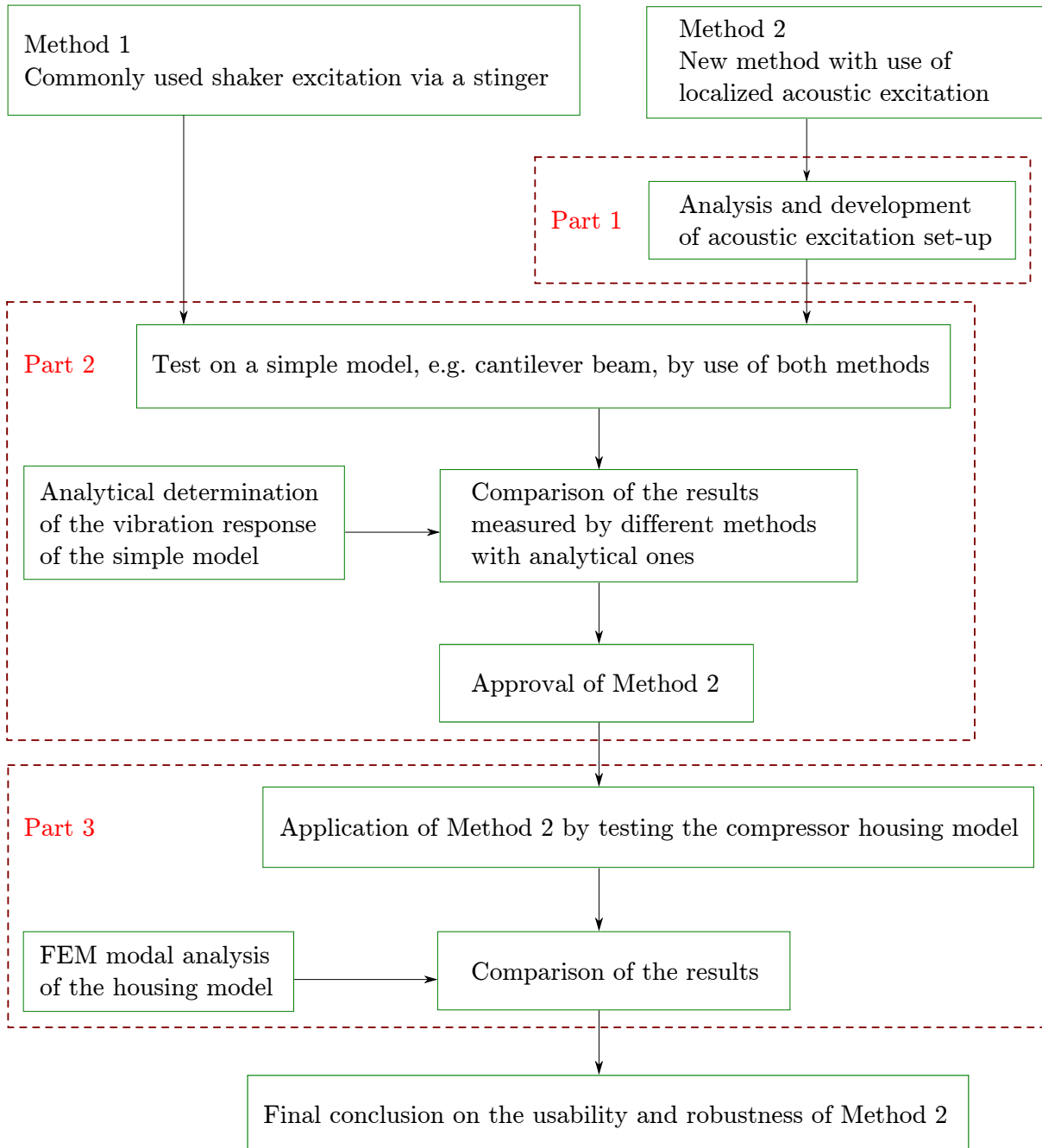


*Figure 1.3: Flow chart to the solution methodology.*

Finally, according to the solution strategy and taking into account that it contains three distinct parts, the problem formulation of the project can be divided onto three sub-problems, which are listed below.

Sub-problem 1:

*Analysis and development of the acoustic excitation set-up.*

Sub-problem 2:

*Application of two methods to the simple structure and comparison with analytical results.*

Sub-problem 3:

*Application of Method 2 to the compressor housing tests.*



# Theoretical basis 2

---

In the following a brief summary of the theory applied to the problems of the project is represented. Among the topics represented are (1) discussions on the theoretical background of measurement techniques applied in the tests, (2) basic acoustic analysis (a simple analysis of the cylindrical wave-guides and definition of impedance of a system), (3) structural (vibration) beam analysis with use of energy and variational principle, and (4) Finite Element Method (FEM) harmonic (mode superposition) analysis that is supposed to be applied to the shell structure of a compressor housing. Each chapter includes references to literature sources and to the sections where application of the theory is made.

## 2.1 Mobility Measurements

In the following section a summary of the theoretical background for the point mobility measurements are briefly represented. Basic information are taken from [Herlufsen, 1984] and [Døssing, 1988].

The main dynamic properties of a mechanical system can be defined by the FRF of a structure, that is a complex function of frequency and serves as a system descriptor, which shows 'input-output' relationships. Schematically the concept of FRF is shown in Figure 2.1, and can be expressed as:

$$H_t(f) = \frac{X(f)}{Y(f)} \quad (2.1)$$

where  $Y(f)$  corresponds to a force applied to excite the structure, and  $X(f)$  is the response of the structure. Both functions are transformed from time into frequency domain.

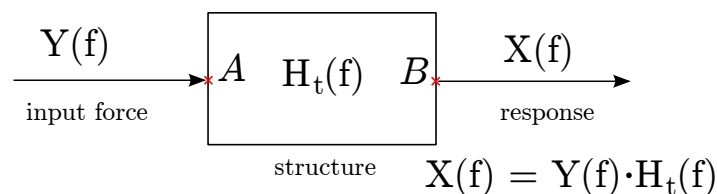


**Figure 2.1:** Schematic expression of the system frequency domain model. Inspired from [Døssing, 1988, p.14].

Consider points  $A$  and  $B$  at the system, see Figure 2.1. If input force is applied at point  $A$  and response is measured at point  $B$ , then function  $H_t$  is called a 'transfer function' between the points  $A$  and  $B$ , and can be denoted as  $H_{tAB}$ .

In the experiments that are undertaken during the project, the dual channel Fast Fourier Transform (FFT) analysis principle is used. The principle scheme of a dual channel FFT analysis procedure, that results into the FRF and coherence function, is shown in Figure 2.2.

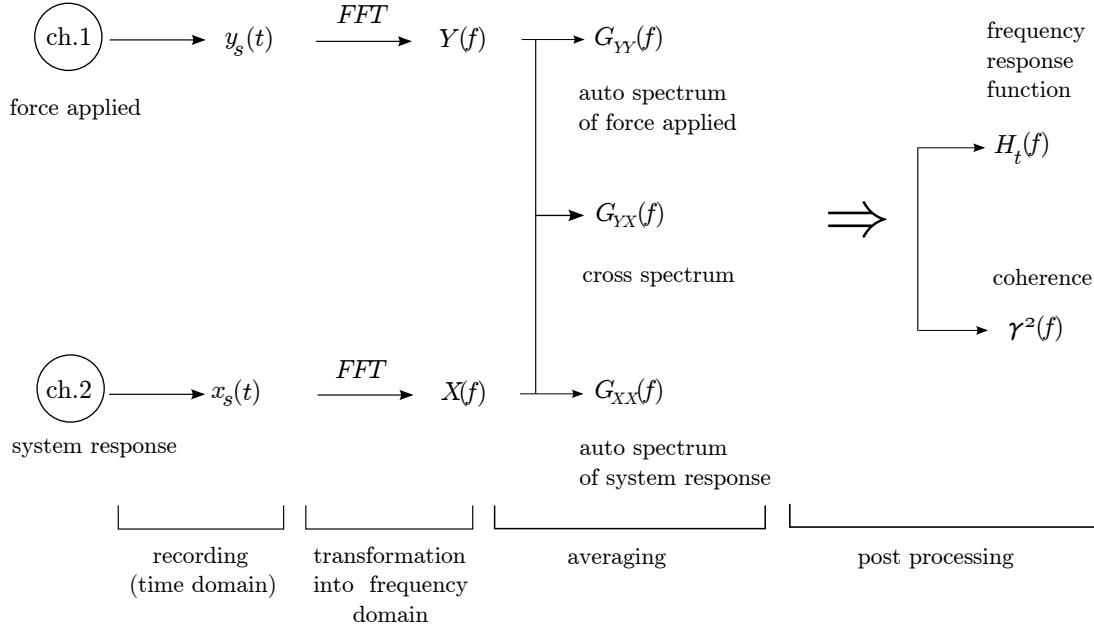


**Figure 2.2:** Scheme of the dual channel FFT analysis. Inspired from [Herlufsen, 1984, p.6].

The procedure consists of a several steps. The first step is a recording of the time history of the signals, which consists of a number of records with specified sampling rate and lengths. It also may include preprocessing of data in time domain. Next step is conversion from time to frequency domain by use of Discrete Fourier Transformation and FFT algorithm. Wherein some averaging technique is used to minimization of the influence of background noise.

An auto-spectrum of signal  $y_s(t)$  and  $x_s(t)$  after transformation into frequency domain is defined as an average of a number of products of the spectra and their complex conjugate (denoted by \*); it can be expressed as follows:

$$G_{YY}(f) = \sum Y^*(f) \cdot Y(f) \cdot \frac{1}{N_{av}} \quad G_{XX}(f) = \sum X^*(f) \cdot X(f) \cdot \frac{1}{N_{av}} \quad (2.2)$$

where  $N_{av}$  is number of averages.

A cross spectrum is determined as a product of the complex conjugate of one spectrum and the other spectrum:

$$G_{YX}(f) = \sum Y^*(f) \cdot X(f) \cdot \frac{1}{N_{av}} \quad (2.3)$$

Using different combination of ratios between auto and cross spectra, different FRF estimators can be calculated. Each of them suit to certain environmental measurement conditions, e.g. noise is either present in the input or in output signals. These estimators are defined as follows:

$$H_1(f) = \frac{G_{YX}(f)}{G_{YY}(f)} \quad H_2(f) = \frac{G_{XX}(f)}{G_{XY}(f)} \quad (2.4)$$

In other cases it is more convenient to use a  $H_3(f)$  estimator:

$$H_3(f) = \sqrt{H_1(f) \cdot H_2(f)} \quad (2.5)$$

when noise is present in both signals.

Besides the FRF, a very useful tool in the analysis is the coherence function. It is defined as follows:

$$\gamma(f)^2 \equiv \frac{|G_{YX}(f)|^2}{G_{XX}(f) \cdot G_{YY}(f)} \quad (2.6)$$

The bounds of the coherence function  $\gamma(f)^2$  are limited from zero to unity, such that  $\gamma(f)^2 = 1$  means good coherence between the signals and  $\gamma(f)^2 = 0$  indicates that coherence is absent. The main property of coherence function is an estimation of linearity of the system, and an assessment of noise influence on the measurements. The coherence function can also be used for estimating if leakage in signals takes place.

Here the points where the coherence function can be used are listed:

- to detect noise at the output and input;
- non-linearity of the system (when random excitation is applied);
- leakage in random excitation

One of the important and beneficial characteristics of FRF is that for a linear system it describes the dynamic properties independently of the excitation type, and can be used for different types of excitation.

Concerning the errors in measurements, there are two types of errors: bias and random. Bias errors are repeating each time and are of the same magnitude, they can be avoided by use of the correct estimator. Random errors can be minimized by increasing the averaging.

## 2.2 Basics of acoustics

In the following, a brief summary of the relevant acoustic theory is given. The concept, formulation and specifics of acoustic wave propagation within a rigid-walled cylindrical tube of constant cross section is represented along with the relevant assumptions. The section is based on the theory found in [Raichel, 2006], [Sorokin, 2005] and [Rienstra and Hirschberg, 2013].

### The wave equation and its solution for the rigid-walled wave guide of constant circular cross-section

The wave equation in its general form i.e. for the pressure perturbation in the acoustic medium can be expressed in the form of:

$$\Delta p - \frac{1}{c^2} \frac{\partial^2 p}{\partial t^2} = 0 \quad (2.7)$$

Here  $p = p(\bar{x}, t)$  is the sound pressure perturbation. It is a function that depends on the position  $\bar{x} = (x, y, z)$  and time  $t$ ,  $\Delta$  is the Laplacian, and  $c$  is the speed of sound in acoustic medium. This equation is derived using the mass, the momentum and the energy conservations laws.

There are several important assumptions that must be taken into account:

1. The viscosity of a fluid is neglected.
2. The mean value of pressure, density and temperature of a unperturbed medium are assumed to be constant and independent on time, the velocity of the fluid is considered to be zero,  $v_0 = 0$ . The propagation of the acoustic wave through the medium can be expressed in a form of a small perturbations of pressure, density and velocity, i.e.  $p_0 + p$ ,  $\rho_0 + \rho$ ,  $v$ .
3. In addition  $p \ll p_0$  and  $\rho \ll \rho_0$ .
4. For the Equation Of Motion (EOM), the constant over time volume forces are not taken into account, the variable volume forces acting from outside do not exist, other outside forces act only through the boundaries.
5. The gradients of constant and variable velocities and a spatial temperature gradient are assumed to be small.
6. The motion of the fluid is vortex-free.
7. The deformation of the fluid is small and stress-strain relations follows the Hooke's law.
8. The fluid is assumed to be homogeneous.

To solve equation 2.7 the separation of variables is applied, so the function  $p(\bar{x}, t)$  is assumed to be represented as the product of the functions:

$$p(\bar{x}, t) = P(\bar{x}) \cdot \Theta(t) \tag{2.8}$$

Assume that acoustic field changes harmonically in time:

$$\Theta(t) = e^{\pm i\omega t} \tag{2.9}$$

where  $i$  is an imaginary unit,  $\omega$  is an angular frequency,  $\omega = 2\pi f$ .

Consider a wave number:

$$k = \frac{\omega}{c} \tag{2.10}$$

Then, Equation 2.7 can be transformed to the form of:

$$\Delta P(\bar{x}) + k^2 P(\bar{x}) = 0 \tag{2.11}$$

Equation 2.11 is the Helmholtz equation.

Consider an acoustic duct of cylindrical cross section, for which a cylindrical coordinates system,  $(r, \psi, x)$  can be used, see Figure 2.3. Here the axis  $x$  is the longitudinal axis of the duct,  $r$  is internal radius of the wave guide. Using the expression of the Laplacian for cylindrical coordinates Equation 2.11 can be written as follows:

$$\frac{\partial^2 p}{\partial x^2} + \frac{\partial^2 p}{\partial r^2} + \frac{1}{r} \frac{\partial p}{\partial r} + \frac{1}{r^2} \frac{\partial^2 p}{\partial \psi^2} + k^2 p = 0 \tag{2.12}$$

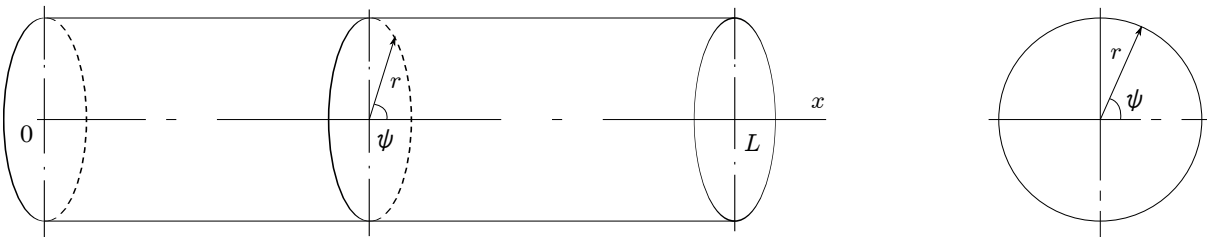


**Figure 2.3:** Cylindrical coordinates system.

Consider the simple case of the radial symmetry, where the acoustic field does not depend on angle  $\psi$ , hence the fourth term in Equation 2.12 is zero:

$$\frac{1}{r^2} \frac{\partial^2 p}{\partial \psi^2} = 0.$$

Then we separate variables considering the function of two variables  $p(r, x)$  is the product of two functions  $R(r)$  and  $\tilde{X}(x)$ :

$$p(r, x) = R(r)\tilde{X}(x) \quad (2.13)$$

doing so we can find the solutions for Equation 2.12. Substituting expression 2.13 into 2.12 and re-arranging we obtain:

$$\frac{\tilde{X}''}{\tilde{X}} = -\frac{R''}{R} - \frac{1}{r} \frac{R'}{R} - k^2 \quad (2.14)$$

Note, that in case of cylindrical coordinates, the wave number  $k$  is turned into a vector, that consists of two components  $\eta$  and  $\zeta$ , that represents the wave numbers for the longitudinal and radial directions of a wave propagation respectively and are related to each other by the next expression:

$$k^2 = \eta^2 + \zeta^2 \quad (2.15)$$

Assume the solution for  $\tilde{X}$  is  $\tilde{X}(x) = e^{i\eta x}$ , then the left part of Equation 2.14 becomes equal to

$$\frac{\tilde{X}''}{\tilde{X}} = -\eta^2 \quad (2.16)$$

Hence, for  $R$  we obtain:

$$R'' + \frac{1}{r} R' + (k^2 - \eta^2)R = 0 \quad (2.17)$$

that represents the equation for the Bessel function of zeroth-order:

$$R = A_1 J_0(\zeta r) + A_2 Y_0(\zeta r) \quad (2.18)$$

Applying condition  $|R| < \infty$  at  $r = 0$  leads to  $A_2 = 0$ , hence the solution for the acoustic field  $p(r, x)$  is:

$$p = A_1 J_0(\zeta r) \cdot e^{i\eta x} \quad (2.19)$$

The values of  $\zeta$  (the wave number in radial direction) can be determined from the Boundary Condition (BC)s, namely taking into account the BCs at the walls of the acoustic duct. Consider a case of the duct of radius  $r = a$  with rigid walls, which is relevant case for the wave guide used in Method 2. Then the pressure is maximum and radial velocity is equal to zero at the boundary. This BC can be written as follows:

$$\left( \frac{\partial p}{\partial r} \right)_{r=a} = -\zeta J_1(\zeta a) = 0 \quad (2.20)$$

The solutions of Equation 2.20 are the roots of Bessel's function of first order (i.e: 0; 3.83; 7.02; etc.). From this the critical frequencies for the duct of radius  $a$  can be calculated, hence the the

condition when there is only plane wave propagates through the duct can be determined.

Determine first critical frequency, which has to satisfy the following conditions:

$$\zeta a = 3.83 \qquad \eta = 0 \qquad (2.21)$$

Recall expression 2.15, where  $\zeta$  can be expressed as:

$$\zeta = \sqrt{k^2 - \eta^2} \qquad (2.22)$$

This leads to following equations:

$$\sqrt{k^2 - \eta^2} = \frac{3.83}{a} \qquad k^2 - \eta^2 = \left(\frac{3.83}{a}\right)^2 \qquad (2.23)$$

The condition of the critical frequency is  $\eta = 0$ , then a simple expression relating radius and wave length can be formulated:

$$ka = 3.83 \qquad (2.24)$$

Having  $k = \omega/c$ ,  $\omega = 2\pi f$  and  $f = c/\lambda$ , ( $\lambda$  is the wave length) the condition either for critical radius or for critical frequency is established:

$$r \leq 0.61\lambda \qquad (2.25)$$

Thus, once we have a defined geometry, the critical frequency can easy be calculated. This condition is to be taken into account in analysis and development of the acoustic excitation set up, to have only plane wave propagating through the wave guide.

In the zero mode case, when  $\zeta = 0$  the expression for the acoustic field becomes simply

$$p = A_0 \cdot e^{ikx} \qquad (2.26)$$

Recall Equations 2.8 and 2.9, the solution for the acoustic field rewritten as:

$$p(x, t) = A_0 \cdot e^{i(kx \pm \omega t)} \qquad (2.27)$$

It is seen Equation 2.27 represents the solution for the wave equation in the one dimensional case, i.e. plane wave equation.

### Definitions of acoustic impedance of a system

Impedance is a useful characteristic of an acoustical system. By definition it represents the ratio between sound pressure and velocity:

$$Z = \frac{p}{v} \qquad (2.28)$$

According to [Rienstra and Hirschberg, 2013, p.36 ], there are the *fluid 'inherent impedance'* is defined as  $\tilde{Z} = \rho_0 c_0$  and *dimensionless 'specific impedance'*  $Z = \tilde{Z} / \rho_0 c_0$ .

For each acoustical system the 'specific impedance' can be determined experimentally, that allows to have a defined analytical model of the system.

To derive the analytical formulation of the 'specific impedance' the velocity potential  $\varphi$  is to be introduced. By definition, [Sorokin, 2005, p.5 ] it can be expressed as following:

$$\vec{v} = \nabla\varphi \qquad p = -\rho_0 \frac{\partial\varphi}{\partial t} \qquad (2.29)$$

Consider a one dimensional sound field of a harmonic form, recall equation 2.27. Then the velocity potential can be expressed as:

$$\varphi = (Ae^{ikx} + Be^{-ikx})e^{-i\omega t} \qquad (2.30)$$

Utilizing Equations 2.29 (note that for one dimensional case  $v = \frac{\partial\varphi}{\partial x}$ ), yields:

$$\begin{aligned} p &= i\rho_0\omega(Ae^{ikx} + Be^{-ikx})e^{-i\omega t} \\ v &= (ikAe^{ikx} - ikBe^{-ikx})e^{-i\omega t} \end{aligned} \qquad (2.31)$$

Substituting coefficients  $A$  and  $B$  with these in a form of  $A = \frac{\tilde{A}}{i\rho_0\omega}$ , and recall that  $k = \frac{\omega}{c_0}$  leads to the following:

$$\begin{aligned} p &= (\tilde{A}e^{ikx} + \tilde{B}e^{-ikx})e^{-i\omega t} \\ v &= \frac{1}{\rho_0 c_0}(\tilde{A}e^{ikx} - \tilde{B}e^{-ikx})e^{-i\omega t} \end{aligned} \qquad (2.32)$$

Finally, according to the definition 2.28 the expression for the 'specific impedance' is as follows:

$$\frac{(\tilde{A}e^{ikx} + \tilde{B}e^{-ikx})\rho_0 c_0}{\tilde{A}e^{ikx} - \tilde{B}e^{-ikx}} = Z \qquad (2.33)$$

The coefficients  $\tilde{A}$  and  $\tilde{B}$  are to be determined from the BCs of the system.

To demonstrate this, consider an acoustic duct (relevant for Method 2), assuming that it is treated as a pipe with cylindrical cross section opened at one end and closed at the other, see Figure 2.4.

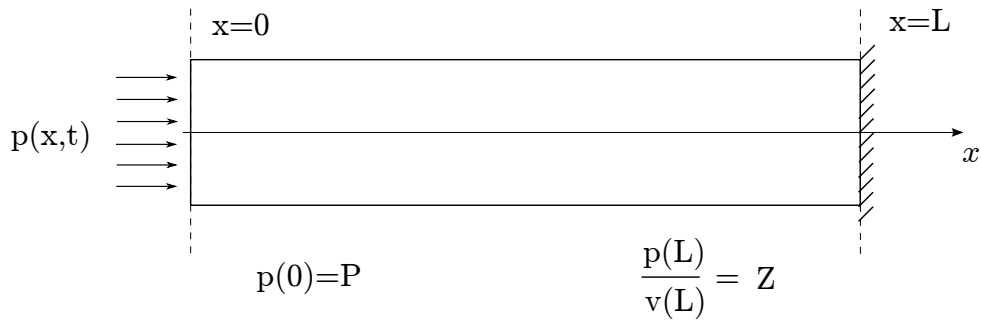


**Figure 2.4:** Scheme of the simplified acoustic duct with open and closed ends and BCs.

Then, taking into account the BCs, Equations 2.32 and 2.33 yield:

$$\begin{aligned} \tilde{A} + \tilde{B} &= P \\ \frac{\tilde{A}e^{ikL} + \tilde{B}e^{-ikL}}{\tilde{A}e^{ikL} - \tilde{B}e^{-ikL}} &= \frac{Z}{\rho_0 c_0} \end{aligned} \qquad (2.34)$$

which is the system of two equations with two unknowns.

From the Equation 2.33 it is seen that specific impedance is a function of a frequency and position and can be a complex number. Furthermore, in case where the reflected wave does not exist, i.e.  $\tilde{B} = 0$ , the 'specific impedance' is equal to the fluid inherent impedance  $\tilde{Z} = \rho_0 c_0$ .

The calculation of a 'specific impedance' is to be used further in the analysis of a acoustic excitation set-up, i.e. Method 2, in Chapter 3

### 2.3 Vibration analysis of a beam

In the following a short theoretical summary of a vibrating beam is given. It is used for the analytical determination of the frequency response of a beam. The section is based on [Irving H. Shames, 2003, Chapter 7, Part A ].

The derivation of the equation of motion for a vibrating beam is based on the fundamental Hamilton's principle:

$$H = \int_{t_1}^{t_2} (T - V - U) dt \qquad \delta H = 0 \qquad (2.35)$$

where  $T$  is the total kinetic energy,  $V$  is the internal potential energy of a structure, and  $U$  is the potential energy of external forces. Considering Bernoulli-Euler beam theory the quantities of Equation 2.35 are given by

$$T = \frac{1}{2} \int_0^L \rho A \left( \frac{\partial w}{\partial t} \right)^2 dx \qquad (2.36)$$

$$V = \frac{1}{2} \int_0^L EI \left( \frac{\partial^2 w}{\partial x^2} \right)^2 dx \qquad (2.37)$$

$$U = \int_0^L q w dx \qquad (2.38)$$

where  $\rho$  is the material density,  $A$  is cross-sectional area,  $E$  is Yuong's Modulus,  $I$  is the area moment of inertia,  $q$  is a load, and  $w$  is the vertical displacement, that depends on time and position, i.e.  $w = w(x, t)$ , see Figure 2.5.

Applying the variational method, the equation of motion for the Bernoulli-Euler beam is formulated as follows:

$$\rho A \frac{\partial^2 w}{\partial t^2} + EI \frac{\partial^4 w}{\partial x^4} = q \qquad (2.39)$$

Note, that for case of free vibration analysis  $q = 0$ .

Assuming that

$$w(x, t) = W(x) \cdot \Theta(t) \qquad (2.40)$$

and separating variables, the solution for  $W(x)$  to the equation 2.39 can be written in a form of:

$$W(x) = A_1 \cos(kx) + A_2 \sin(kx) + A_3 \cosh(kx) + A_4 \sinh(kx) \quad (2.41)$$

where

$$k = \sqrt[4]{\frac{\rho \cdot A \cdot \omega^2}{E \cdot I}} \quad (2.42)$$

The constants  $A_i$  are to be found from the BCs, which for a cantilever beam with origin  $x = 0$  at the clamped end, see Figure 2.5, are as follows:

1. at the clamped end,  $x = 0$ , the displacement  $W(x)$  and the slope  $W'(x)$  are zero:

$$W(0) = 0 \quad W'(0) = 0 \quad (2.43)$$

2. at the free end,  $x = L$ , the bending moment  $M = EIW''(x)$  and the shear force  $Q_s = EIW'''(x)$  are zero:

$$EIW''(L) = 0 \quad EIW'''(L) = 0 \quad (2.44)$$

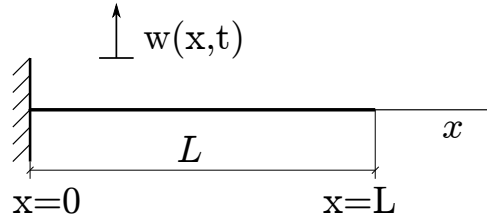


**Figure 2.5:** Scheme of a cantilever beam.

Solving four equations 2.43 and 2.44 and substituting coefficients  $A_i$  into 2.41, the function of vertical displacement  $x$  and frequency  $f$ ,  $W(x, f)$ , is obtained (e.g. see Maple calculations in Appendix D). The denominator of this function is the frequency equation for the cantilever beam:

$$1 + \cos(kL) \cdot \cosh(kL) = 0 \quad (2.45)$$

The Equation 2.45 corresponds to [Irving H. Shames, 2003, p.333 ], and its roots are the natural frequencies of the cantilever beam. This approach can be used to determine the relevant experimental frequency range, which is the base for the FFT analysis settings and equipment selection.

### Forced vibration analysis

In the experimental part of the project the vibration of a cantilever structure occurs due to the excitation of the structure with an external force applied at a certain point, which is on the centreline ( $x$ -axis) of the beam, see Figure 2.6.

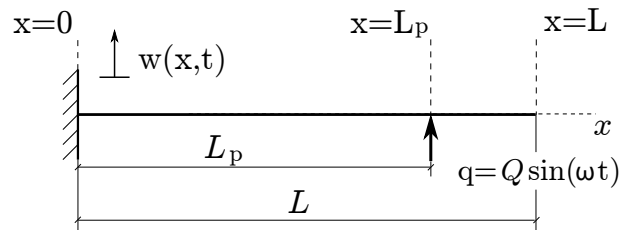


**Figure 2.6:** Diagram for the cantilever beam and forced vibration

To determine the vertical displacement, the beam is divided into two parts at the point of force application,  $x = L_p$  and the equation of displacement  $W(x)$  is formulated for the each part:

$$\begin{aligned} W_A(x) &= A_1 \cos(kx) + A_2 \sin(kx) + A_3 \cosh(kx) + A_4 \sinh(kx) \\ W_B(x) &= B_1 \cos(kx) + B_2 \sin(kx) + B_3 \cosh(kx) + B_4 \sinh(kx) \end{aligned} \quad (2.46)$$

The coefficients  $A_i$  and  $B_i$  are to be determined from the boundary and compatibility conditions. The BCs for the clamped and free ends, i.e. for  $x = 0$  and  $x = L$ , are the same as for the free vibration case, Equations 2.43 and 2.44:

$$\begin{aligned} W_A(0) &= 0 & EIW_B''(L) &= 0 \\ W_A'(0) &= 0 & EIW_B'''(L) &= 0 \end{aligned} \quad (2.47)$$

For the point  $x = L_p$  four following equations are established:

$$\begin{aligned} W_A(L_p) &= W_B(L_p) \\ W_A'(L_p) &= W_B'(L_p) \\ EIW_A''(L_p) &= EIW_B''(L_p) \\ EIW_A'''(L_p) - EIW_B'''(L_p) &= Q \end{aligned} \quad (2.48)$$

Thus, we obtain a system of eight equations with eight unknowns. Now the expressions for the displacement,  $W_A(x)$  and  $W_B(x)$  are determined and can be used for a comparison with FRF obtained from measurements.

### Inclusion of addition mass and moment of inertia.

To measure vibration one or several transducers need to be attached to the structure. The inertia of the devices (masses and centroidal moments of inertia) can influence the vibration response. Usually transducers are chosen according to the recommendations and standards in order to have negligible influence and good accuracy of the results obtained. Nevertheless, in case of the considerable addition masses and moments of inertia of the devices, their contribution can be accounted for in the analysis.

Consider the case, where the transducers are connected to the excitation point,  $x = x_m = L_p$ , see Figure 2.7.

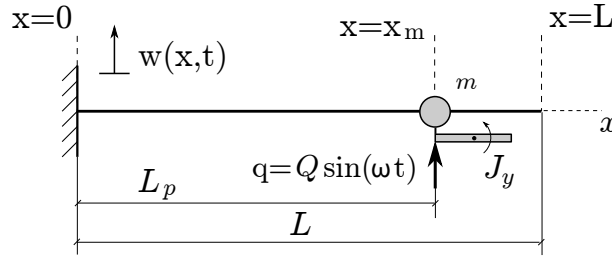


**Figure 2.7:** Diagram of a cantilever beam with additional mass and rotational inertia.

To solve this problem, the mass and moment of inertia are added to the total energy of Equation (2.36)

$$T = \int_0^L \frac{1}{2} \rho A \left( \frac{\partial w(x,t)}{\partial t} \right)^2 dx + \frac{1}{2} m \left( \frac{\partial w(x_m,t)}{\partial t} \right)^2 + \frac{1}{2} J_y \left( \frac{\partial w(x_m,t)}{\partial x \partial t} \right)^2 \quad (2.49)$$

where  $m$  is the mass and  $J_y$  is moment of inertia. After applying Hamilton's principle, Equation 2.35, the added turms will contribute to the continuity conditions 2.48, which gives

$$\begin{aligned}
 W_A(L_p) &= W_B(L_p) \\
 W'_A(L_p) &= W'_B(L_p) \\
 EIW''_A(L_p) - EIW''_B(L_p) - J_y\omega^2 W'_A(x_m) &= 0 \\
 EIW'''_A(L_p) - EIW'''_B(L_p) &= Q - m\omega^2 W_A(x_m)
 \end{aligned} \tag{2.50}$$

In fact, due to the contribution of the additional mass and moment of inertia the natural frequencies of a beam are shifted. The response of the structure can be seen by plotting either  $W_A$  or  $W_B$ , see calculations in Maple documents, Appendix D. Due to very complicated denominator of the displacement function, it is not possible (at least very time consuming) to use the approach for calculation of natural frequencies described earlier for the free vibration of a pure cantilever beam, see Expression 2.45. But it is easy to determine the frequencies by plotting either the denominator, and check where the curve crosses  $x$ -axis, or the entire function and look for peaks.

The approach of calculation natural frequencies and frequency response function in terms of compliance is to be used for the analytical analysis of the cantilever structure, see Chapter

## 2.4 FEM, modal and harmonic (mode superposition) analysis

In the following a short summary of the FEM modal and harmonic mode superposition analysis is represented. This method is applied for the numerical determination of dynamic characteristics of a compressor housing, by use of the commercial software ANSYS 14.5. The section is based on [Cook *et al.*, 2002, Chapter 11 ].

For a discrete mechanical system, the dynamic equilibrium equation is of the form:

$$[M] \{\ddot{D}\} + [C] \{\dot{D}\} + [K] \{D\} = \{R^{ext}\} \tag{2.51}$$

where  $[M]$  is the mass,  $[C]$  is the damping,  $[K]$  is the stiffness matrix,  $\{D\}$  is the displacement, and  $\{R^{ext}\}$  is the external force vectors.

To determine the natural frequency for a free undamped vibration ( $\{R^{ext}\} = 0, [C] = 0$ ), the 'generalized eigenvalue problem' is to be solved:

$$\begin{aligned}
 ([K] - \omega^2 [M]) \{\bar{D}\} &= \{0\} \\
 \Downarrow \\
 \det([K] - \omega^2 [M]) &= 0
 \end{aligned} \tag{2.52}$$

In this case the number of natural frequencies corresponds to number of Degrees Of Freedom (DOF), i.e. number of equations in the system 2.52.

The harmonic mode superposition analysis is the method for solving forced vibration problems. It involves replacing displacements in the equation 2.51 to modal parameters by using  $[M]$ -orthonormalization of eigenvectors:

$$\{D\} = [\phi] \{S\} \tag{2.53}$$

Then the system of equilibrium equations in modal parameters are decoupled:

$$\{\ddot{S}\} + [2\xi\omega] \{\dot{S}\} + [\omega^2] \{S\} = \{Q\} \tag{2.54}$$

which represents the system of  $n$  equation of a type:

$$\ddot{s}_i + 2\xi_i\omega_i\dot{s}_i + \omega_i^2 s_i = q_i \tag{2.55}$$

where  $\xi_i$  is a damping of an  $i$ -th mode.

After solving the decoupled equilibrium equations in modal coordinates, the solution is transformed into original problem using the relation 2.53.

The advantage of this method is the ability to determine modal damping  $\xi_i$  to each mode experimentally, and then include it in the numerical simulation.

# Design and analysis of acoustic excitation set up 3

In the following, the main features of the experimental set up with localized acoustic excitation are analysed. Two new designs with focus on robustness and usability are suggested. An analysis of the characteristics of the acoustic field for new modifications is performed analytically and experimentally. Advantages and disadvantages of different approaches are discussed.

## 3.1 Analysis and technical improvements of existing design

The main difference of the alternative method for mobility measurements is localized excitation of the structure by acoustic waves. The experimental set up suggested and used by Secop GmbH is shown in Figure 3.1.

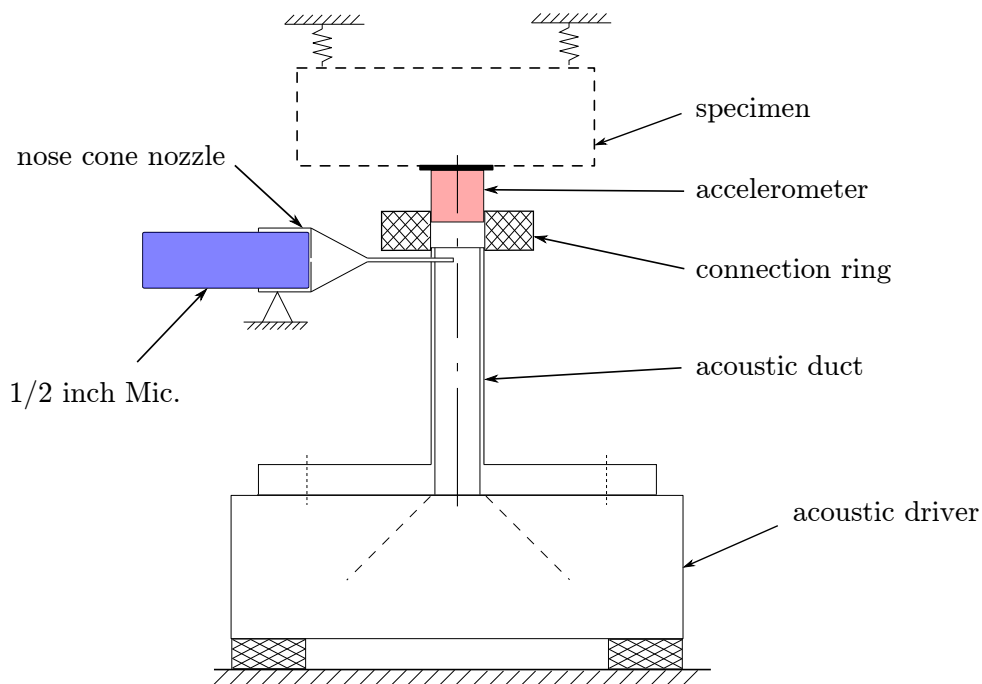


*Figure 3.1: The configuration of the set up suggested by Secop.*

The method involves the following principal parts in the experimental set up:

1. an accelerometer connected to a structure to measure the motion of the structure (system response  $x_s(t)$ )

2. a microphone, to measure the sound pressure level, which serves as a reference signal (excitation force  $y_s(t)$ )
3. an acoustic driver, to excite the acoustic field with the required sound pressure level and certain form of excitation
4. an acoustic duct, which serves as a wave guide
5. components for providing sealing and connections of the parts, such as connection ring and silicon

Due to the difference in transducer positions relative to input and output responses, an estimation of the accuracy is needed. Immediately can be seen that the closer positions of the transducers are to each other, the more accurate results can be obtained, as the force applied to the structure is registered closer to the accelerometer surface, where it is applied. The ideal solution is when the measurement of the force applied to the structure occurs at the point of its application, otherwise the transfer function between the points of measurement and application have to be determined.

The initial configuration of the set up suggested by Secop GmbH, see Figure 3.1, includes an accelerometer with a cylindrical housing, a foam connection ring, 1/2 inch microphone connected by a probe cone with a thin tube nozzle, and the acoustic duct fastened to the acoustic driver. To avoid leakages of the sound pressure the connection of the thin tube nozzle to the duct is sealed by silicon. The geometrical parameters of the set up allows to take a probe of sound pressure very close to the accelerometer surface, hence the quality of the results is of high accuracy. At the same time, the position of the parts can not be kept absolutely the same each time, hence the measured data can differ for the same system for each single measurement session.

Concerning the robustness of the actual set-up, several points can be concluded: (i) it is quite time consuming to assemble all parts: firstly, due to the dimensions of microphone and requirements to have an extra holder for it; secondly, the microphone consists of several parts, which also have to be assembled; (ii) the set up is not effective with respect to re-movability (mobility), i.e. to conduct measurements on different points, requires extra operations for disassembling and assembling of all the parts.

To improve the robustness of the existing set up a new design including two different modifications of the adaptor named 'm#1' and 'm#3', see Figure 3.2, is introduced.

The principle scheme of adaptor m#1 is shown in Figure 3.2a. The main changes of the adaptor modification m#1 in comparison to the initial set up are: (i) the use of a smaller microphone (for the present set-up 1/4 inch microphone B&K Type 4935 used), which is inserted directly into the acoustic duct; (ii) the outer diameter of the duct tube is increased so that the foam connection ring can be placed upon the top of the tube, and fixed by the pad/bead in axial direction, hence have a constant fixed position with respect to the tube for each measurement session.

The principle scheme of modification m#3 is represented in Figure 3.2b. The concept of the device was suggested by Brüel&Kjær, as a prototype to a more robust and accurate solution. The main idea is to place both transducers into a single rigid housing, which can be connected by a soft connector (e.g. foam or rubber ring) through an acoustic duct (e.g. flexible hose or rigid wave guide), to the acoustic driver. In this case, in contrast to adaptor m#1, the distance between the transducers is constant and it is not influenced by the soft connection ring.

The advantages of adaptor m#3 are: (i) higher robustness due to the simple connection and mobility of the device, (ii) the closer location of the acoustic centre of microphone to the point of excitation, i.e. accelerometer surface. Furthermore the rigid housing of the device does not allow

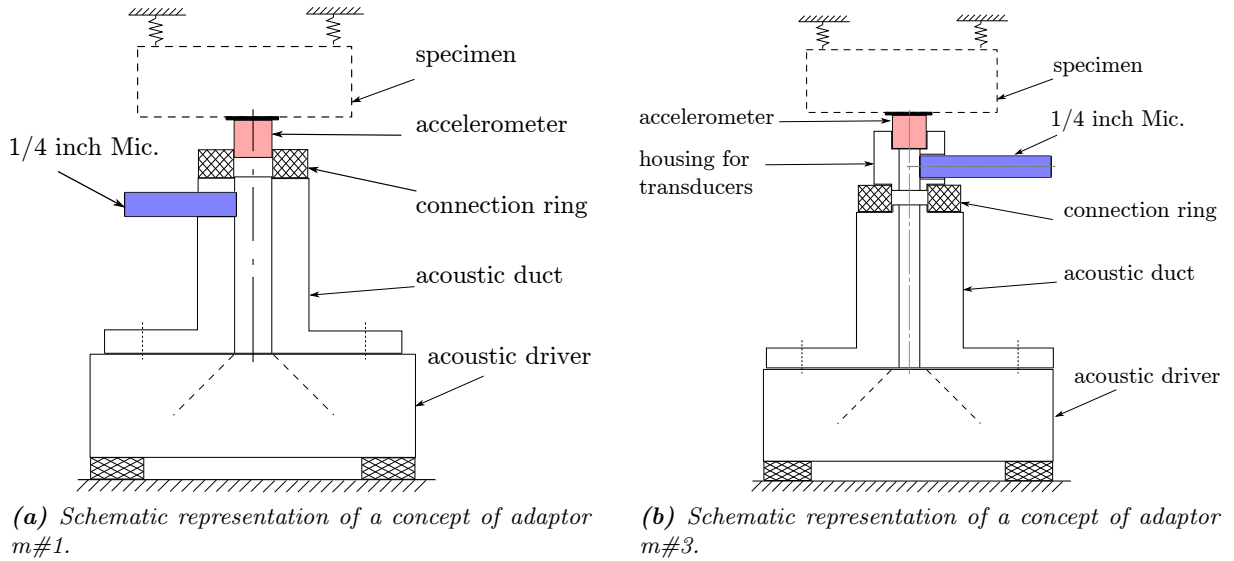


**Figure 3.2:** Representation of the concepts of two modifications of a new design.

any mutual displacement between the transducers and therefore keeping the transfer function between the acoustic centre of the microphone and the surface of the accelerometer constant. In case of adaptor m#1 the transfer function between the transducers may depend on the possible deformation of the connection ring due to its flexibility, hence this affects the accuracy of the measurements.

The disadvantages of adaptor m#3 is the higher inertia (and mass) of the device, which in turn might affect the dynamic characteristics of a system, including the FRF. The influence of the additional mass and moment of inertia is to be investigated in the vibration analysis of a cantilever structure, see Chapter 4.

### Manufacturing of the adapters

For the experiment to be conducted two suggested modifications of adaptors were manufactured, wherein several considerations were incorporated.

Firstly, the main geometrical parameters, such is the height and the internal diameter of the acoustic duct are inspired by the original adaptor from the Secop GmbH set-up. Secondly, taking into account preferences with respect to the characteristic of acoustic field, i.e. the plane wave condition, Equation (2.25) is satisfied, such that the diameter of the acoustic channel set to be  $D_{ch} = 5$  mm.

The dimensions of the top part of the adaptor m#1, where the connection ring is placed, is chosen similarly to the diameter of the cylindrical accelerometer (B&K Type 4993 V), which is equal to 7 mm. The rubber ring was chosen from the materials found in the vibro acoustic lab, with no data of the material properties available.

For the tests with the adaptor m#3 the accelerometers B&K Type 4507 B 004 and Type 4507 B 005, and the set of 6 '1/4 inch' microphones B&K Type 4935, were used. The construction of the accelerometers includes the cubic housing with dimensions 10x10x10 mm, this led to special design of the top part of the adaptor, which combines both transducers in a single housing.

A sketch of the adaptor m#3 is shown in Figure 3.3. Drawings of the adaptors m#1 and m#3 are represented in Appendix A.

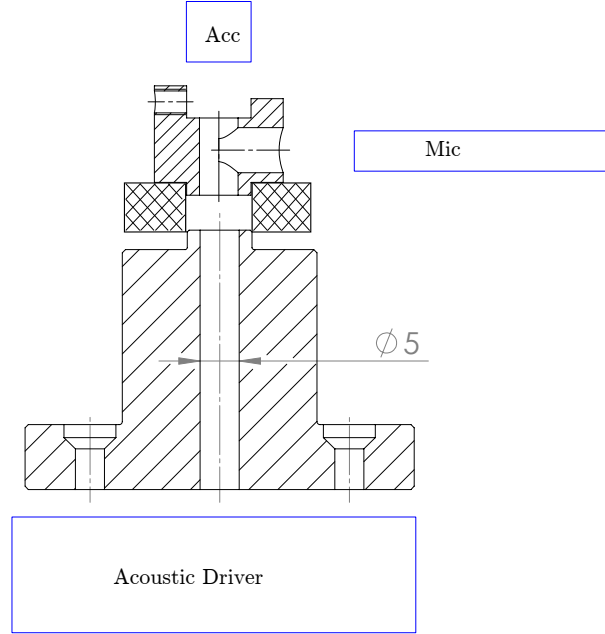


**Figure 3.3:** Configuration of m#3.

### 3.2 Experimental investigation of the adaptors m#1 and m#3.

To investigate how the acoustic field depends on the geometrical parameters and sealing conditions of adaptors m#1 and m#3 several measurement sessions were conducted.

Consider the internal channel of the adaptors as the wave guide with a cylindrical cross section, and designate the points of the transducers placement as  $A$  for the top transducer,  $B$  for the axis of the reference microphone and  $C$  for the bottom part of the channel, see Figure 3.4, 'adaptor wave guide' part. The aim of the test is to measure and compare the transfer function  $H_{tAB}(f)$  between the points  $A$  and  $B$ , which are the positions of the transducers in the adaptors. Particular points of interest are: (i) examination of the influence of the sealing of the acoustical channel on the FRF between the points  $AB$  for the m#3; (ii) verification of the influence of changing in distance  $AC$  for the modification of the adaptor m#3; (iii) the investigation of the dependency on the changing the distance  $AB$  for the adaptor m#1.

The results of measurements are also aimed to be used for comparison with analytical analysis of the wave guides, and determining of the acoustic impedance of the systems.

The principle scheme of the experimental set-up is shown in Figure 3.4. To determine the FRF by means of sound pressure an accelerometer from the initial set up is replaced by a microphone (*mic2*), which is fixed rigidly by a holder connected to the concrete block.

The apparatus used in measurements are listed in Table 3.1.

Device	Type	Serial number
Vibration analyzer	Bruel&Kjaer 3560-C (3109+7536)	2277049
Acoustic driver 'Artificial Mouth'	Bruel&Kjaer 4216	146181
Power amplifier	Bruel&Kjaer 2706	2120369
Array microphone (1)	Bruel&Kjaer 4935	2079317
Array microphone (2)	Bruel&Kjaer 4935	2252304
Laptop with B&K PULSE SW	LabShop v.16.1.0.84	

**Table 3.1:** Apparatus and devices used in measurements.

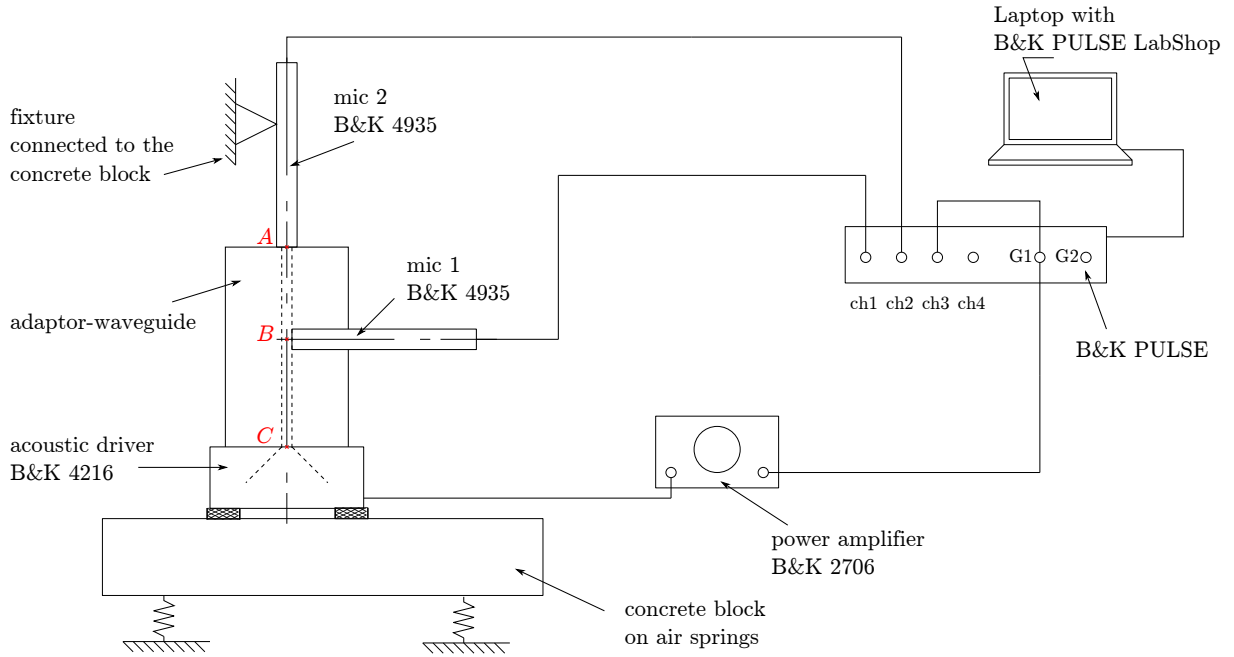


**Figure 3.4:** Principle scheme of the experimental set-up for the investigation of properties of adaptors m#1 and m#3.

### Choice of the effective frequency range

Taking into account that the application of the method is for point mobility measurements of a flexible shell structure of a compressor housing, a prior estimation of the natural frequencies of a housing model have been done, see Chapter 5. The first 14 natural frequencies are in the range from 3 kHz to 6 kHz. Following to the specification of the microphone properties, see Appendix C, Table C.1, the guaranteed frequency range of the microphone is up to 5 kHz, and general frequency range is up to 20 kHz.

To cover the required frequency bounds the upper frequency limit used in the experiment is set to 10 kHz for the FFT analyzer and to 12.5 kHz for the generator. The settings of FFT analyser are given in Table 3.2.

Parameter	Value
Number of lines	6400
Frequency span	10 kHz
Number of averages	100
Time	21,76 s
Overlap	66,67%

**Table 3.2:** Settings of the FFT analyser.

However, to have an accurate estimation of the acoustic field properties, the effective frequency range considered for further analysis is chosen to be limited to 5 kHz.

For all experiments documented in the present report random noise was chosen as the type of excitation. It can be justified by high robustness and accuracy of the method if it is applied to the linear systems, according to [Døssing, 1988].

### Experimental investigation of properties of adaptor m#3

To investigate how the transfer function  $H_{TAB}(f)$  for m#3, depends on the sealing of the duct and how it depends on the changing of the length of the acoustic channel  $AC$  several variations of the assembly, see Figure 3.4, were performed. The experimental set-up, 'adaptor wave guide', with m#3 shown in Figure 3.5.



*Figure 3.5: Experimental set up with modification m#3.*

The different assemblies of the adaptor wave guide include the combinations of the set-up considering the sealing of the microphone 2 (measurement sessions M1, M2 and M3), use the connection of the top and bottom parts of the adaptor with and without the connection ring (M1, and M4), and finally use of m#3 without bottom part (M5). To each of the measurement session special name (mark) has been assigned.

The descriptions and the details for the combinations of the set up for the 'sealing of the top microphone (mic2)' case, with the appropriate marks assigned are represented in Figure 3.6. The comparison plot for measurement sessions M1 (good sealing), M2(not proper sealing) and M3(no sealing) in terms of FRF estimator H3, Bode Plots 'Magnitude/Phase', is shown in Figure 3.7.

From the plot, Figure 3.7, it is seen that for an untight sealing the amplitude decreases. The results are as expected. In the case of an untight sealing, part of the acoustic pressure 'dissipates' through the tiny openings in the end of the channel and are not reflected by the membrane of the microphone.

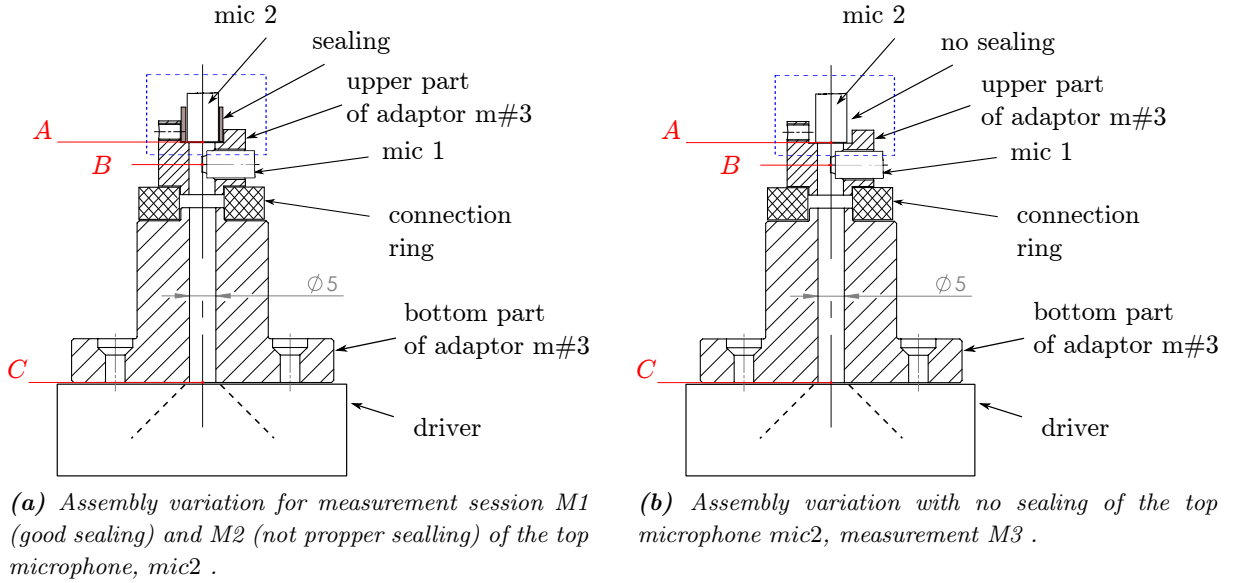


**Figure 3.6:** Experimental set up for the 'adaptor wave guide section' for measurements sessions M1, M2 and M3.

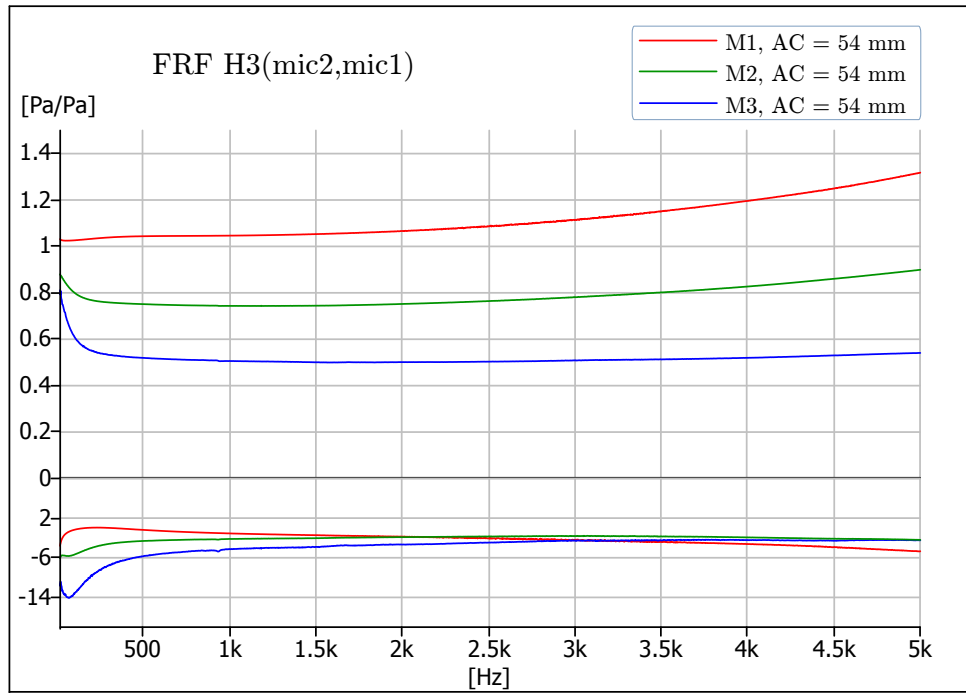


**Figure 3.7:** The transfer functions of the acoustic field between the transducers placement AB, in terms of FRF estimator H3, Bode Plots 'Magnitude/Phase', for measurement sessions M1, M2 and M3.

To investigate the influence of the change in distance  $AC$  on the transfer function, the measurements M4 (no connection ring) and M5 (no bottom part of the adaptor) were conducted, see sketches of the adaptor assembly variations in Figure 3.8. For case M4 the distance  $AC$  was reduced from 54 mm (for the original M1 case) to 49mm, and for case M5 effective length of the duct  $AC$  was reduced to 20 mm.

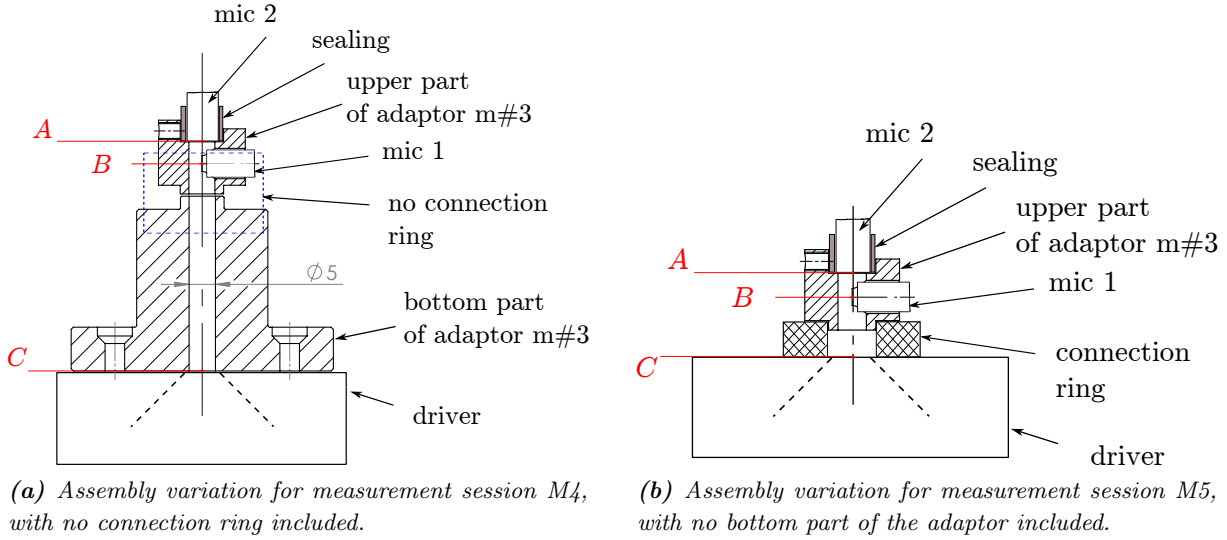


**Figure 3.8:** Experimental set up for the 'adaptor wave guide section' for measurements sessions M4 and M5.

The results of the test in terms of FRF estimator H3, Bode Plots 'Magnitude/Phase' are represented in Figure 3.9. As it was expected, the curves for the cases with different length

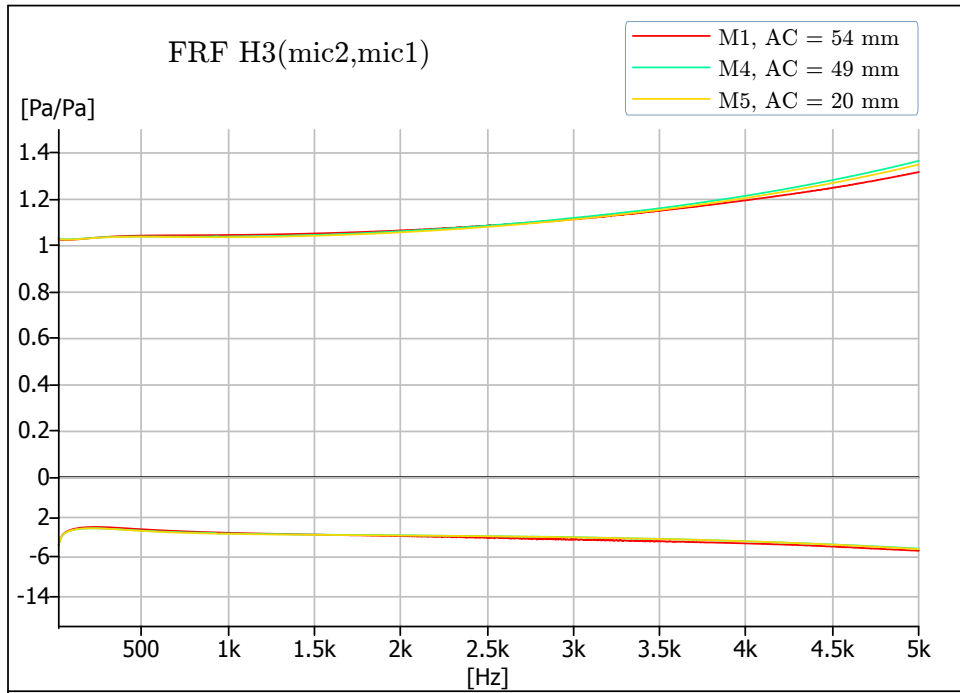


**Figure 3.9:** The transfer functions of the acoustic field between the transducers placement AB, in terms of FRF estimator H3, Bode Plots 'Magnitude/Phase', for measurement sessions M1, M4 and M5.

of the acoustic channel are in a good agreement, hence the transfer function  $H_{tAB}(f)$  is the characteristic of the acoustic field between the points A and B, and does not depend on the general length of the acoustic channel. This statement is also to be verified by analytical calculation of the transfer function for the model of the device.

### Experimental investigation of properties of adaptor m#1

The picture of the experimental set up, with adaptor m#1 is shown in Figure 3.10.

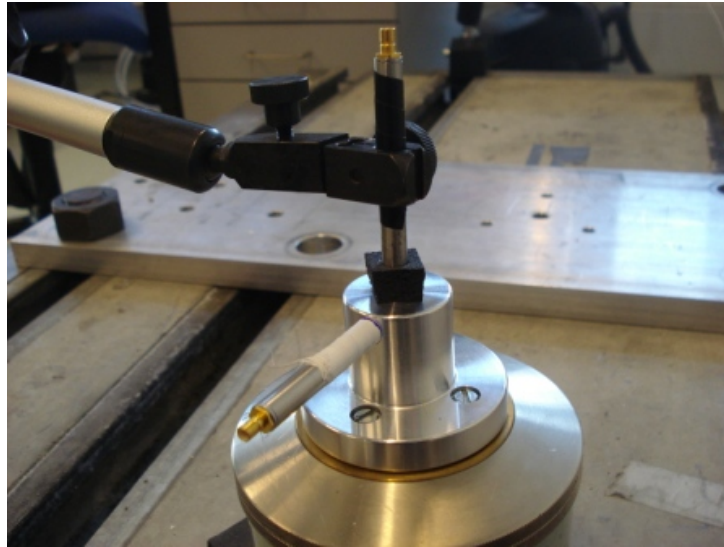


*Figure 3.10: Experimental set up with adaptor m#1.*

The part of measurements conducted on the adaptor m#1 is aimed to determine the transfer function for the acoustic field between the points  $A$  and  $B$ , see Figure 3.4, when the distance  $AB$  is gradually changed. For this purpose a set of four measurements with increasing the distance  $AB$  from 7 to 10 mm with a step of approximately 1 mm were conducted. The measurement sessions are named M6, M7, M8 and M9 respectively.

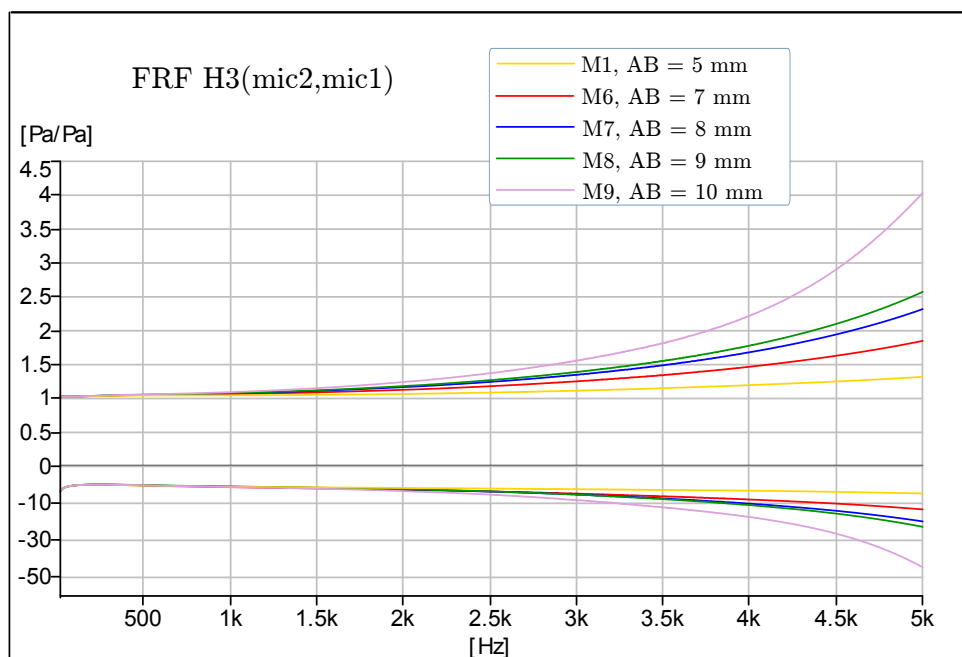


*Figure 3.11: The transfer functions of the acoustic field between the transducers placement  $AB$ , in terms of FRF estimator  $H3$  for the adaptors m#1 and m#3.*

To compare the transfer function  $H_{tAB}(f)$  for the adaptors m#1 and m#3 results from measurement M1 are included into the comparison plot, Figure 3.11. In case of M1 distance  $AB$  is constant, as the transducers are fixed in the common rigid housing, and equal to 5 mm.

The marks assigned to the measurements with corresponding distances  $AB$  and the Bode Plots 'Magnitude/Phase' of the FRF in terms of the estimator  $H3$  are shown in Figure 3.11.

From the plots it is seen that the transfer function of acoustic field depends on the change in distance between the points, such that the longer the distance is the more deviation from the  $H_t(f) = 1$  can be observed.

### 3.3 Analytical analysis of the acoustic excitation setup

The purpose of the analytical analysis is to make a model of the system used in the experiments, and to determine the transfer function  $H_{tAB}(f)$  analytically. Then, the model obtained can be used in the analytical or numerical vibration analysis of cantilever and shell structures, where it might be necessary to correlate the amplitudes of the FRFs taking into account the transfer function of the acoustic field between the transducers placement.

Using the definition of a transfer function, see Equation 2.1, for the relevant problem it can be written as:

$$H_{tAB}(f) = \frac{p(L_A, f)}{p(L_B, f)} \quad (3.1)$$

where  $p(L_A, f)$  and  $p(L_B, f)$  is the sound pressure amplitudes at the points  $A$  and  $B$  of the acoustical system.

The scaled sketch of the acoustic channel for adaptor m#1 is shown in Figure 3.12. As was stated earlier the specifics of m#1 is that the transducers are separated by a soft rubber or foam ring, which is indicated by the dashed line on the scheme. The distance  $AB$  can vary each time when assembling and disassembling the set up.

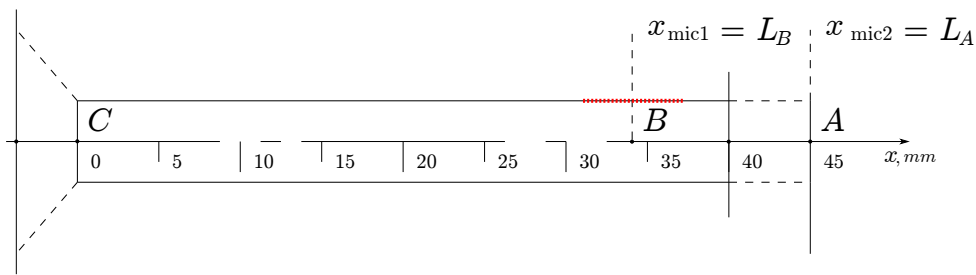


**Figure 3.12:** Scaled sketch of the acoustic channel for the adaptor modification m#1.

The scaled scheme of m#3 is shown in Figure 3.13. Here the distance  $AB$  is constant and equal to 5 mm.

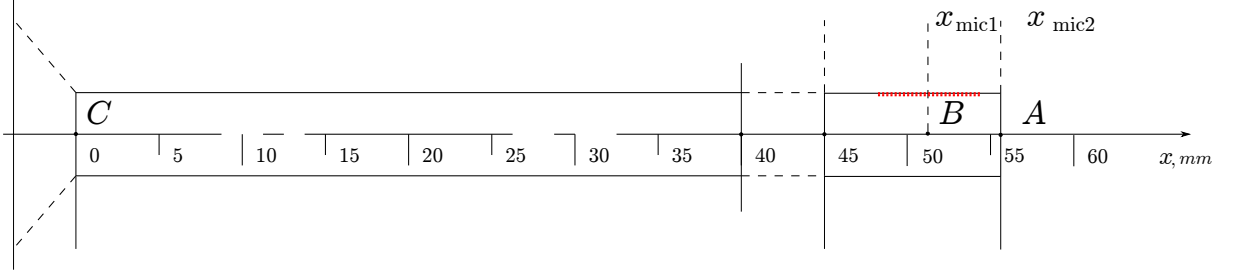


**Figure 3.13:** Scaled sketch of the acoustic channel for the adaptor m#3.

It was proved experimentally, that the transfer function does not depend on the general length of the acoustical channel, hence for m#3 only the top part, where both of the transducers are placed, can be considered for the analysis, see the scheme in Figure 3.14.

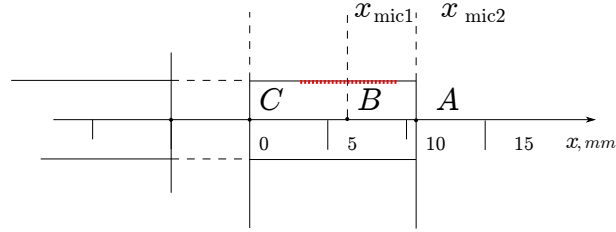


**Figure 3.14:** The effective length of the acoustic channel for adaptor m#3.

To determine the pressure amplitude for the points  $A$  and  $B$ , the approach represented in Chapter 2, Section 2.2 is used.

Recall the expression for the pressure (2.31):

$$p = i\rho_0\omega(Ae^{ikx} + Be^{-ikx})e^{-i\omega t} \quad (3.2)$$

Substituting it into (3.1) leads to the expression for the transfer function  $H_{tAB}(f)$ :

$$H_{tAB}(f) = \frac{Ae^{ikL_A} + Be^{ikL_A}}{Ae^{ikL_B} + Be^{ikL_B}} \quad (3.3)$$

where  $k = \omega/c$  is a wave number,  $A$  and  $B$  are the coefficients to be determined.

For the first stage, to determine the coefficients consider the acoustic duct as the tube with one end opened and the other perfectly closed. Then the coefficients can be determined from the following BCs, so that the pressure amplitude is equal to some value  $P$  at the opened end; and the specific impedance  $Z$  tends to infinity, due to the sound velocity is equal to zero at the closed end. When setting the impedance to a large number, the next plots are obtained, see Figure 3.15. There are three cases M1, M6, and M9 considered, that corresponds to distance  $AB$  equal to 5, 7 and 10 mm respectively.

As can be seen from the plots, Figure 3.15, the experimental curves deviate from analytical ones, and deviation increases with increasing frequency.

To obtain the analytical solution closer to the experimental one the specific impedance of the system has to be determined using the data from measurements. These calculations include a number of complicated and long expressions, which were solved by using the commercial software Maple 16. Corresponding Maple documents are represented in Appendix E.

The results represented in the report are calculated for the cases M6 and M9 for adaptor m#1,

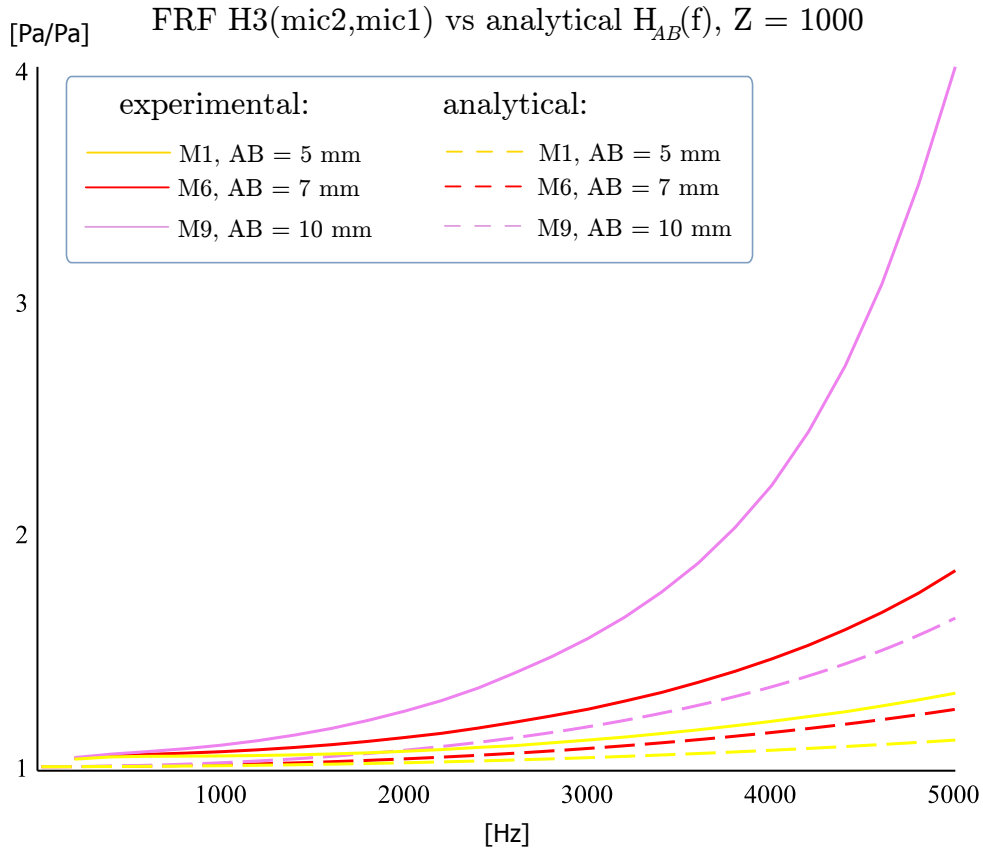


**Figure 3.15:** Comparison plot of the experimental and analytical result of the transfer function with impedance tend to infinity.

and M1 for adaptor m#3.

The specific impedance determined is shown graphically in Figure 3.16 in terms of the real and the imaginary part of  $Z$ .

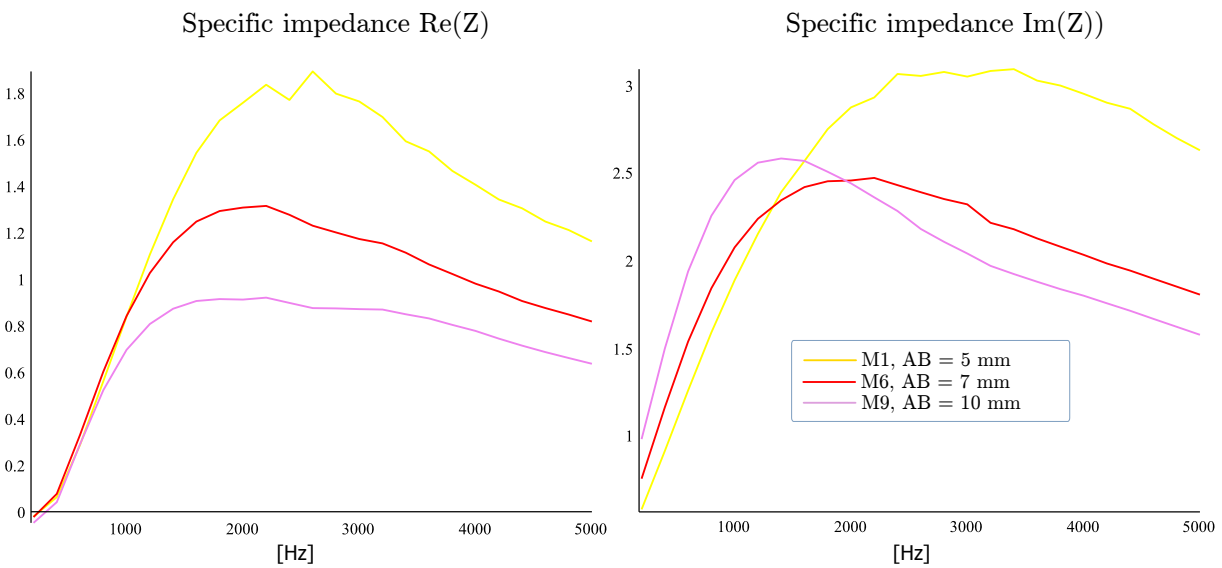


**Figure 3.16:** Specific impedance for the cases M6, M9 and M1; real and imaginary part vs frequency.

It is seen that the determined specific impedance is a complex number that depends on frequency. Substituting the value for the impedance in the FRF calculations the next analytical curves are

obtained, see Figure 3.17.

In case of the use of the specific impedance of the system, the analytical curves are in agreement

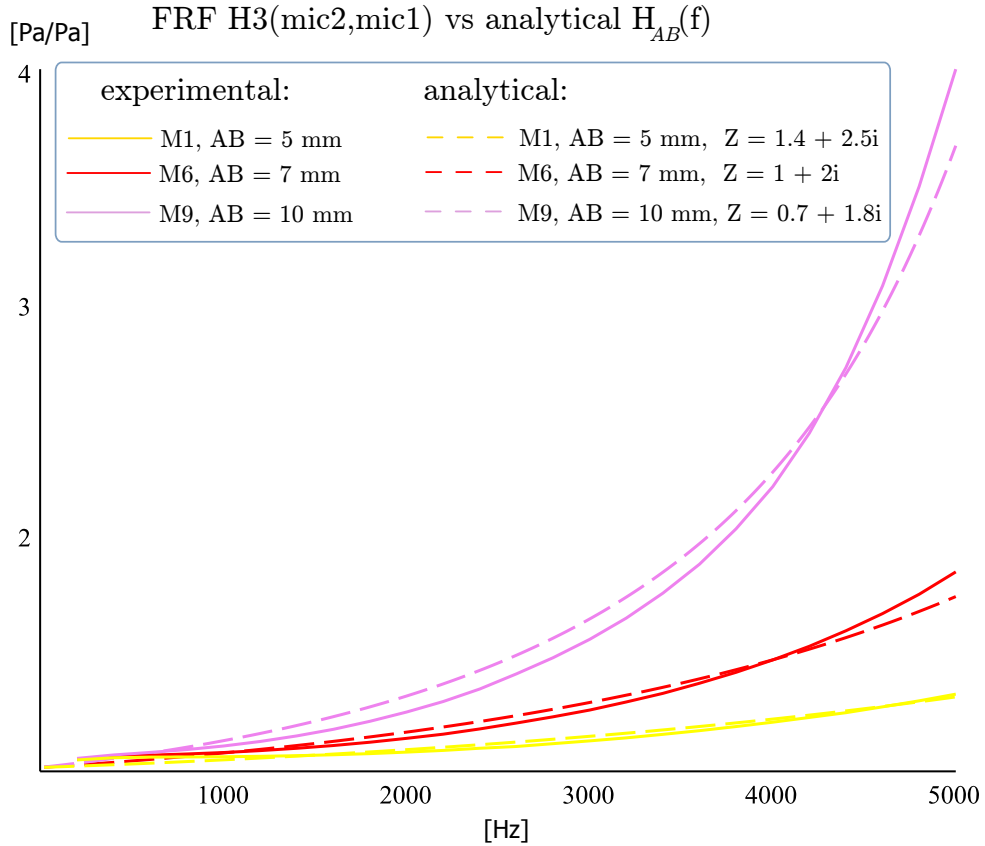


**Figure 3.17:** Comparison plot of the experimental and analytical result of the transfer function with impedance determined used the data from measurements.

with experimental ones. To obtain less deviation between the curves, a curve fitting procedure can be applied to define the impedance as a function of frequency, which can be included into the analytical solution for the transfer function  $H_{tAB}(f)$ .

### 3.4 Summary

In this chapter the solution to the first sub-problem of the project is suggested. Two new designs with several improvements with respect to the robustness and usability of the acoustic excitation set up are introduced and analysed. The investigation of the acoustical properties, mainly with the aim to determine the transfer function between the points of the transducers placement are performed experimentally and analytically. The principle points to be considered for the further application of the devices for the measurements and analytical analysis are summarised:

- The sealing of the acoustic channel is of crucial importance for the resulting FRF, therefore special attention has to be paid to avoiding leakages of sound pressure in the next experiments.
- The general distance/length of the duct does not affect the final result, that is proved analytically and experimentally, hence the method can be used with wave guides, either rigid adaptors or flexible hoses, of different length. The important detail of the acoustic

excitation set up is to keep the distance, sealing and general BCs between the points  $AB$  the same for each measurement session.

- Adaptor m#1 has flexibility in the distance between the transducers that leads to uncertainties and does not improve the accuracy of the final results.

# Vibration analysis of a cantilever structure 4

In this chapter vibration analysis of a cantilever beam is presented. The dynamical properties of the structure are determined both analytically and experimentally by application of the methods introduced in the previous chapters, i.e. the localized acoustic excitation by use of adaptor m#3, and the conventional measurement technique using shaker via stinger excitation of the structure. The analytical vibration analysis of the structure is based on the approach presented in Chapter 2, Section 2.3, i.e. Bernoulli-Euler beam theory and Hamilton's principle. An assessment and comparison of the new and conventional methods are done both experimentally and analytically.

## 4.1 Specimen and cantilever structure setup

In this section, a cantilever beam design and its properties, along with construction and features of the experimental set-up are introduced.

With the purpose to conduct measurements on a cantilever structure a thin slender beam has been designed and manufactured. Standard structural steel *S235* has been used as the material for the beam. The individual number, s6, has been assigned to the specimen to ease the data processing. Geometry and dimensions of the specimen is shown in Figure 4.1.

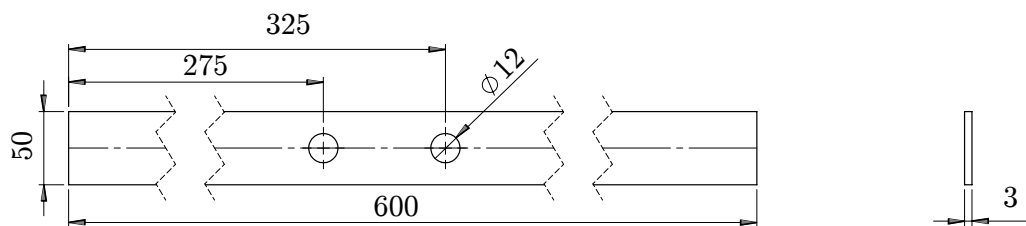


*Figure 4.1: Sketch of the specimen s6.*

The cantilever structure is fixed by four bricks, see picture with details of the experimental set-up in Figure 4.2. The number of bricks allows to position the beam at different distance from the base, i.e. to use the exciter set-up of different heights. The bricks are tightened to the base plate by two M12×1.75 studs (a double-arming bolts) of 350 mm in length, which in turn is fastened to the concrete block by four bolts. To isolate the mechanical system from the influence of outer sources a connection of the concrete block to the floor is made through four air springs.

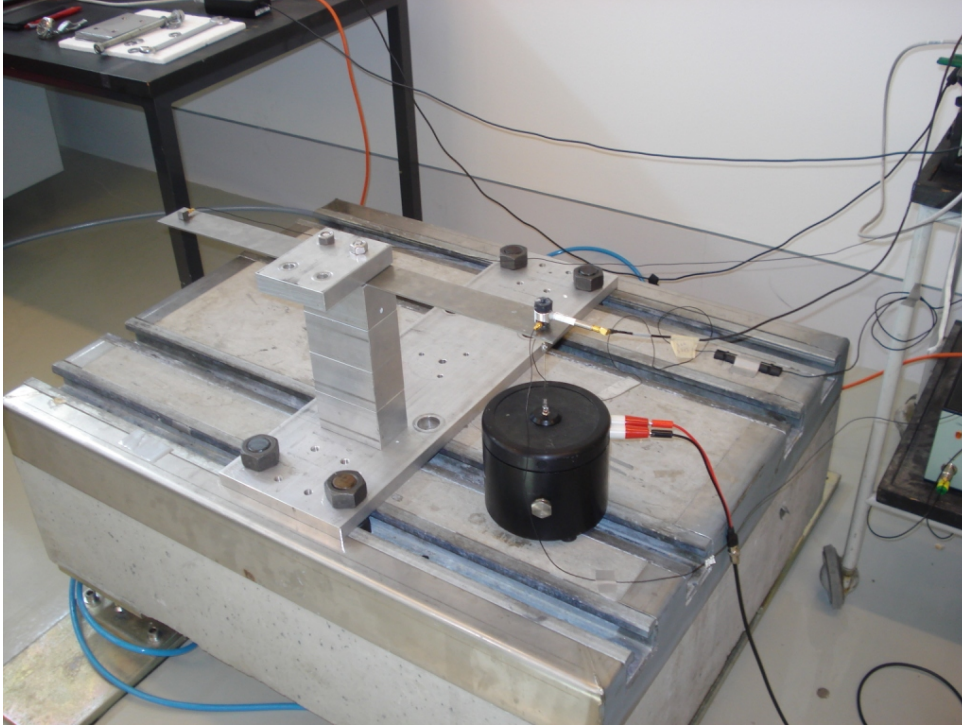


*Figure 4.2: Example of the experimental set-up with construction of a cantilever beam fixture.*

To guaranty the same BCs at the clamped end for each measurement session, an experimental study on the clamping condition has been done. A moment of 75 N/m is found to be sufficient to have the stiffest possible clamping. The M12×1.75 fixture studs are tightened each time with the defined moment by a torque spanner.

### Determination of the material properties for specimen s6

Recall Equations (2.45) and (2.42):

$$1 + \cos(kL) \cdot \cosh(kL) = 0$$

where

$$k = \sqrt[4]{\frac{\rho \cdot A \cdot \omega^2}{E \cdot I}}$$

from which is seen, that the material properties, density,  $\rho$ , and elastic modulus,  $E$ , have to be defined.

For the material of beam s6, which is steel S235, the properties are:

- $E$  in the range from 190 to 210 GPa,
- $\rho$  in the range from 7700 to 8030 kg/m<sup>3</sup>,

according to [steels, 2011].

The wide range of the density and the elastic modulus values leads to large tolerances of the analytically determined natural frequencies. To avoid these kinds of uncertainties the approximate values of density and elastic modulus have been evaluated for the specimen s6. The density of the material is determined using measured mass and calculated volume of the

specimen. Young's Modulus is determined indirectly using the data from measurements. Calculating the volume of specimen s6 and determining the weight of the specimen the approximate value for the density is found to be:

$$\rho = \frac{M_s}{V_s} = \frac{688.3 \cdot 10^{-3} [kg]}{89.321 \cdot 10^{-6} [m^3]} \approx 7706 \left[ \frac{kg}{m^3} \right] \quad (4.1)$$

To have an idea of the magnitudes of natural frequencies within the frequency range, which is considered to be from 0 to 3.5 kHz, and Young's Modulus limits, free vibration analysis using the Equation (2.45) was performed, see Maple document in Appendix D.

The values for the six first natural frequencies are listed in Table 4.1.

Frequency #, [Hz]	$f_1$	$f_2$	$f_3$	$f_4$	$f_5$	$f_6$
for $E = 190$ Gpa	38.5	241	676	1324	2189	3269
for $E = 210$ Gpa	40.5	254	710	1392	2301	3437

**Table 4.1:** First six natural frequencies for specimen s6.

Note, that the deviation of the natural frequencies depending on the elastic modulus of the material is approximately 5%.

To find the value of Young's Modulus closer to the actual one the data from measurements of the auto spectrum from the accelerometer attached to the symmetric part of the cantilever beam is used. The symmetric part of the cantilever beam with attached accelerometer is shown in the sketch of the experimental set-up for the test with shaker via stinger excitation, see Figures 4.2 and 4.13.

The auto spectrum of signal *acc2* from measurements M14 is shown in Figure 4.3. The peaks

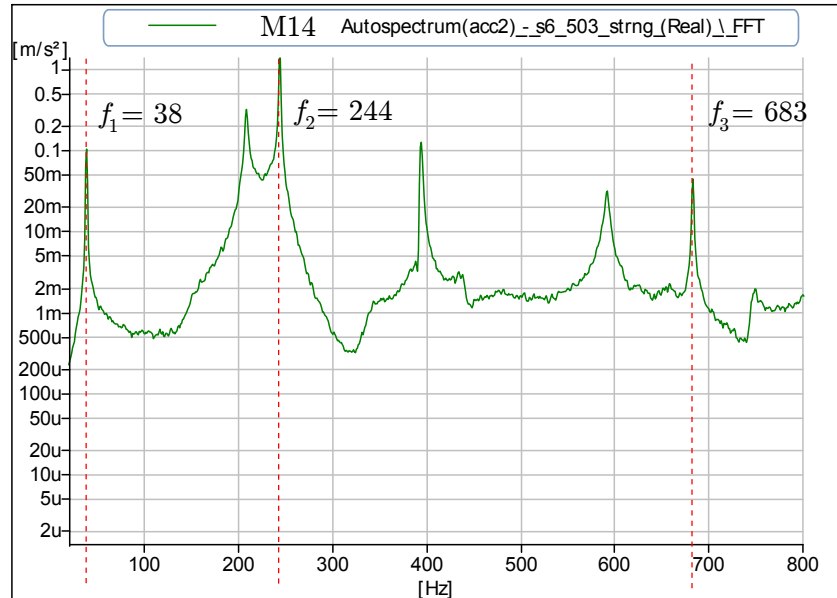


**Figure 4.3:** Auto spectrum of the *acc2* from the 'shaker via stinger' experiment.

of the curve which correspond to the natural frequencies of the bending modes of the beam are marked by the dash lines. The discussion on the nature of the peak frequencies other than represented bending modes is given in the end of the section.

From the experimental data, the value for the first natural frequency,  $f_1 = 38$  Hz, is determined.

This is close to the value of the natural frequencies with Young's Modulus  $E = 190$  GPa. Including the additional mass of the accelerometer attached to the cantilever beam by using the approach described in Section 2.3, a more exact value of Young's Modulus is determined.

The mass of the accelerometer used for the measurement of the vibration at the symmetric part of the beam is determined to be 0.005 kg. Using the approach presented in Section 2.3 with lowest value of  $E = 190$  GPa, the first natural frequency is determined (graphically in the range of frequencies from 35 to 45 Hz) to be  $f_1 = 37.5$  Hz, that deviates from the measured frequency by 1.3%.

By iteratively increasing the value of Young's Modulus by 5 GPa, the first frequency is found to be  $f_1 = 38.04$  Hz, the deviation from the measured frequency is 0.1%.

For further calculations the properties of beam s6 are considered to be as following,  $\rho = 7706$  kg/m<sup>3</sup> and  $E = 195$  GPa.

A comparison plot of the compliance of beam s6 with added mass of 0.005 kg for  $E = 190$  GPa,  $E = 195$  GPa and  $E = 210$  GPa along with the frequencies obtained from measurements (vertical lines) are shown in Figure 4.4.

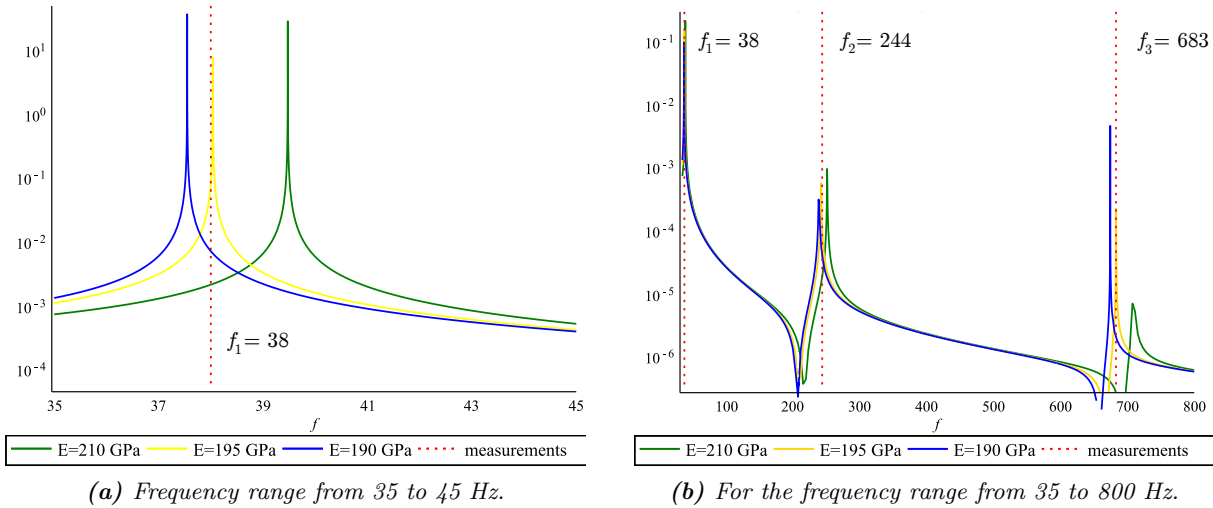


Figure 4.4: Comparison plot for the different  $E$ .

### Discussion on the peak frequency from the *acc2* auto spectrum

Considering the peaks from the curve M14 (auto spectrum from *acc2*), see plot in Figure 4.3, which indicate other types of bending modes of the beam, three frequencies are observed. They are at  $f_{AS1} = 208$  Hz,  $f_{AS2} = 394$  Hz, and  $f_{AS3} = 592$  Hz.

By conducting numerical simulation of the modal analysis for the specimen s6, frequency  $f_{AS2} = 394$  Hz was determined to be the one of first torsional modes. It is noticed that the peak sharpness of this frequency is similar to the sharpness of the peaks for bending modes. This indicates a similar level of damping for these frequencies.

Considering peaks at  $f_{AS1} = 208$  Hz and  $f_{AS3} = 592$  Hz less sharpness is observed, that indicates a different nature of damping is present.

Furthermore, comparing the plots of the compliance of beam s6 with the included mass of the accelerometer, see Figure 4.4b, and the auto spectrum of *acc2*, Figure 4.3, a coincidence can be noticed between the frequency of the first anti-resonant point in the analytical solution and the second peak frequency for the auto spectrum,  $f_{AS2} = 208$  Hz. The displacement of the

beam as a function of  $x$  for this frequency is shown at Figure 4.5. From the plot it is seen that

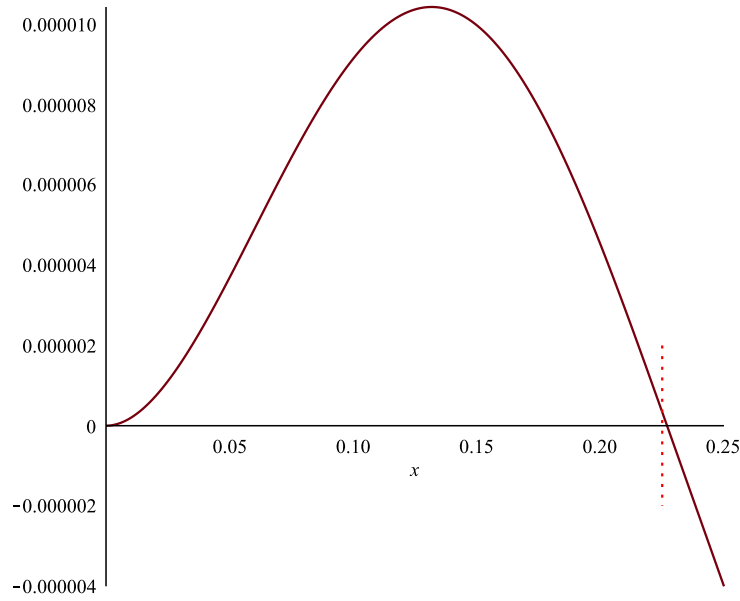


**Figure 4.5:** Displacement vs  $x$  for the frequency  $f=208$  Hz

the transducer is placed almost at the nodal point, hence the corresponding peak at the auto spectrum plot cannot show the resonance frequency of bending mode.

Analysing other possible sources that might produce the peaks in the auto spectrum consider the sketch of the experimental set-up with shaker via stinger excitation, see Figure 4.6. The

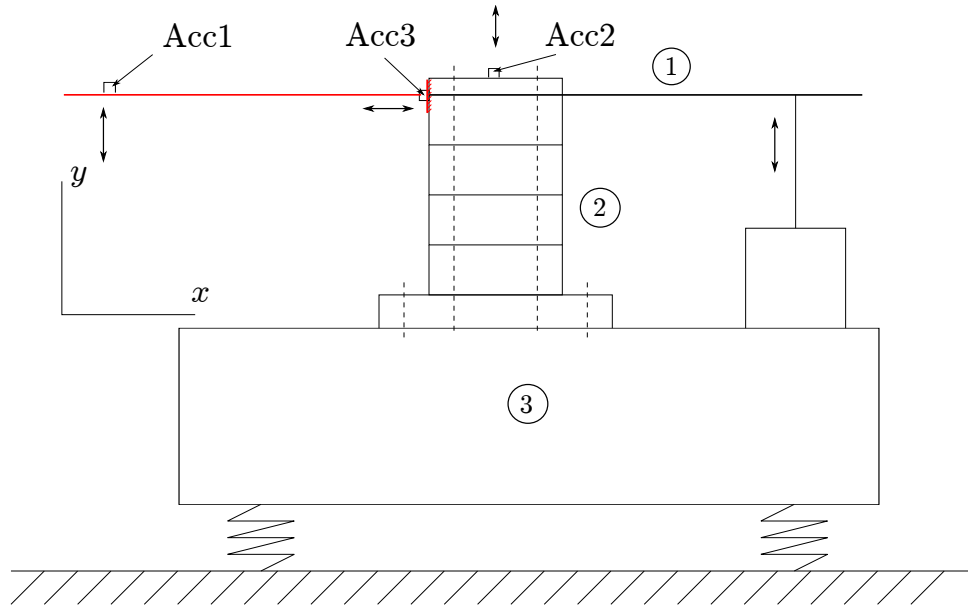


**Figure 4.6:** Sketch of the experimental set-up with indication of possible vibrating parts.

concrete block 3 being a massive part is not considered for this case, but the fixture 2 can be the source of additional vibrations. To verify this assumption a test with use of two extra accelerometers for measuring the response of the fixture can be conducted. Alternatively, either analytical or numerical vibration analysis of the fixture can be performed, but these tasks are out of the scope of the project.

### 4.2 Acoustic excitation experiment

To determine dynamic characteristics of a cantilever structure experimentally using localized acoustic excitation of the structure, several measurement sessions were conducted on beam s6 by use of adaptor m#3.

A sketch of the experimental set-up is shown in Figure 4.7.

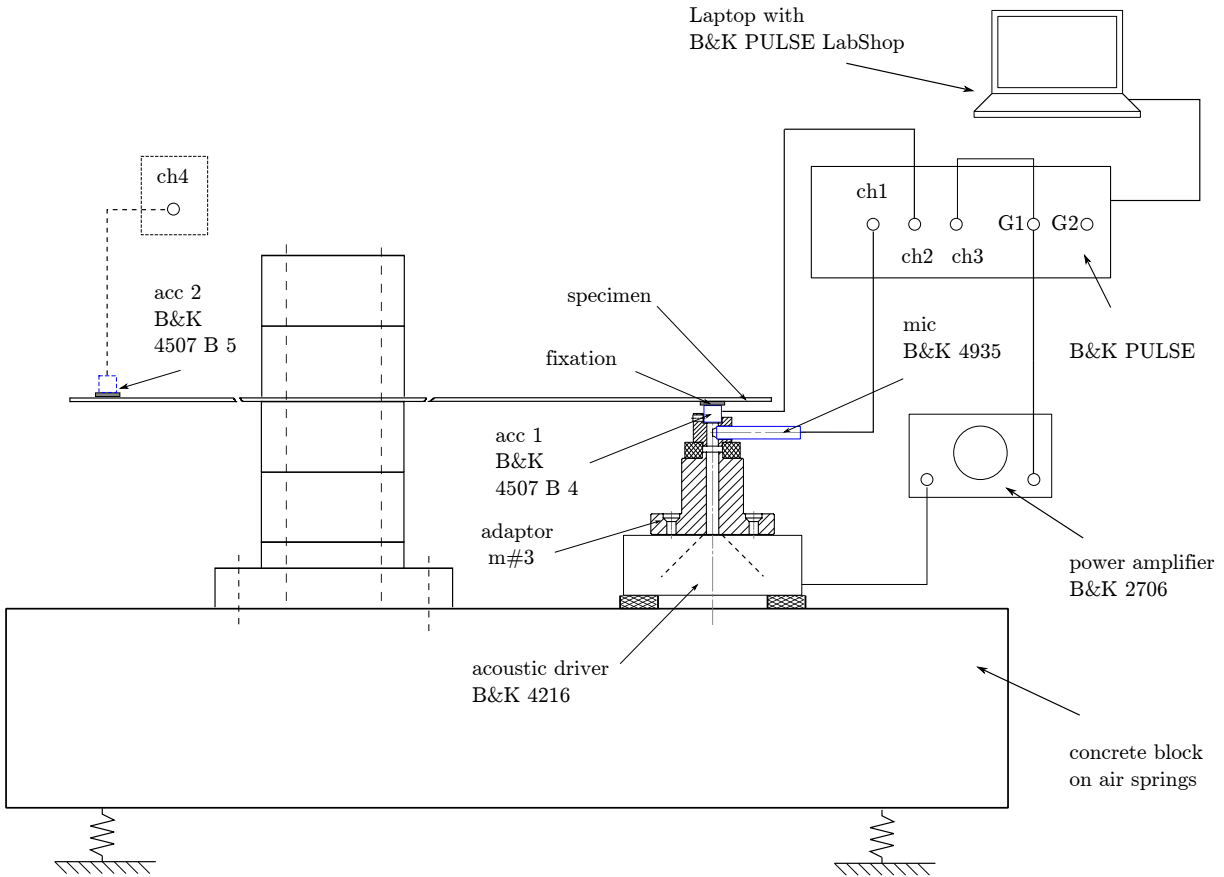


Figure 4.7: Sketch of the experimental set-up to the test with localized acoustic excitation of the structure.

A list of apparatus used in the measurements is given in Table 4.2.

Device	Type	Serial number
Vibration analyzer	Bruel&Kjaer 3560-C (3109+7536)	2277049
Acoustic driver 'Artificial Mouth'	Bruel&Kjaer 4216	146181
Power amplifier	Bruel&Kjaer 2706	2120369
Array microphone (1)	Bruel&Kjaer 4935	2079317
Accelerometer (acc1)	Bruel&Kjaer 4507 B 4	2154316
Accelerometer (acc2)	Bruel&Kjaer 4507 B 5	2154481
Laptop with B&K PULSE SW	LabShop v.16.1.0.84	

Table 4.2: Apparatus and devices used in measurements of the point mobility by the acoustic excitation method.

To be able to obtain comparable results using different approaches the FRF is measured at a specific point of the beam. This point is set to be at 25 mm from the free end. The position of the device used in the test (the top part of adaptor m#3, including the accelerometer and microphone) is installed so that the centreline of the adaptor passes through the point mentioned above, see Figure 4.8.

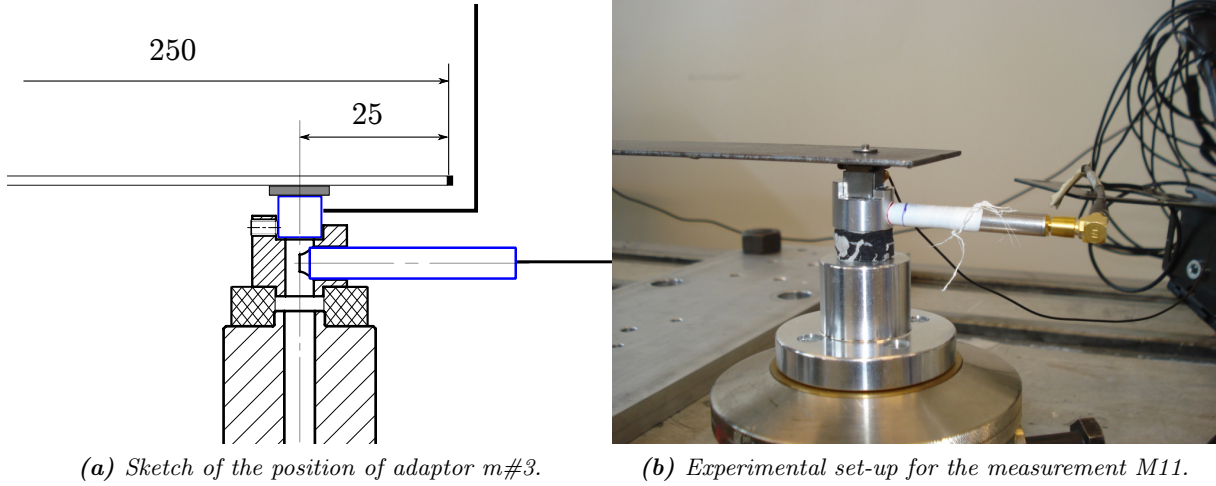


**Figure 4.8:** Location of the transducers, acoustic excitation set-up.

### Choice of the effective frequency range

As a rule, the choice of the frequency range for the test depends on the frequency range of interest for the given problem, and the limitations of the apparatus used in the measurement chain. For the case of the cantilever beam  $s_6$  by the prior analytical estimation, see section 4.1, e.g. Table 4.1, the first six natural frequency of a beam  $s_6$  is found to be in a range from 30 Hz to 3.5 kHz. The upper frequency limit is not exceed the limitations of the devices used, except the mounting clip UA 1407. The limitations of apparatus are listed in Table C.1, Appendix C. Based on the analysis requirements and limitations of the apparatus used in the measurements the upper frequency limit for the FFT analyser and signal generator is set to 3.2 kHz. As in the prior measurements conducted on the acoustic excitation set up, Section 3.2, random type excitation, which is fast and accurate is used. The settings of the FFT analyser are listed in Table 4.3.

Parameter	Value
Number of lines	3200
Frequency span	3.2 kHz
Number of averages	100
Time	34 s
Overlap	66.67%

**Table 4.3:** Settings of the FFT analyser.

There are several methods to attach the transducers to the specimen. The basic ones are described in [Mark Serridge, 1987, section 4.4, pp. 88 - 105]. Besides this accelerometers B&K of Type 4507 B have an option to be mounted on the special fixations, see specification [Brüel&Kjær, 2012a].

In the presented measurement sessions for transducers mounting two principally different methods were used. The first one is mounting through the plastic clip B&K UA 1407 with use of the grease smearing of the contact surfaces. The upper frequency limit for such kind of connection is 3 kHz, see Table C.1, Appendix C. This session is denoted as M10.

Second method is mounting on a thin layer of bee's wax, the measurement is denoted as M11 and M12. This method gives good bonding between the transducer and the specimen. According to [Mark Serridge, 1987, p.90, Fig.4.7 ] the upper frequency limit for such a connection is up to 6 kHz. The disadvantage of the bee's wax connection in contrast to the plastic mounting clip is that the method cannot guaranty exactly the same placement of the transducer from measurement to measurement.

The FRF for the measurements sessions M10 (mounting clip fixation) and M11 (bee's wax fixation) on beam s6 is shown in Figure 4.9. From the plot it is seen that the mounting clip

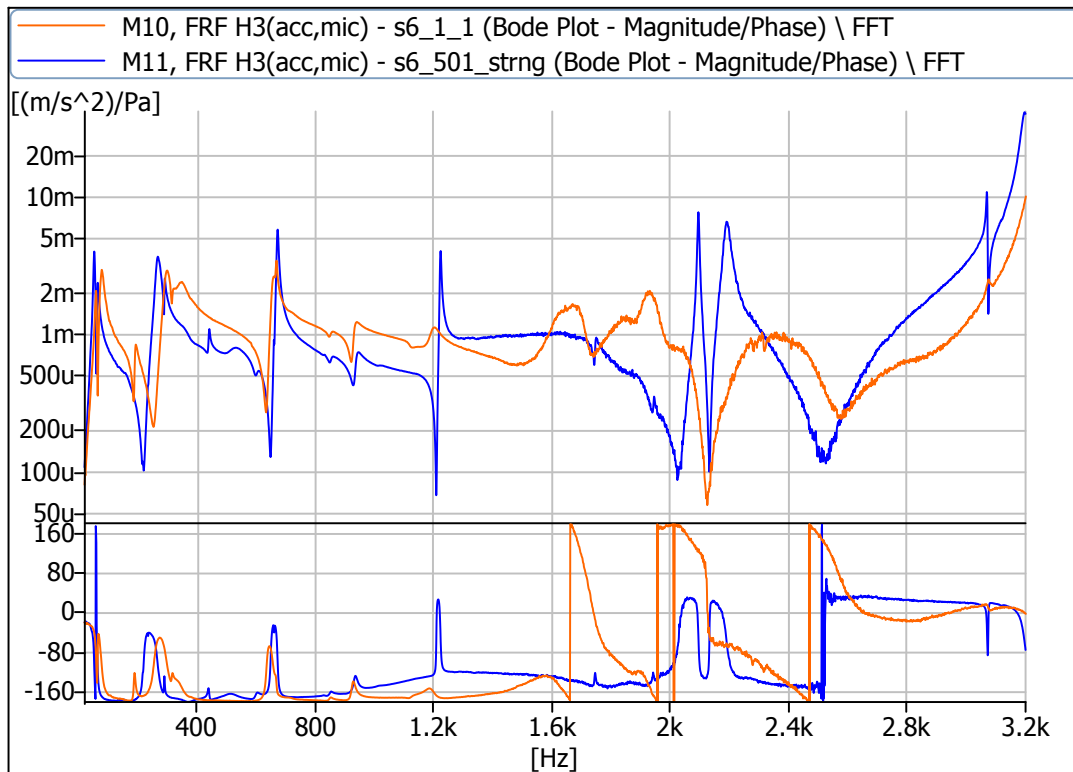
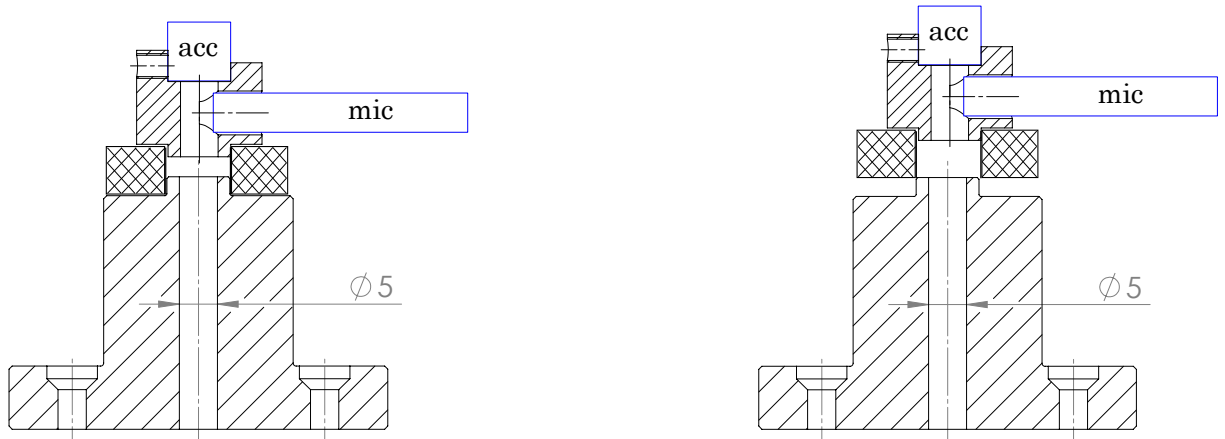


*Figure 4.9: Comparison plot for the clip vs wax fixation*

works good for the frequency range up to 1.5 kHz, which corresponds to the upper frequency limit for the plastic clip B&K UA 1407 with dry connection. For the frequencies higher then 1.5 kHz the resonance peaks are absent. Thus, for the further tests the mounting by the bee's wax is considered as the best available method.

Considering the BCs of the cantilever beam the condition of the absolutely free end is violated, as the adaptor m#3 has connection through the rubber connection ring that might influence the FRF of the system. To check the influence of the connection two measurement sessions with different method to connect the bottom part of the adaptor to the connection ring were applied. The methods of connection are shown in Figure 4.10. They are called as the 'full' and 'touch' connections with corresponding measurement sessions M11 and M12. The results of the sessions M11 and M12 are represented on Figure 4.11.



(a) Assembly variation for measurement session M11 ('full connection').

(b) Assembly variation for measurement session M12 ('touch connection').

**Figure 4.10:** Experimental set up of the connection type for measurements sessions M11 and M12.

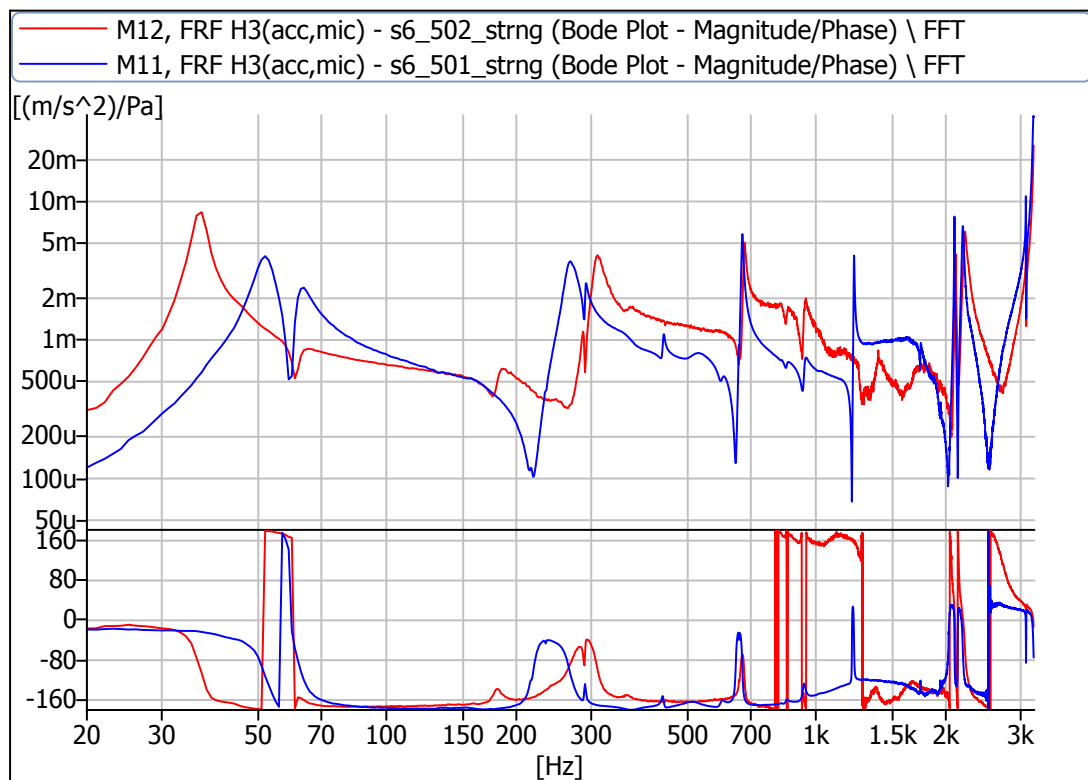


**Figure 4.11:** Comparison plot for the cases of M11 and M12

From the results obtained an influence of the type of connection of the top part of the adaptor to the bottom part of the set-up is noticed. Large deviation for the first natural frequency can be explained by the introducing of additional stiffness (stiffness of the connection ring) to the free end of the beam, that leads to increase in the value of natural frequency. Good agreement in the peaks is observed for the third natural frequency. The general appearance of the curves has minor deviation both in the amplitudes and in slope due to the difference of the BC of the free end, which is introduced by the rubber ring connection.

### 4.3 Analytical vibration analysis.

Analytical solution to the model of the cantilever beam used in the experiments are done using the theory discussed in Chapter 2, Section 2.3.

To determine the compliance of the beam s6 analytically and to see the influences of additional mass of the top part of adaptor  $m\#3$  and moment of inertia of the microphone, three different cases are considered. They are (i) forced vibration analysis of a pure cantilever beam; (ii) analysis of a cantilever beam with added mass; and (iii) consideration of the addition mass and the moment of inertia.

For the pure cantilever beam the analysis is performed by solving the system of Equations (2.47) and (2.48) and determining the Equations (2.46) for the displacement of the point of the excitation,  $x = L_p = 225$  mm.

For the cases accounted for the additional mass and the moment of inertia Equations (2.50) are used, which include the contribution of the mass and the moment of inertia.

The addition mass of the complete top part of adaptor  $m\#3$  includes the masses of accelerometer, microphone, connection ring and the housing, and is measured to be:

$$M_{add} = 0.0295 [kg] \quad (4.2)$$

The moment of inertia of the microphone is calculated to be:

$$J_{mic} = \frac{1}{3} M_{mic} \cdot L_{mic}^2 = \frac{1}{3} \cdot 0.01 \cdot 0.035^2 = 4.08 \cdot 10^{-6} [kg \cdot m^2] \quad (4.3)$$

where  $M_{mic} = 0.01 kg$  is the mass of microphone B&K type 4935, see Table C, and  $L_{mic} = 0.035 m$  is the distance from the center of mass of the microphone to the vertical axis of the adaptor  $m\#3$  top part.

The comparison plot including three cases is shown in Figure 4.12. From the plot it can be

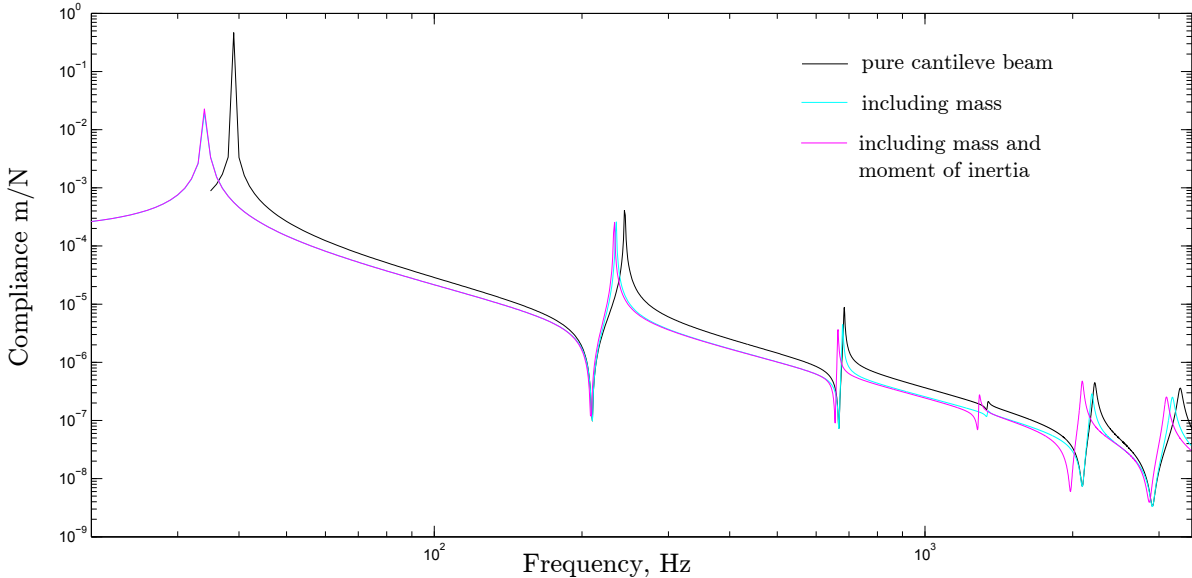


**Figure 4.12:** Comparison plot for the analytical vibration analysis of cantilever beam s6.

noticed that in general the addition inertia influences the compliance of the system and it has to be taken into account to obtain more accurate results. The large deviation (14.7 %) is observed between the 'pure cantilever beam' (39 Hz) and the rest two curves (34 Hz) for the first natural frequency. For next two frequencies deviation decreases gradually. But if at the first frequency

the curves for the mass and moment are identical, then with increasing frequency the difference between the curves increases. And the influence of the moment of inertia of the microphone becomes noticeable.

Thus, for the comparison to the measurement results, the analytical solution, which accounts for additional inertia of the device, is used.

#### 4.4 'Shaker via stinger' experiment

In the following the dynamic properties of a cantilever structure are determined experimentally by the conventional method, i.e. well known 'shaker via stinger' excitation of a structure.

The principle scheme including the sketch of the experimental set-up for the test with 'shaker-stinger' excitation is represented in Figure 4.13.

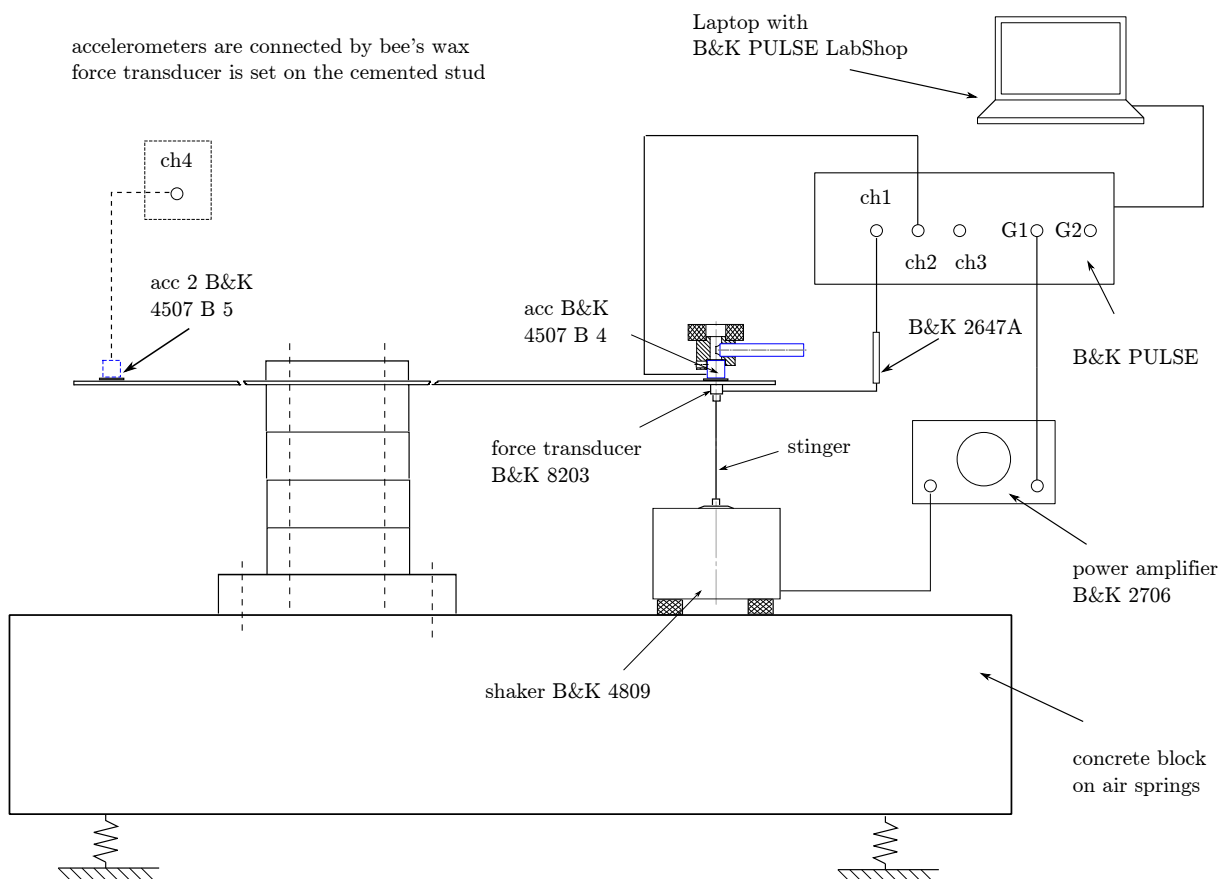


**Figure 4.13:** Experimental set-up for the 'shaker-stinger' experiment.

In this method a force transducer is used to measure the force applied. The transducer can be fixed to a structure in several different ways. For the present test the connection through the cement stud, which is glued to the structure with epoxy glue, is applied. To have the system with a dynamic properties like in the acoustic excitation test, the same additional mass and moment of inertia are introduced by attaching the complete top part of adaptor m#3, including the connection ring and the microphone, see Figure 4.13.

The transducers placement is kept the same as in the acoustic excitation test, i.e. 25 mm from the free end, see Figure 4.14. For this case a misalignment of the transducers can affect the accuracy of the FRF of a system.

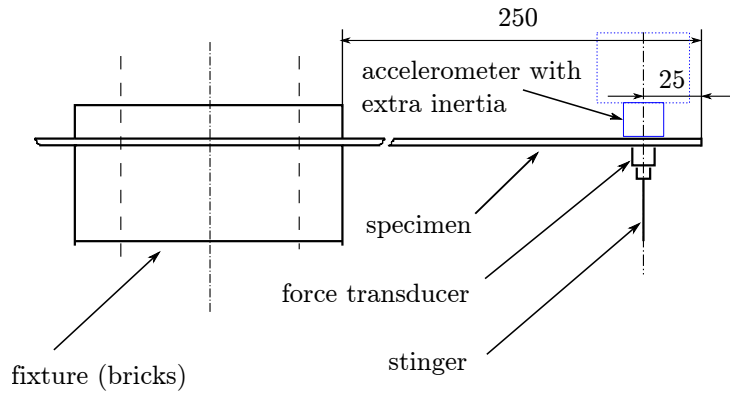


**Figure 4.14:** Position of the transducers in the 'shaker-stinger' experiment.

The details of the shaker via stinger connection of the experimental set-up is shown in Figure 4.15.

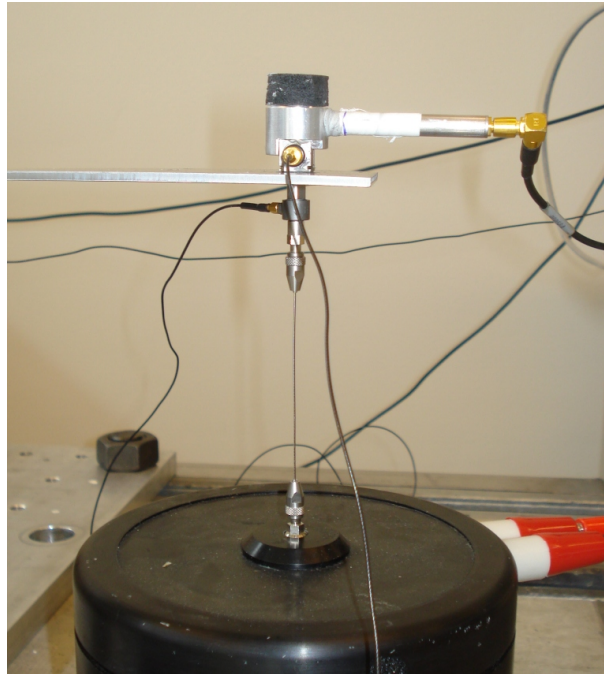


**Figure 4.15:** Detail view of the shaker via a stinger connection.

The apparatus used in the experiment are listed in Table 4.4.

Device	Type	Serial number
Vibration analyzer	Bruel&Kjaer 3560-C (3109+7536)	2277049
Vibration exciter	Bruel&Kjaer 4809	1583461
Power amplifier	Bruel&Kjaer 2706	2120369
Force transducer	Bruel&Kjaer 8203	1887706
Charge to DeltaTron converter	Bruel&Kjaer 2647A	2207158
Accelerometer (acc1)	Bruel&Kjaer 4507 B 4	2154316
Accelerometer (acc2)	Bruel&Kjaer 4507 B	2154481
Laptop with B&K PULSE SW	LabShop v.16.1.0.84	

**Table 4.4:** Apparatus and devices used in measurements of the point mobility by the 'shaker via stinger' method.

The excitation frequency range and the settings of the FFT-analyser are identical to those in the acoustic excitation experiment, i.e. 3.2 kHz for generator, see Table 4.5.

Parameter	Value
Number of lines	3200
Frequency span	3.2 kHz
Number of averages	100
Time	34 s
Overlap	66.67%

**Table 4.5:** Settings of the FFT analyser.

Two measurement sessions were done with different levels of the signal amplification, that is denoted by M13 for weak and M14 for strong amplifications of the excitation signal. The plot with the FRF of the two cases is shown in Figure 4.16. Comparing the results an agreement

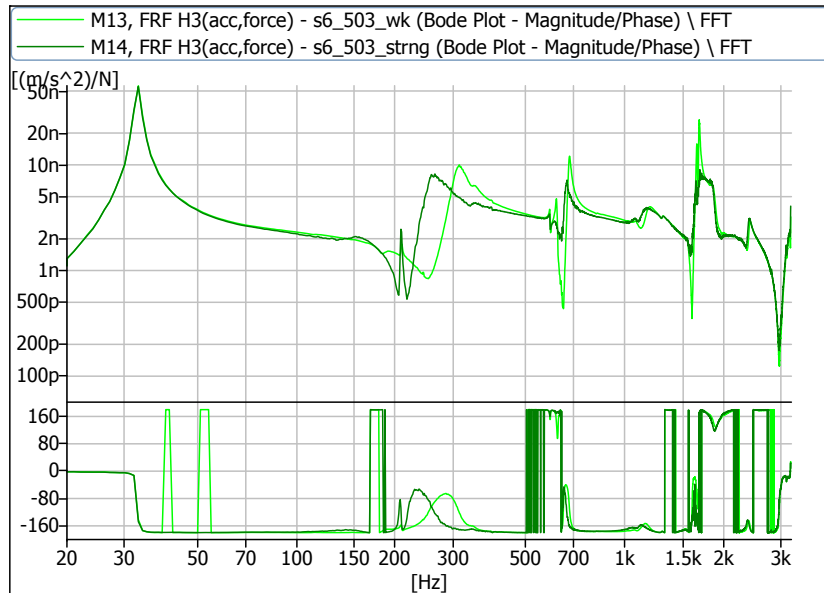


**Figure 4.16:** Comparison plot for the 'shaker via stinger' experiment for the weak and strong amplification of the signal.

in curves at the frequency range from 20 to 150 Hz is observed and the peak frequency, which corresponds to the first natural frequency is clearly seen. When increasing the frequency value, a slight disagreement in peak amplitudes can be noticed particularly for the frequencies  $f_3$  and  $f_5$ . For the second natural frequency region a disagreement both in the peaks and in the slopes of the curves can be seen. Such dissimilar behaviour of the curves can be explained by studying the specifics of the shaker via a stinger connection, where the requirement for a stinger is always to work in tension when exciting the structure. It is very thin and not a stiff part of the excitation set-up, and it is not capable to excite the structure in compression. In case of the strong excitation signal the stinger can turn from the tension state to compression state and at this time the structure can experience a kind of release from the pre-stressed condition, which leads to some kind of a shock excitation. In such a case the motion is registered by the accelerometer but the force applied is not. This gives the bad coherence between the signals. Checking the coherence function for the two cases, see Figure 4.17, the better coherence for the measurement session with a weaker amplification signal is seen. The bad coherence for the stronger excitation

signal for the measurements M14 is probably due to not sufficient pre-stress condition of the beam.

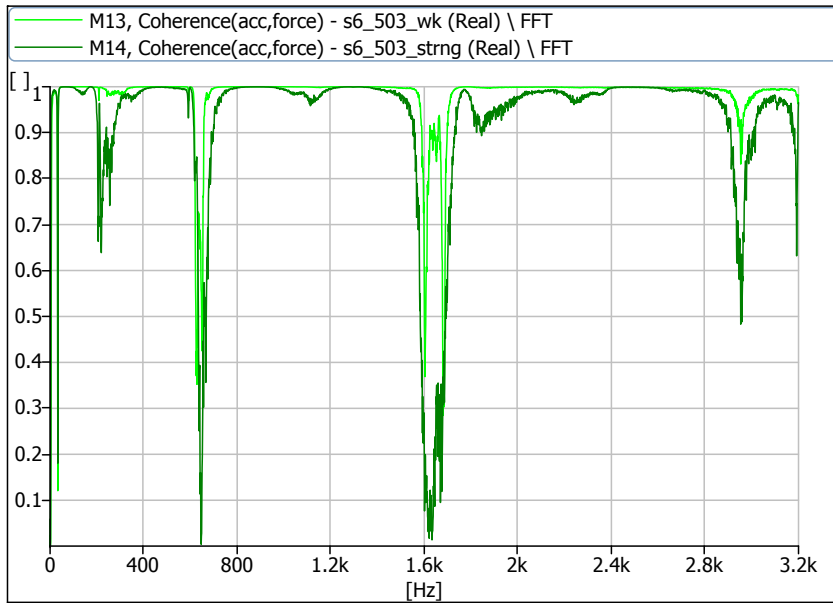


*Figure 4.17: Coherence function from the M13 and M14.*

Finally, the results of measurements M13 are concluded to be more accurate and is to be used for the comparison with the one from the acoustic excitation method and the analytical ones.

## 4.5 Comparison of the results

The results obtained by the different approaches are represented in a form of a comparison plot, see Figure 4.19. Here all the results are represented in the form of compliance with units of  $m/N$ . The compliance was obtained from the measured accelerance data by the applying the 'j $\omega$ ' weighting approach (using the B&K PULSE notation  $j$  is denoted for the imaginary unit, and  $\omega$  is the angular frequency).

To convert pressure value into force the simple definition of pressure is used:

$$P = \frac{Q}{A} \quad (4.4)$$

where  $P$  is sound pressure measured by the microphone, and  $A$  is the effective area where the sound pressure acts. For the case of adaptor m#3 effective area is calculated as the surface of the accelerometer plus the bottom surface of the top part of the adaptor, see Figure 4.18.

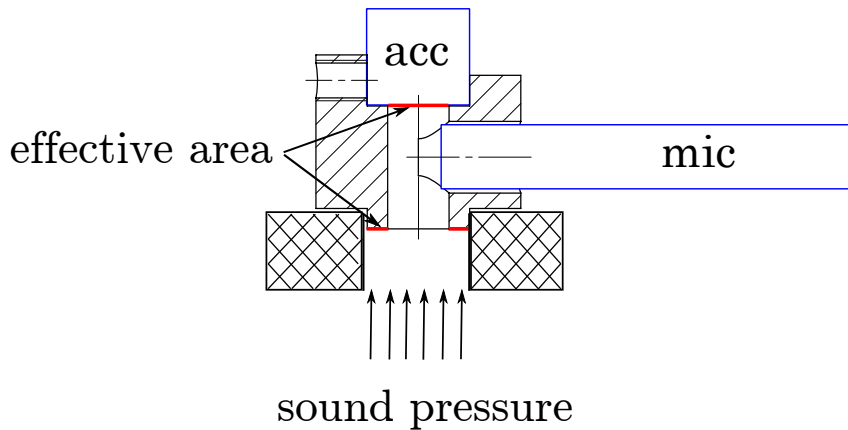


**Figure 4.18:** Sketch of the effective area where sound pressure acts.

Analysing the comparison plot, Figure 4.19, a general agreement in the slope and amplitude for all curves can be noticed. For the first natural frequency the experimental curve M13 ('shaker via stinger' measurement session) has the best fit to the analytical solution, whereas the largest deviation can be observed for the acoustic excitation 'full connection' curve, M11. Such large

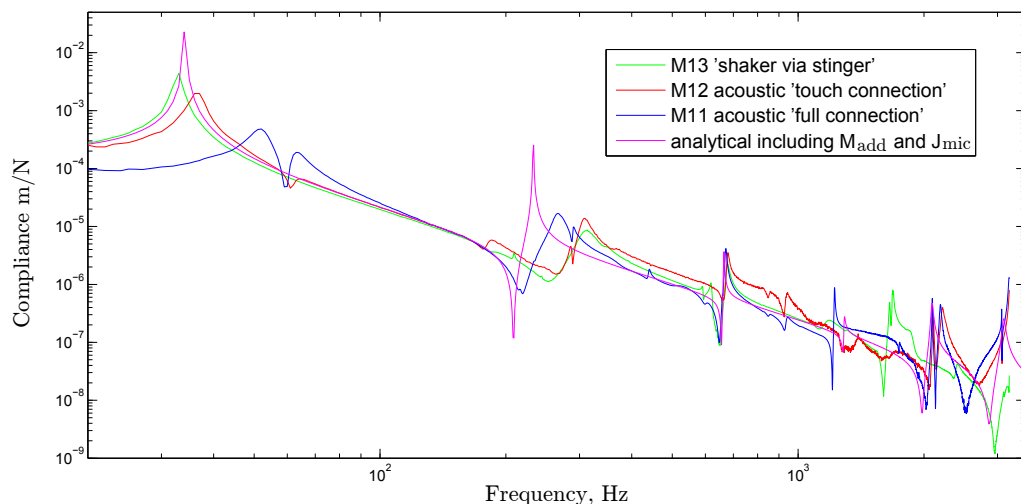


**Figure 4.19:** Comparison plot for the both measurements methods and analytical estimation.

deviation can take place due to the added stiffness from the experimental set-up connection to the free end of the cantilever beam. The obtuse form of first natural frequency peak is evidence of the definite amount of damping presented in the acoustic excitation set-up.

The best agreement is observed for the natural frequency  $f_3 = 665$  Hz, the value is taken from the analytical case. The deviation of results measured from the analytical solution limits to 1% in comparison to measurement M11 (acoustic 'full connection'), and 2.3% comparing to measurement M12 (acoustic 'touch connection') for the frequency value, at the same time the amplitudes of the frequency  $f_3$  are very close in magnitudes.

For natural frequency  $f_5 = 2092$  Hz for the analytical solution the peak coincides with acoustic excitation results, but these observations can not be reliable, since the analytical solution for the high frequency range Timoshenko beam theory has to be applied, [Irving H. Shames, 2003, section 7.7, pp. 348 - 349, figures 7.7 and 7.8 ].

## 4.6 Summary

In the chapter the second part of the project are presented. Two measurement methods are applied to a simple structure, i.e. cantilever beam, to determine dynamical characteristics in a form of FRF.

The specimen and the relevant BCs have been modelled analytically with further comparison of the results.

To obtain analytical solution the material properties have been determined with values of density and Young's Modulus close to the real ones. Indirect method of evaluation of the Young's Modulus using the data from a single channel vibration measurements has been applied.

After the experiment was performed and the results compared to analytical solution, the main points to summarise are:

- in general the results obtained by different methods are in agreement
- estimating the robustness, the acoustic excitation set-up is much faster with respect to assembling the parts and attaching the transducers to the structure
- for some of the cases, e.g. for the first natural frequency the 'shaker via stinger' shows better accuracy and agreement with analytical solution in comparison with acoustic excitation method
- for some cases, e.g. for the frequency  $f_3$  all three methods show very good agreement
- the influence of the connection ring properties such as stiffness has to be further investigated, as for the 'touch' connection the results differ in comparison to 'full' connection set-up
- difference in the peaks for the 'touch' and 'full' connection decreases with increasing of frequency range, as was expected due to the convergence of the natural frequencies for the same specimen but with different BCs with increasing the frequency order [Rao, 2005, pp. 613, Figure 8.15 ]
- comparison for the higher order frequencies has to be done with accounting for Timoshenko beam theory for the analytical analysis and frequency limits of the apparatus used in the experiment.

# Vibration analysis of a shell structure 5

---

In the following dynamic characteristics of a complex shell structure is analysed. A housing of a positive displacement compressor, commonly used in refrigerators, is considered as the shell structure. Vibration analysis represented in this chapter includes point mobility measurements with the localized acoustic excitation. Results obtained from measurements are to be compared with ones from the FEM, where harmonic mode superposition analysis is performed on the shell model of the pure housing. Finally, brief summary with conclusion is represented.

## 5.1 Experimental part

To determine FRF at the single point of a shell structure several measurement sessions on the housing provided by Secop GmpH were conducted. The example of experimental set-up is represented in Figure 5.1.



*Figure 5.1:* Picture of experimental set-up; pure housing suspended on four rubber bands and acoustic exciter with adaptor m#3.

The sketch of experimental set-up is shown in Figure 5.2. As it is seen from the sketch the

specimen is fixed through the springs, which are soft rubber bands, to the rigid fixation, which is the ceiling of the room. There are four bands glued to the housing, see Figure 5.1. Positions of the bands fixation and points of excitations are shown in Figure 5.3. The excitation unit, i.e. acoustic driver with adaptor m#3 is placed on the concrete block with air springs connected to the floor. Such configuration has only single energy transmission path between the exciter and the specimen, hence guaranty good accuracy of the results.

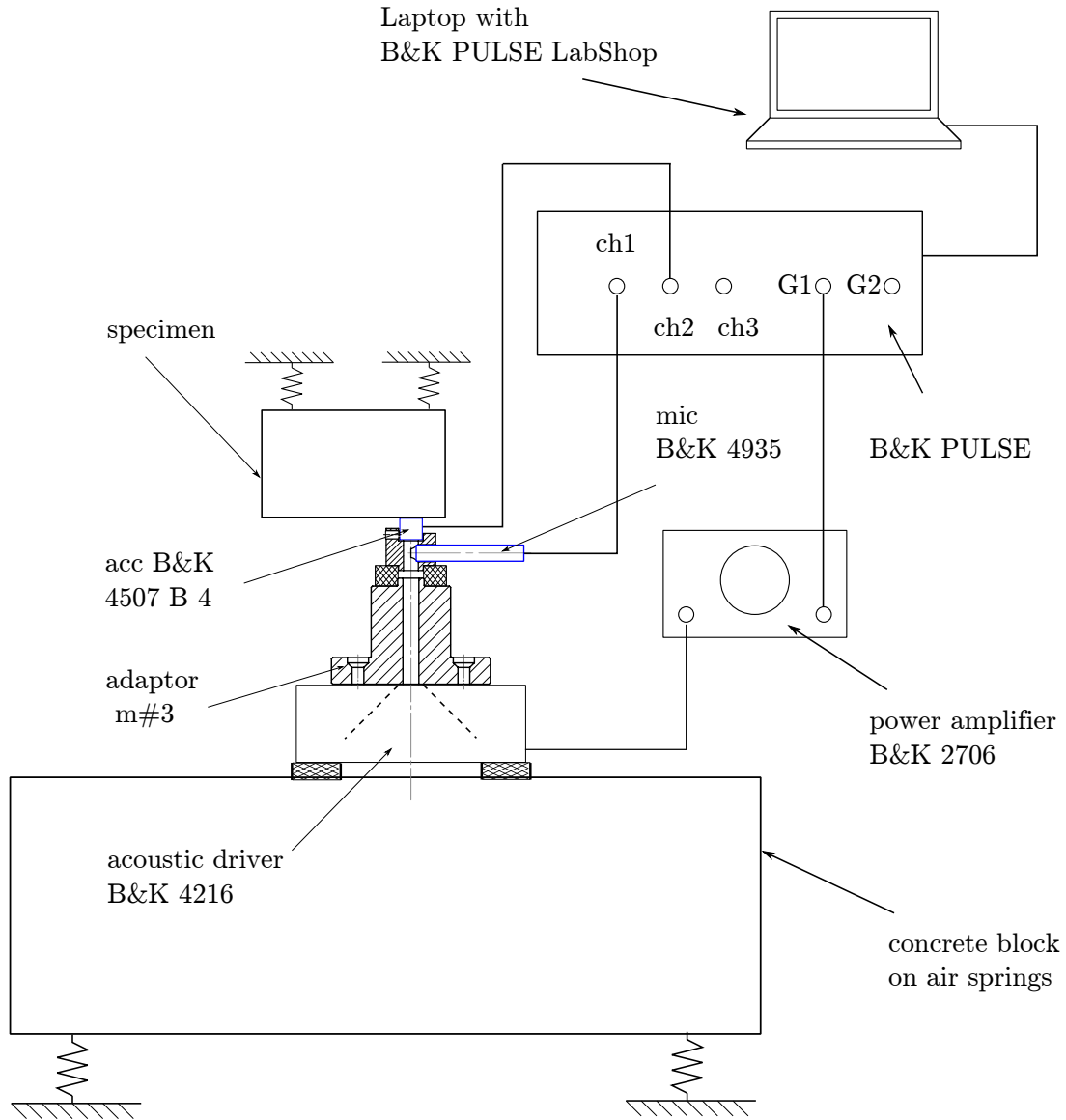


**Figure 5.2:** Sketch of the experimental set-up for the vibration measurements of compressor housing.

The compressor housing is the stiff elastic shell structure with complex geometry, which is manufactured by welding of two parts made of a sheet metal with a thickness of approximately 3 mm. Thickness of the shell is not uniform as it has a welding seam around the body and four spring holder positions inside the housing.

To investigate how FRF depends on the location of the point of application, two positions for measurements are considered, see Figure 5.3.

The points and corresponding measurement sessions are denoted as:

- p1 for the 'corner' position at one of the internal spring holder placement;
- p2 for the 'middle' position at the bottom part of the housing where thin low curved shell structure is placed.

- ✗ placement of the band connection points
- ✕ measurement points for cases p1 and p2

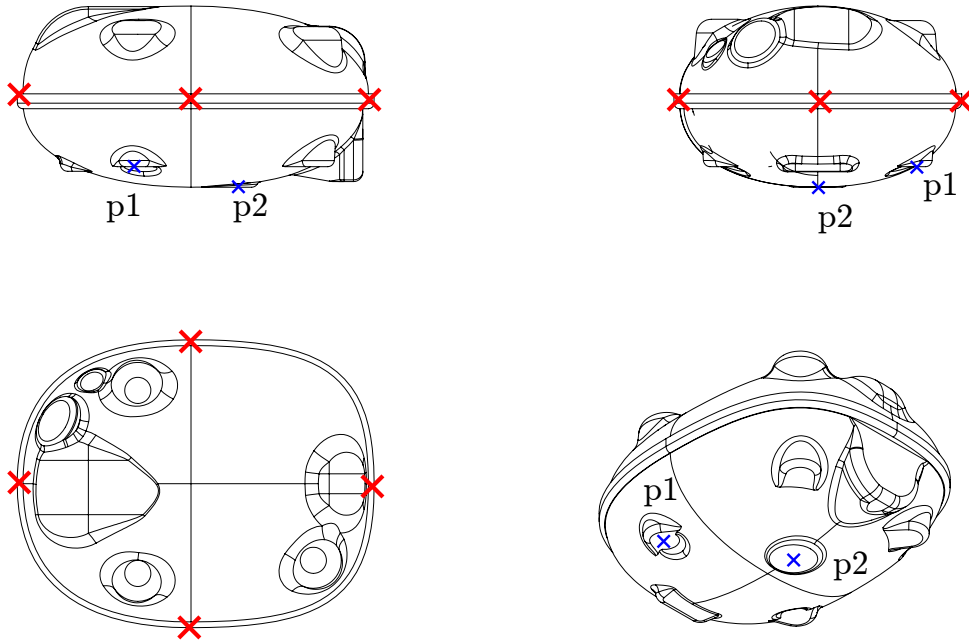


**Figure 5.3:** Sketch of the pure housing with indication of the fixation rubber band points and points of excitation for cases p1 and p2.

Apparatus used in the measurements are listed in Table 5.1.

Device	Type	Serial number
Vibration analyzer	Bruel&Kjaer 3560-C (3109+7536)	2277049
Acoustic driver 'Artificial Mouth'	Bruel&Kjaer 4216	146181
Power amplifier	Bruel&Kjaer 2706	2120369
Array microphone	Bruel&Kjaer 4935	2079317
Accelerometer	Bruel&Kjaer 4507 B 4	2154316
Laptop with B&K PULSE SW	LabShop v.16.1.0.84	

**Table 5.1:** Apparatus and devices used in measurement sessions p1 and p2.

The frequency range relevant for the measurements of the FRF is chosen from the preliminary assessment of the structure characteristics and limitations of the devices used in the measurements. From FEM modal analysis first eight natural frequencies (excluding the rigid body motion modes) are found to be in a range from 3 kHz to 5 kHz. The upper frequency range of the devices is limited by the properties of array microphone B&K Type 4935, which is of 5 kHz following to the guaranteed specification, see Table C.1 in Appendix C. This leads to

the choice of the upper frequency limit both for the excitation signal and for the FFT analyser settings to be 6.4 kHz, see Table 5.2. The method of excitation is set to be a random noise, due to robustness and accuracy, which are proved by the prior measurements conducted on beam s6.

Parameter	Value
Number of lines	6400
Frequency span	6.4 kHz
Number of averages	100
Time	34 s
Overlap	66.67%

**Table 5.2:** Settings of FFT analyser for p1 and p2 measurements.

To attach the transducer to the specimen bee's wax fixation is used as the best available one. Two different placement p1, and p2 of the device connection are shown in Figure 5.4.



(a) Details of the connection for measurement session p1 ('corner').



(b) Experimental set-up for the session p2.

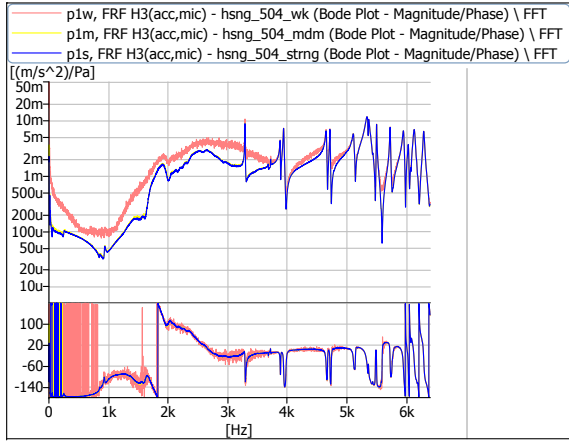
**Figure 5.4:** Details of the assemblies of the sessions p1 and p2.

### Verification of linearity and assessment of background noise influence

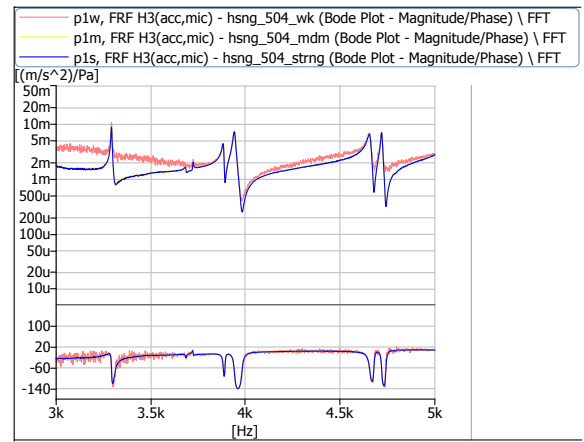
As it is discussed in Chapter 2, Section 2.1, for the linear system resulting FRF does not depend on the type of excitation and level of the signal amplification. To verify if the compressor housing has linear dynamical properties several measurement sessions of the case p1 with different level of the excitation signal amplification were conducted. The sessions are denoted as follows:

1. 'p1w', for the weak signal amplification;
2. 'p1m', for the medium amplification;
3. 'p1s', for the strong signal.

The results for three cases are shown in a form of FRF H3, Bode plot in Figure 5.5. For the entire frequency span, see Figure 5.5a, and for the relevant frequency range, see Figure 5.5b.



(a) FRF for the cases *p1w*, *p1m* and *p1s* for the entire frequency range.

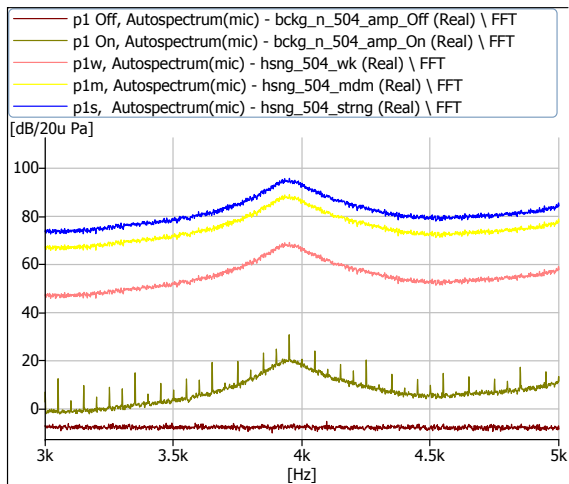


(b) FRF for the cases *p1w*, *p1m* and *p1s* for relevant frequency range.

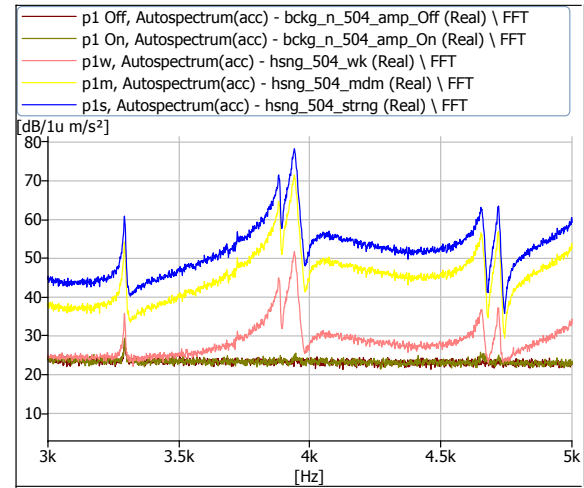
**Figure 5.5:** FRF for the cas *p1* with different level of amplification of excitation signal.

From the comparison plot of the responses with different signal amplification clearly seen that the weak signal is not sufficient to excite structure to obtain good results. Coincidence of the curves from 'p1m' and 'p1s' measurement sessions prove that the system is linear with respect to the dynamic properties.

To have more detailed information about the level of background noise, the records were done with the amplifier switched off (denoted as 'p1 Off') and switched on (denoted as 'p1 On'). The plots with the results of the auto spectra for the microphone and the accelerometer are shown on Figure 5.6a, and 5.6b respectively.



(a) Auto spectrum of microphone signal.



(b) Auto spectrum for accelerometer signal.

**Figure 5.6:** Assesment of the background noise level, measurement sessions *p1 Off*, *p1 On*, *p1w*, *p1m* and *p1s*.

From the plots with background noise level several points are to be noticed:

- From the auto spectrum of microphone signal 'p1 On' presence of 50 Hz harmonics hum noise is seen. The problem is found to be due to electro magnetic field (particularly coming from the B&K power amplifier Type 2706 when the power is on) that is picked up by the 'banana'-cable, which connects the exciter with the power amplifier. The problem could not to be solved during the project time, hence the certain amount of the hum noise is presented in the measurements. Nevertheless, from the plot, Figure 5.6a, is also seen that the level between the auto spectra of the microphone signal from the background noise measurement session, i.e. 'p1 On', is much lower then the level of the auto spectra from the measurement sessions 'p1w', 'p1m' and 'p1s', and the difference between them exceeds 10 dB.
- From the auto spectra of the accelerometer signal, see Figure 5.6b, it is clearly seen that the level of the weak amplification signal, 'p1w', is close to the background noise level. This can explain bad quality of the FRF form measurements 'p1w'.
- In general difference in the auto spectra from the measurements with different level of the signal amplification shows the same scaling factor, which is prove the linearity of the system.
- Results from measurement session 'p1w' can not be used for the further analysis due to influence of the background noise.

To have more detailed quality assessment of sessions *p1m* and *p1s* the coherence between the signals can be compared. The plot of the coherence of 'p1m' and 'p1s' for the relevant frequency range are shown in Figure 5.7. From the plot, Figure 5.7, very good coherence with minor

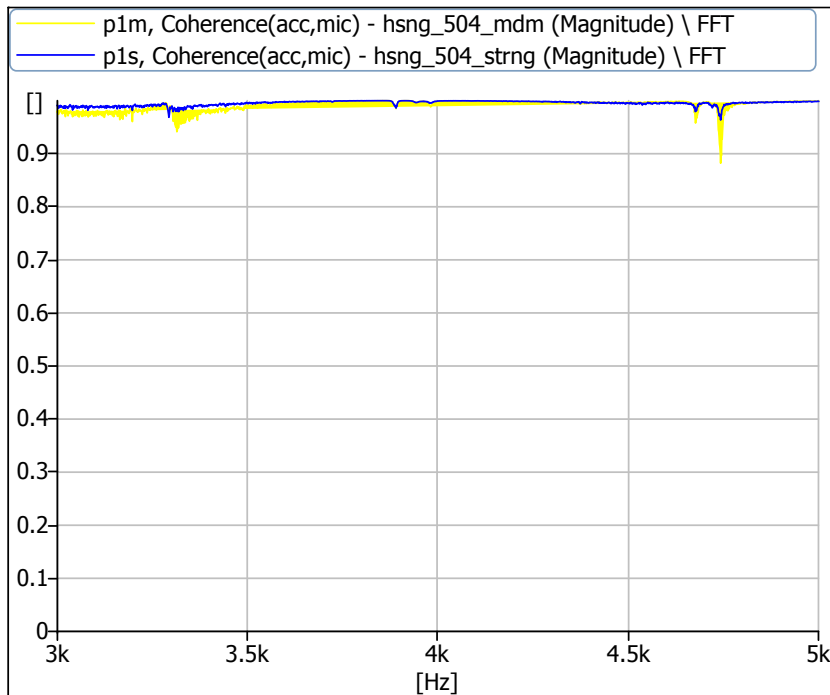


*Figure 5.7: Coherence function for the measurements p1m and p1s*

deviation from the unit value for both cases is observed, which is one more prove for the linearity of the system, and evidence of the absence of the leakages of the sound pressure. Better coherence

is noticed for the measurements with stronger amplification, hence the settings of the case 'p1s' are considered to be the best and to be used for the measurement with application at the point p2.

### Results from p1 and p2 sessions

The results from measurements p1 and p2 by means of FRF are shown in Figure 5.8. From the plot noticeable difference in the curves appearance is observed. However, the deviation for the first natural frequency between  $f_1(p1) = 3292$  kHz and  $f_1(p2) = 3210$  kHz is approximately of 2.5%. The sharpness of the peaks from p1 case refer to the smaller damping rate in comparison to the p2 case, which is also confirmed by the different slopes of the corresponding phase curves. The shift in the first mode frequency can be explained by the difference in properties of the

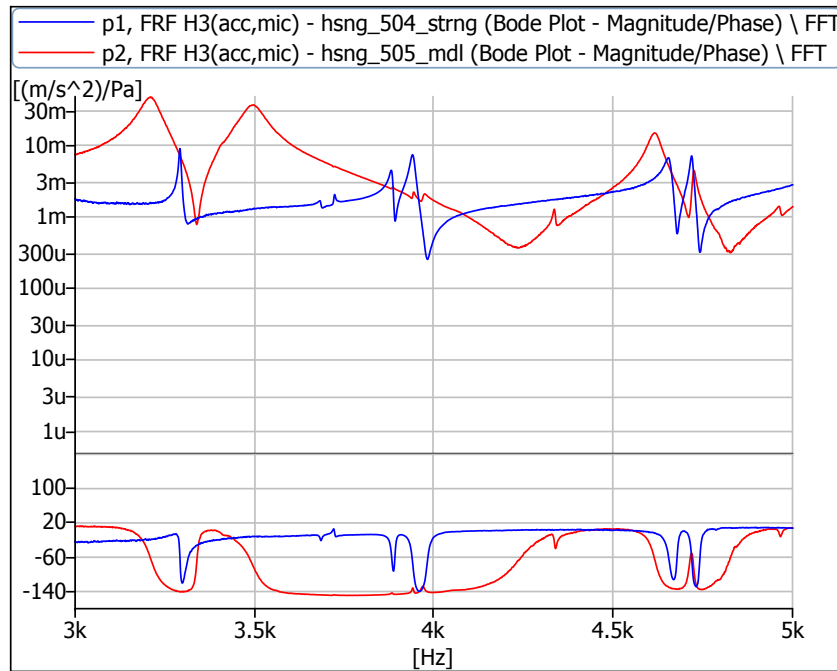


*Figure 5.8: Results from measurements p1 and p2*

structure at the local regions of the application points. The higher value of the first frequency for the case p1 indicates the higher level of the local stiffness due to the high degree of curvature at the location of the application point. The possible difference in the curvature and thickness of the shell structure also tend to influences the results. The mode shapes and position of the resonant and anti-resonant points have to be considered for the explanation of the difference in the curves p1 and p2.

## 5.2 FEM analysis and comparison with measurements.

To compare results from measurements with numerical calculations FEM analysis of the pure housing model was performed. The basic steps of the analysis with comparison of the results to the measurements are represented in following.

To run the simulations of the vibration analysis of the housing the original Computer Aided Design (CAD) model was provided by Secop GmbH. Further pre- and post- processing with the model of a housing are done with help of commercial software Solid Works and ANSYS 14.5. Using the advantage of ANSYS Workbench the model of simplified experimental set-up and

automatic meshing were done and an input file was written. The input file with the meshed model of the housing was further used for the FEM harmonic mode superposition analysis in ANSYS Mechanical APDL, where a simple (self written) macro script was applied.

For the FEM model of the housing body 'SHELL 181' (four node) element is used. In order to simulate the BCs of the suspended housing, four spring-dumper elements 'COMBIN 14' are added to the points of the connections of rubber bands suspension. The element formulation allows to define stiffness and dumping of the spring attached. The approximate stiffness of the rubber bands were determined in a simple test, and set to be 20 N/m per each spring. Springs ground connection is simulated by using 'TARGET 170' element with the position, which provides the actual length of the rubber bends.

The model of the experimental set-up created in Workbench and the meshed model transferred into Mechanical APDL, with the springs elements attached, and points of the excitation force application are shown in Figure 5.9.

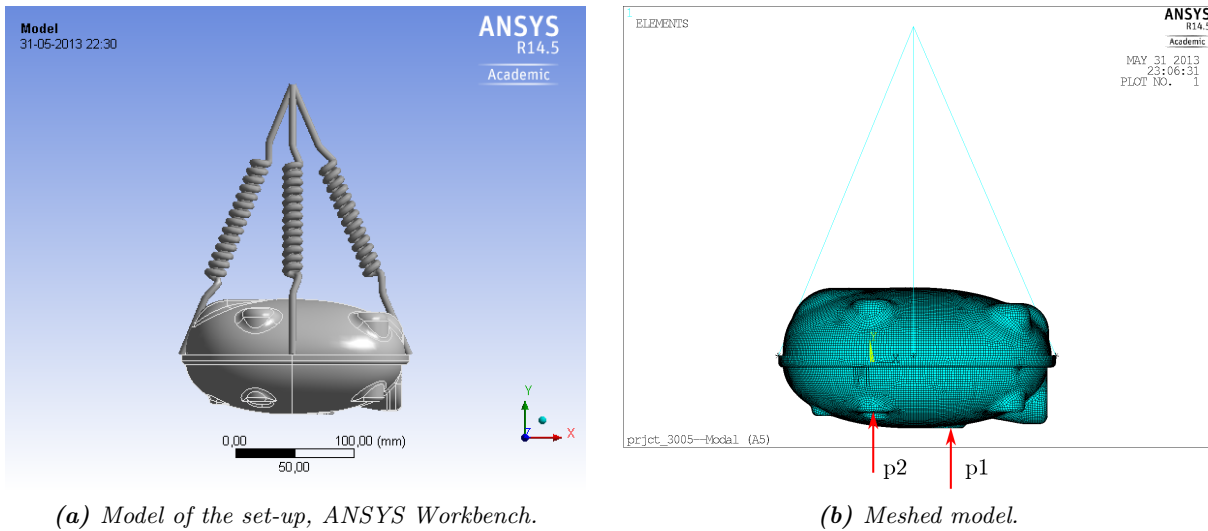


**Figure 5.9:** Models of the housing used in FEM.

As it is stated in Chapter 2, Section 2.4 in the mode superposition analysis damping ratio can be defined for every mode. The damping ratios for the cases p1 and p2 are taken from the measurement results calculated by LabShop PULSE. For case p1 ten, and for case p2 seven first resonant frequencies are included for the mode superposition analysis. Corresponding damping ratios are listed in Table 5.3.

$\xi_i, \%$	$\xi_1$	$\xi_2$	$\xi_3$	$\xi_4$	$\xi_5$	$\xi_6$	$\xi_7$	$\xi_8$	$\xi_9$	$\xi_{10}$
case p1	0.08	0.19	0.19	0.18	0.26	0.1	0.45	0.45	0.43	0.21
case p2	0.73	0.86	0.15	0.18	0.36	0.11	0.22			

**Table 5.3:** Damping ratio included into the FEM analysis for cases p1 and p2.

From the modal damping data, especially for the case p1, it is seen the tendency of increasing in the damping ratio with increasing of frequency. However, for the case p2 increasing of the damping ratio is observed stepwise, for the definite frequency spans, i.e. it increases from  $\xi_1$  to

$\xi_2$ , then from  $\xi_3$  to  $\xi_5$ , and finally from  $\xi_6$  to  $\xi_7$ .

The settings used for the mode superposition analysis are listed in Table 5.4.

Parameter	Value
Lower frequency limit	3000 Hz
Upper frequency limit	5000 Hz
Number modes to include	p1 10 p2 7
Number of sub-steps	2000
Excitation force	1 N

**Table 5.4:** Settings of FEM mode superposition analysis.

Following the settings of the frequency span and number of the sub-steps the frequency resolution is equal to 1 Hz . Excitation force is applied at the nodes, which approximately correspond to the transducer centreline placements. Using the value of 1 N for the force amplitude the resulting response is to be obtained in m/N, that is the units of FRF in terms of compliance. To be able to compare numerical results with the measured ones the FRF, which are written in a form of accelerance, from measurements p1 and p2 are converted into the compliance by use of 'j $\omega$ ' weighting.

Numerical solutions for both cases along with the FRF obtained by measurements are represented in a form of comparison plot in Figure 5.10 for case p1, and Figure 5.11 for case p2.

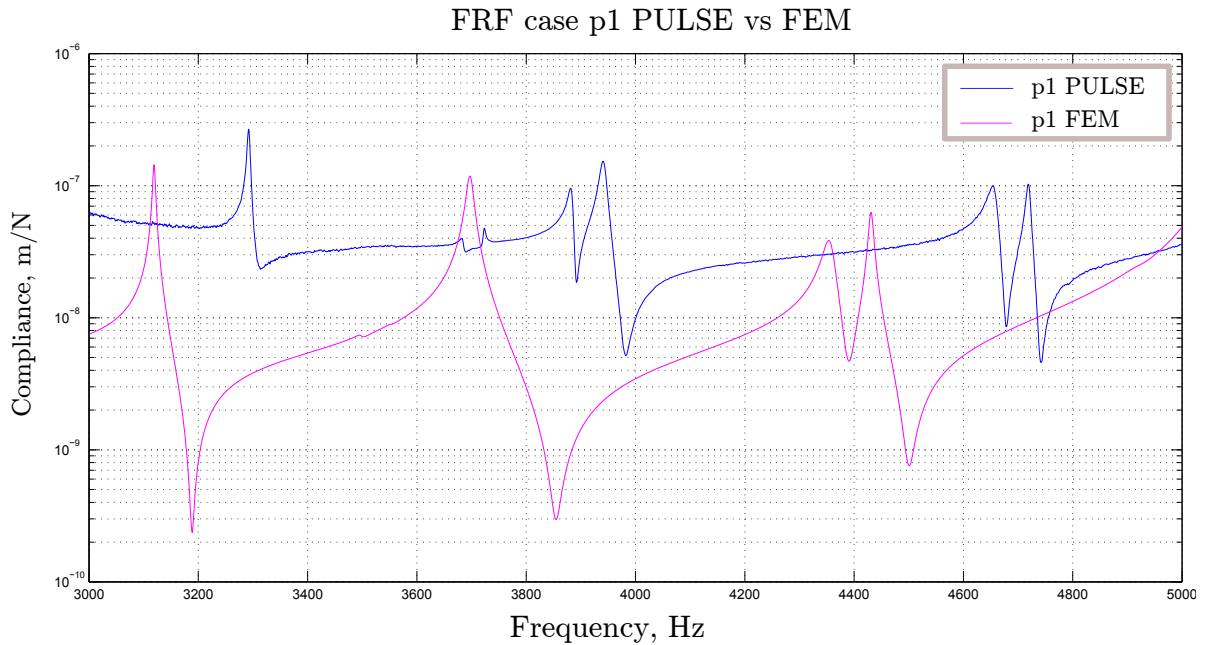


**Figure 5.10:** Comparison plot for case p1.

As it is seen from the comparison plot for case p1, Figure 5.10, the curve from measurements is not in complete agreement to the numerical results. The main deviation is in the peak frequencies values, see Table 5.5, which is in average differs by 6%.

Frequency #	PULSE	FEM	Deviation
	Hz	Hz	%
$f_1$	3292	3119	5.3
$f_2$	3941	3697	6.2
$f_3$	4655	4354	6.5
$f_4$	4719	4431	6.1
	average $\approx$		6.0

**Table 5.5:** Comparison of the peak frequencies value for the PULSE and FEM p1 case.

Such equal shift in the peak frequencies can be due to the difference in the physical properties and geometry of the actual housing and the numerical model. In fact, the numerical model of the housing has the uniform thickness, that is not a case for the point p1, where the internal spring holder is placed. The thicker shell and high degree of curvature make the local area around point p1 stiffer, that leads to the frequency shift. On the other hand, the correspondence in the peak amplitudes order and general slope of the curves means that the principle agreement between the numerical and actual models is achieved.

In contrast the agreement in the numerical and measured results for case p2 is rather good, see Figure 5.11.

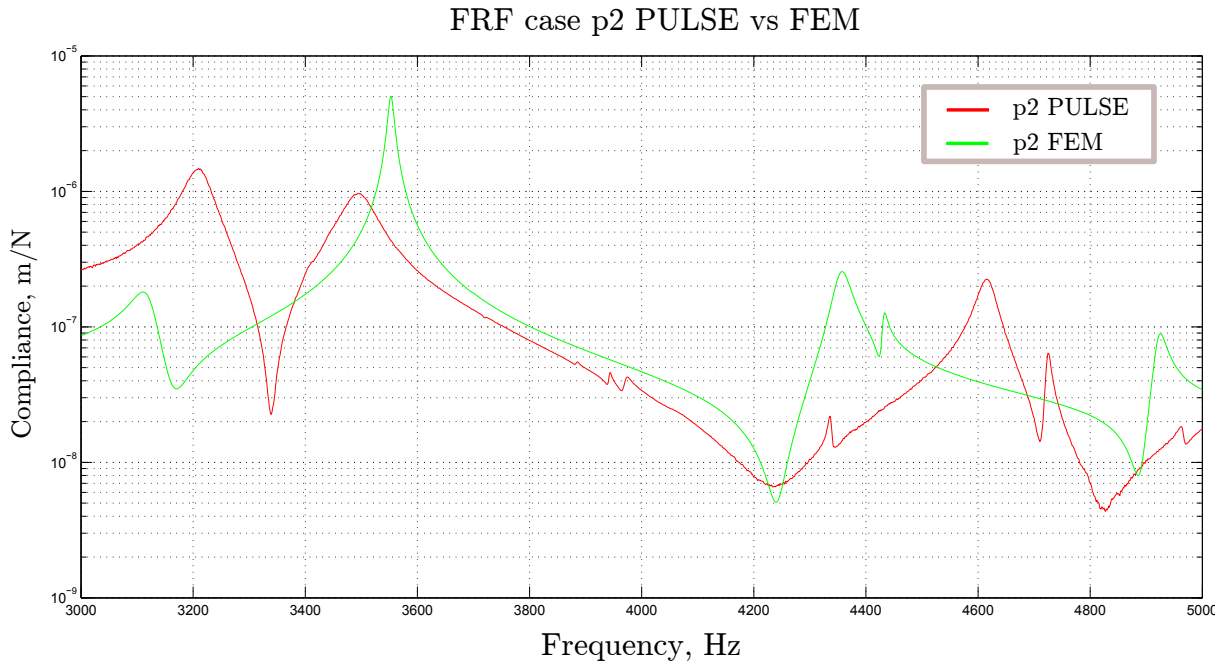


**Figure 5.11:** Comparison plot for case p2

In spite of some disagreement in the peak frequencies, general slope of the curve and particularly for the frequency span from 3600 Hz to 4200 Hz, points that the numerical model is in better correspondence to the real one, then in case of p1. It could be explained that in the middle of the bottom part of the housing, where point p2 is placed, the housing has low degree of curvature and uniform thickness, as it is in the numerical model. The values of the peak frequencies with the deviation are given in Table 5.6. The average deviation in the frequencies value by 3.5 % can be considered as a good result.

Frequency #	PULSE	FEM	Deviation
	Hz	Hz	%
$f_1$	3210	3113	3.0
$f_2$	3494	3552	1.7
$f_3$	4616	4355	5.7
	average $\approx$		3.5

*Table 5.6: Comparison of the peak frequencies value for the PULSE and FEM, case p2.*

### 5.3 Summary

In the final part of the project the localized acoustic excitation method is applied to the vibration analysis of a shell structure. The results from measurements are compared with the ones from numerical simulation. During the experimental investigation assessment of the level and influence of background noise are done along with the verification of the linearity of the mechanical system.

Finally the main points are summarised:

- in general the application of the method introduced is proved to be usable;
- for the complex shell structure the dynamic characteristics such as the natural frequencies and FRF are sensitive to the point where the analysis is applied;
- numerical simulations conducted on the shell model with uniform thickness gives good results in the case where the numerical model is close to the actual one;
- further investigation on the influence of additional inertia and extra BCs, that takes place with attaching the top part of the adaptor m#3 connected through the rubber connection ring have to be carried out;
- alternative method to measure point mobility can be applied to compare the results obtained.



# Conclusion 6

---

The master thesis project was carried out with the main aim to analyse strengths and weaknesses of the novel method for point mobility measurement, which employs localized acoustic excitation of a structure. The idea, suggested by Secop GmbH, is elaborated and developed with the main focus on robustness and usability of this emerging approach, which should be able to provide users with accurate and reliable results.

Following this line several modifications of the experimental set-up are suggested. The modification denoted as 'adaptor m#3', see Figure 3.2b, is judged to be the best with respect to both robustness and accuracy. The main feature of this modification is combination of two transducers into a single unit. This combination allows to increase robustness significantly in comparison with both the initial set-up configuration and conventional methods, mainly due to less number of operational steps and compactness of the set-up.

The advantage of adaptor m#3 is that the transfer function between the effective surface of an accelerometer and the acoustical centre of a microphone is constant, which improve the accuracy of the device.

The main disadvantage of adaptor m#3 is relatively high translational and rotational inertia of the device that needs to be taken into account as investigated in Chapter 4.

The application of adaptor m#3 to vibration analysis of a cantilever beam allows to verify the usability and accuracy of the device. Analysing the test results accuracy of the method can be assessed as good, and robustness concluded to be high. For example, using a quick bee's wax connection of the adaptor to the beam it can be easy replaced for testing at different points, which in contrast is not possible to do with conventional 'shaker-via-stinger' excitation.

Applying acoustic excitation method with use of adaptor m#3 to the point mobility measurement of a complex shell structure the results obtained are compared to ones from FEM analysis. The results from measurements and numerical simulations are to a certain extent in agreement, but more detailed description of the design features for the numerical model of compressor housing has to be done. Due to the model is of complex geometry non-uniform thickness more advanced CAD model has to be used.

Finally from the work done and results obtained it is concluded that adaptor m#3 can be used for determining the dynamical properties of different types of mechanical systems. The proposed design of adaptor m#3 can serve as the prototype, which after more detailed investigation and the use of more advanced combination of transducers can be developed further in a more robust and accurate device.



# Discussion 7

The work done during the master project results in a design suggestion of the device, denoted as 'adaptor m#3', which can be considered as the prototype of a more advanced device. Thereby several features concerning the design and analysis, which have not been covered in the present report, can be considered for the further development of the device. The points for discussion are mainly concerned with the improvement of accuracy and reliability of the measurements.

## Geometry, concept and design features of adaptor m#3

For the prototype of the adaptor to be designed and applied, equipment has been provided by Brüel&Kjær, from which the key parts for the design of the common housing are the accelerometers B&K Type 4507 and array microphone B&K Type 4935. The main influence on the geometry of the top part of adaptor m#3 is coming from the microphone dimensions, as it must be accommodated in the common housing. The parameters of the microphone are 7 mm in diameter, 65 mm in length and the weigh is 10 g, see Table C.1, appendix C, which for the case of the test carried on beam s6, are considerable and together with inertia of the device must be accounted for.

The use of an alternative microphone type with smaller length and weight, B&K Type 4597 (34 mm in length and of 3.4 g in weight), see specification [Brüel&Kjær, 2012b, ], could decrease influence of inertia and improve the accuracy of the results.

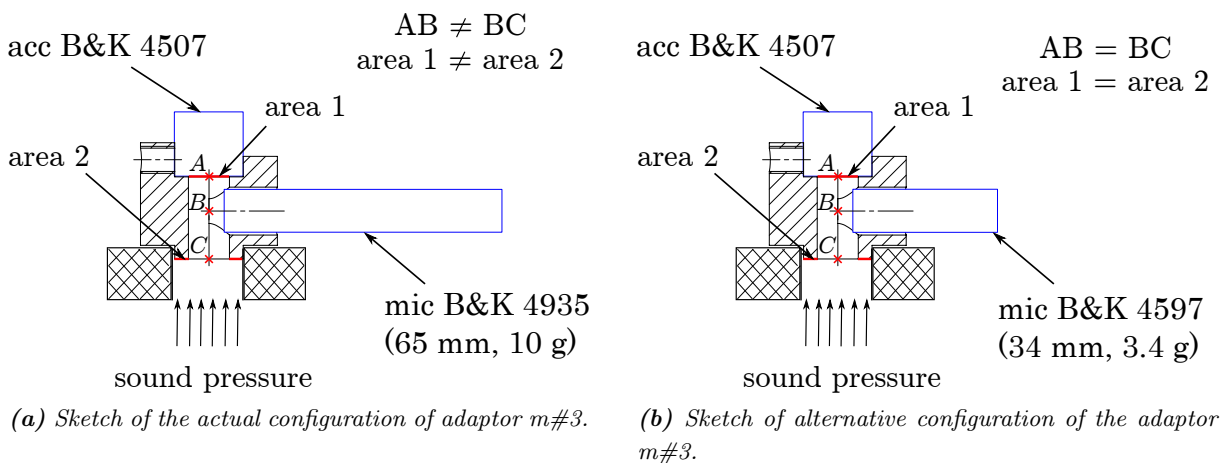


**Figure 7.1:** Suggestion of improvement to the adaptor m#3.

The use of a 1/8 inch microphone could also, besides inertia, decrease the distance between its acoustical centre and the active surface of the accelerometer, that could significantly improve

accuracy of the results obtained .

Part of work on development and analysis of adaptor m#3 includes the calculation and measurement of the transfer function,  $H_{AB}(f)$ , between the points A and B in the acoustic channel of the adaptor, see sketch in Figure 7.1. However, transformation of the sound pressure into the point force also accounted for the 'area 2', which means that the transfer function between points B and C must be taken into account. It is easy to show that under the conditions  $area1 = area2$  and  $AB = BC$ , transfer functions  $H_{AB}(f)$  and  $H_{BC}(f)$  will cancel each other out, hence lead to the best possible accuracy. This statement can be proved analytically for the idealized case, but needs to be verified experimentally.

### **Properties and influence of the connection ring**

As it is seen from the experimental part of the vibration analysis of cantilever structure, the rubber connection ring influences the boundary condition of the free end of the beam. To have a complete mathematical model of this case the stiffness of connection ring, and probably its damping, can be estimated either experimentally or iteratively, and be included into the analytical calculation. In case of achieving the agreement of the results, the properties of the connection ring should be included into the numerical model.

### **Housing analysis**

Comparison of experimental and numerical results reveals the discrepancy between the measurements and numerical predictions for the housing. For the case of such a complex shell structure 2-D shell finite element model is found to be insufficient to simulation of the actual dynamic behaviour. To solve the problem more detailed modelling with use of solid 3-D elements, especially at the zones of large curvature and non-uniform thickness could be used. To estimate the accuracy of the experimental results obtained by use of the localized acoustic excitation and adaptor m#3 an alternative and reliable method can be used. For example, dynamical properties can be determined by use of a hammer excitation or a shaker via stinger in combination with an impedance head. The alternative configuration of the 'stinger - force transducer - accelerometer' can also be considered.

# Bibliography

---

- Brüel&Kjær, 2012a.** Brüel&Kjær. *PRODUCT DATA*. URL: <http://www.bksv.com/doc/bp1841.pdf>, 2012. Downloadet: 29-05-2012.
- Brüel&Kjær, 2012b.** Brüel&Kjær. *PRODUCT DATA*. URL: <http://www.bksv.com/doc/bp2172.pdf>, 2012. Downloadet: 03-06-2012.
- Brüel&Kjær, 1998.** Brüel&Kjær. *Product Data, Array Microphone Type 4935*, 1998.
- Cook, Malkus, Plesha, and Witt, 2002.** Robert D. Cook, David S. Malkus, Michael E. Plesha, and Robert J. Witt. *Concepts and applications of finite element analysis*. ISBN: 978-0-471-35605-9, Fourth Edition. Wiley, 2002.
- Døssing, 1988.** Ole Døssing. *Structural Testing. Part 1: Mechanical Mobility Measurements*. Brüel&Kjær., 1988.
- Herlufsen, 1984.** H. Herlufsen. *Technical Review, No.1 - 1984. Dual Channel FFT Analysis (Part 1)*. Brüel&Kjær., 1984.
- Irving H. Shames, 2003.** Clive L. Dym Irving H. Shames. *Energy and Finite Element Methods in Structural Meshanics*. ISBN: 0-89116-942-3. Taylor and Francis., 2003.
- Mark Serridge, 1987.** Torben R. Licht Mark Serridge. *Piezoelectric accelerometer and vibration preamplifier handbook*. K Larsen & Søn A/S., 1987.
- Raichel, 2006.** Daniel R. Raichel. *The Science and Applications of Acoustics*. ISBN: 978-0387-26062-4, Second Edition. Springer, 2006.
- Rao, 2005.** S. S. Rao. *Mechanical Vibrations*. ISBN: 013-196751-7, 4. edition. Pearson Prentice Hall, 2005.
- Rienstra and Hirschberg, 2013.** S. W. Rienstra and A. Hirschberg. *An introduction to Acoustics*. Eindhoven University of Technology, 2013.
- Sorokin, 2005.** S. V. Sorokin. *Lecture notes on machine acoustics*. AAU, 2005.
- steelss, 2011.** steelss. *DATA TABLE FOR:CARBON STEEL:S235*. URL: <http://www.steelss.com/Carbon-steel/s235.html>, 2011. Downloadet: 26-05-2012.



# Appendix



# Appendix contents

---

Appendix A Blueprints	a-3
Appendix B Mode shapes of cantilever beam s6	a-7
Appendix C Technical characteristics of the devices used in the measurements	a-9
Appendix D Maple calculation for cantilever beam	a-11
Appendix E Maple calculation for acoustic excitation set-up	a-23

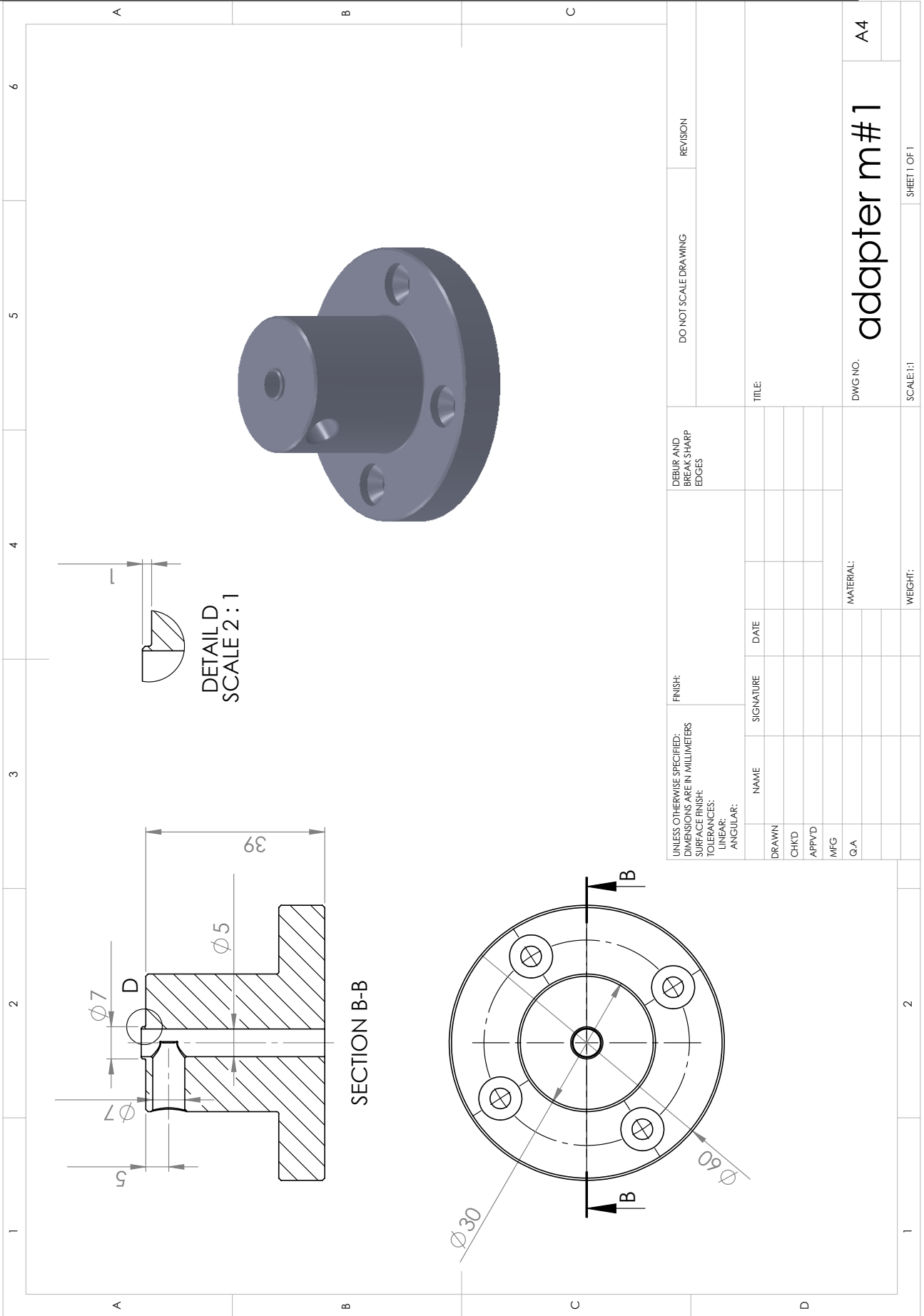


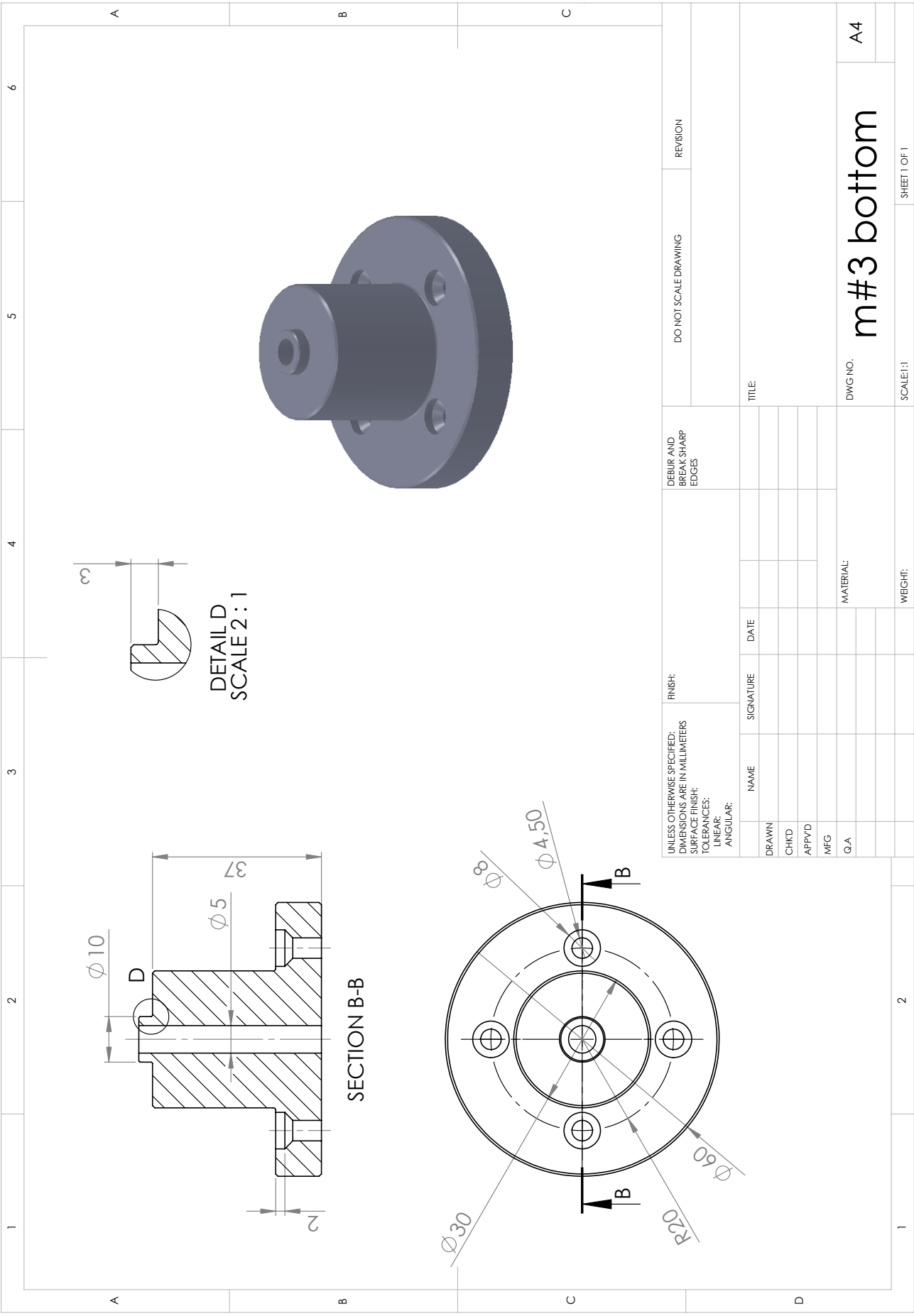
# Blueprints **A**

---

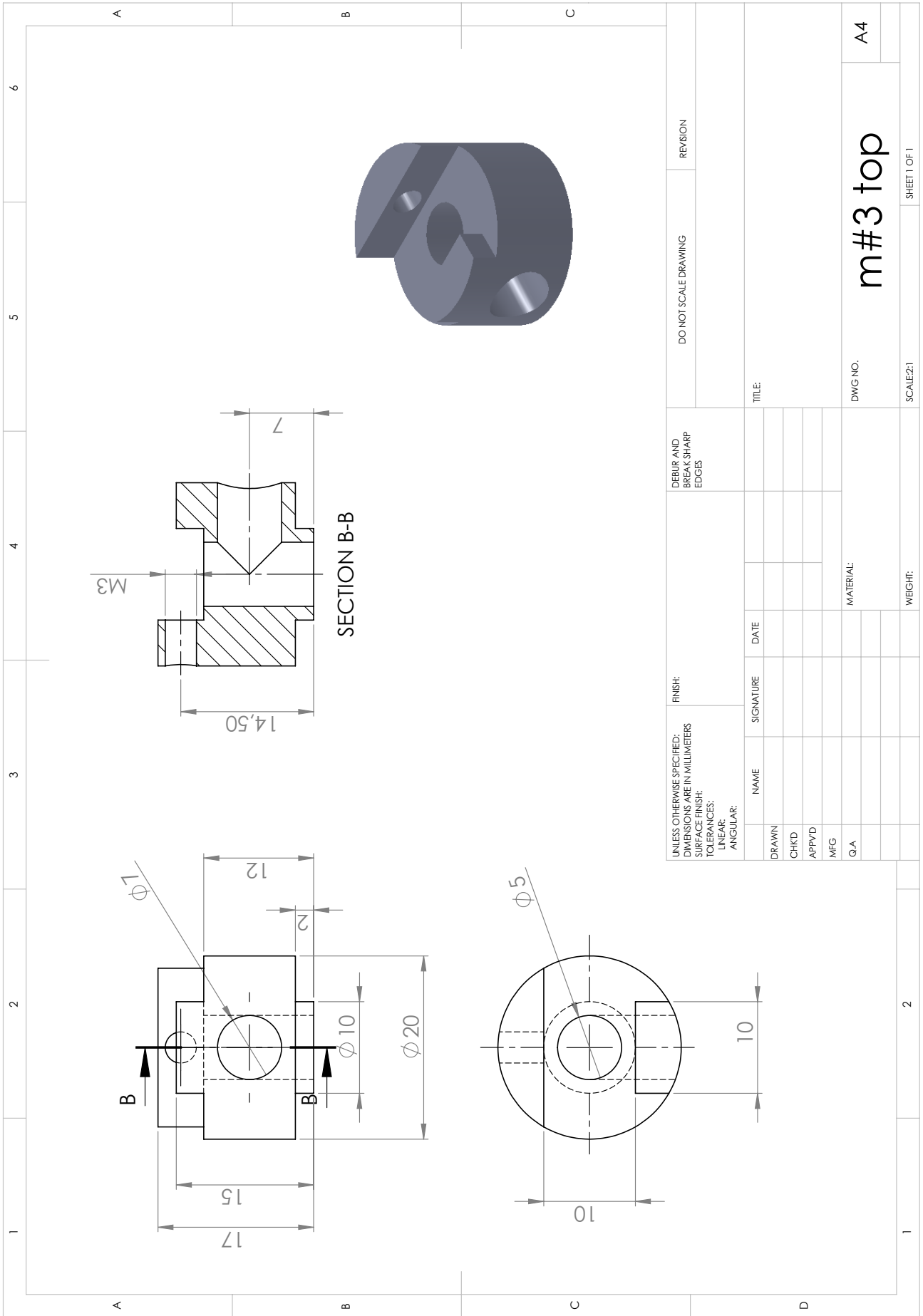
In this appendix the blueprints of the adaptor m#1 and m#3 used in the experimental part of the project are given.

A. BLUEPRINTS





UNLESS OTHERWISE SPECIFIED: DIMENSIONS ARE IN MILLIMETERS		FINISH:		DEBUR AND BREAK SHARP EDGES		DO NOT SCALE DRAWING		REVISION	
SURFACE FINISH:		TOLERANCES:		NAME		SIGNATURE		DATE	
LINEAR:		ANGULAR:		DRAWN		CHKD		APPRD	
				MFG		Q.A		MATERIAL:	
				TITLE:				DWG NO.	
								SCALE: 1:1	
								WEIGHT:	
								SHEET 1 OF 1	
								A4	
								m#3 bottom	



# Mode shapes of cantilever beam s6

# B

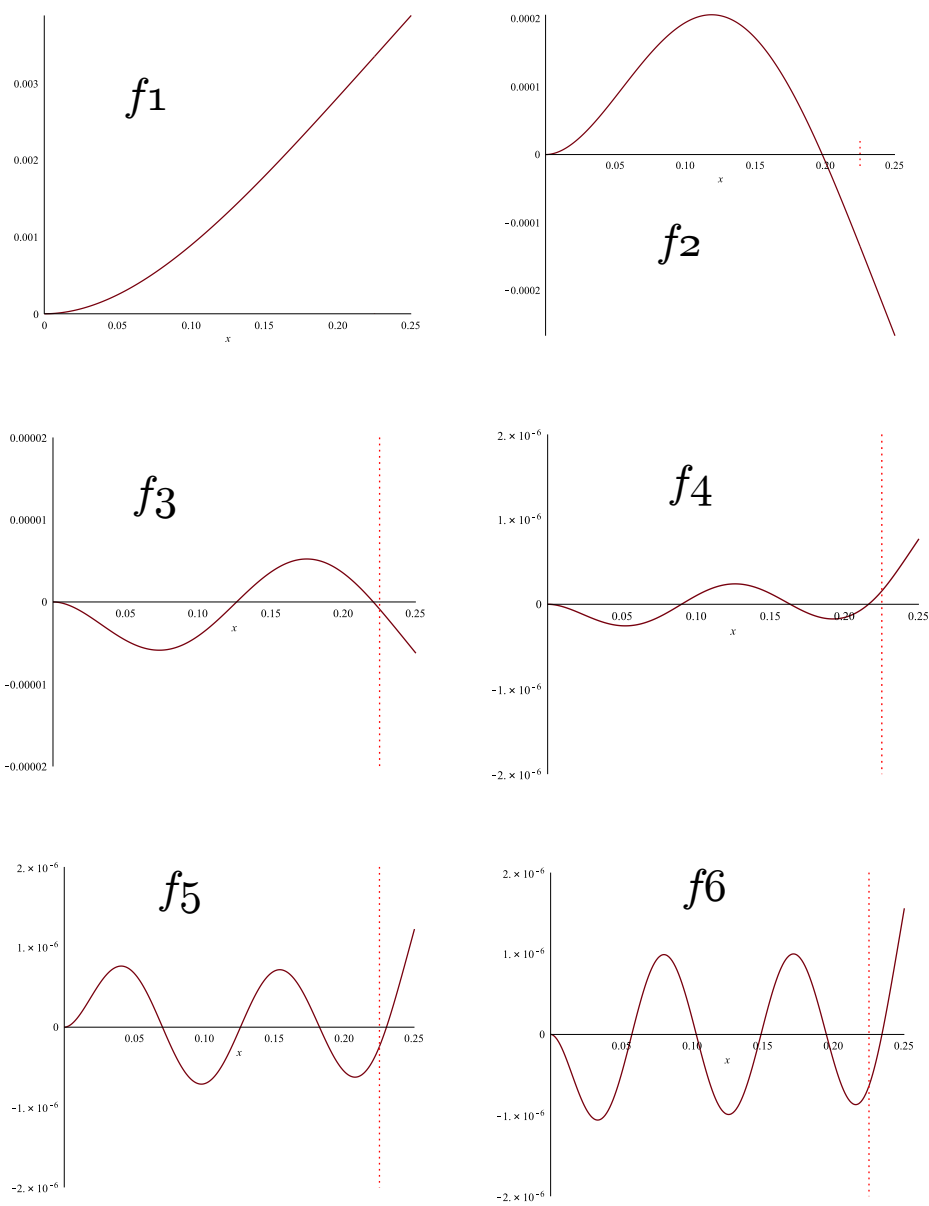


Figure B.1: Mode shapes of beam s6



# Technical characteristics of the devices used in the measurements



The relevant technical characteristics, taken from the B&K Product Data specifications, [Brüel&Kjær, 2012a],[Brüel&Kjær, 1998] for the devices used in the measurements are summarised in Table C.1:

<b>Microphone B&amp;K Type 4935</b>	
Pressure-field response (re 250 Hz)*	$\pm 1$ dB, 100Hz to 3 kHz $\pm 2$ dB, 3 kHz to 5 kHz
<b>FREE-FIELD FREQUENCY RESPONSE</b>	
0° incidence free-field response (re 250 Hz)**	+5, -2 dB, 5 kHz to 20 kHz
Nominal Sensitivity	5.6 mV/Pa
PHASE MATCH	100 to 3000Hz: $\pm 3^\circ$ 3000 to 5000Hz: $\pm 5^\circ$ relative to a factory reference
Dimensions and Weight	Diameter: 7 mm Length: 65 mm Weight: 10 g
<b>Accelerometer B&amp;K Type 4507 B 004</b>	
Sensitivity	10 mV/ms <sup>-2</sup>
Frequency Range, 10 %	0.3 Hz - 6 kHz
Phase Response, $\pm 5^\circ$	2 Hz -5 kHz
Weight:	4.8 gram
<b>Accelerometer B&amp;K Type 4507 B 005</b>	
Sensitivity	100 mV/ms <sup>-2</sup>
Frequency Range, 10 %	0.4 Hz - 6 kHz
Phase Response, $\pm 5^\circ$	2 Hz - 5 kHz
Weight:	4.8 gram
<b>Mounting clip UA 1407</b>	
Upper limiting frequency, 10 %:	
Dry mounting	1.5 kHz
Grease mounting	3 kHz
Weight:	0.4 gram

**Table C.1:** Specifications of the transducers, where (\*) denoted for guaranteed specifications and (\*\*) is for general specifications.



# Maple calculation for cantilever beam

# D

---

In the following the maple documents where calculations of the cantilever beam dynamic properties are represented.

## Determination of the natural frequencies for the fixed-free beam

*restart*

**solution for the free vibration equation:**

$$Wx := A1 \cdot \cos(k \cdot x) + A2 \cdot \sin(k \cdot x) + A3 \cdot \cosh(k \cdot x) + A4 \cdot \sinh(k \cdot x)$$

$$A1 \cos(kx) + A2 \sin(kx) + A3 \cosh(kx) + A4 \sinh(kx) \quad (1.1)$$

**taking into account the b.c.-s**

for the clamped end, at  $x = 0$

**deflection ( amplitude at  $x=0$  )  $W(0) = W_0 = 1$  (assumed)**

$$eq1 := eval(Wx, x=0) = 1$$

$$A1 + A3 = 1 \quad (1.2)$$

**slope  $Wx' = 0$**

$$eq2 := eval(Wx', x=0) = 0$$

$$A2 k + A4 k = 0 \quad (1.3)$$

for the free end, at  $x = L$

**bending moment  $M = 0$**

$$eq3 := eval(E \cdot J \cdot Wx'', x=L) = 0$$

$$E J (-A1 \cos(kL) k^2 - A2 \sin(kL) k^2 + A3 \cosh(kL) k^2 + A4 \sinh(kL) k^2) = 0 \quad (1.4)$$

**shear force  $Q = 0$**

$$eq4 := eval(E \cdot J \cdot Wx''', x=L) = 0$$

$$E J (A1 \sin(kL) k^3 - A2 \cos(kL) k^3 + A3 \sinh(kL) k^3 + A4 \cosh(kL) k^3) = 0 \quad (1.5)$$

calculation of constants  $A_i$

*# B:=solve( {eq1, eq2, eq3, eq4}, {A1, A2, A3, A4})*

*# assign(B)*

*# A1*

*B := solve( {eq1, eq2, eq3, eq4}, [A1, A2, A3, A4])[1]*

$$\left[ A1 = \frac{-\sinh(kL)^2 + \cos(kL) \cosh(kL) + \cosh(kL)^2 - \sin(kL) \sinh(kL)}{\sin(kL)^2 - \sinh(kL)^2 + \cos(kL)^2 + 2 \cos(kL) \cosh(kL) + \cosh(kL)^2}, A2 \right. \quad (1.6)$$

$$= \frac{\cos(kL) \sinh(kL) + \sin(kL) \cosh(kL)}{\sin(kL)^2 - \sinh(kL)^2 + \cos(kL)^2 + 2 \cos(kL) \cosh(kL) + \cosh(kL)^2}, A3$$

$$= \frac{\cos(kL)^2 + \cos(kL) \cosh(kL) + \sin(kL)^2 + \sin(kL) \sinh(kL)}{\sin(kL)^2 - \sinh(kL)^2 + \cos(kL)^2 + 2 \cos(kL) \cosh(kL) + \cosh(kL)^2}, A4 =$$

$$\left[ - \frac{\cos(kL) \sinh(kL) + \sin(kL) \cosh(kL)}{\sin(kL)^2 - \sinh(kL)^2 + \cos(kL)^2 + 2 \cos(kL) \cosh(kL) + \cosh(kL)^2} \right]$$

*assign(B)*

*Wx*

$$\begin{aligned} & \frac{(-\sinh(kL)^2 + \cos(kL) \cosh(kL) + \cosh(kL)^2 - \sin(kL) \sinh(kL)) \cos(kx)}{\sin(kL)^2 - \sinh(kL)^2 + \cos(kL)^2 + 2 \cos(kL) \cosh(kL) + \cosh(kL)^2} & (1.7) \\ & + \frac{(\cos(kL) \sinh(kL) + \sin(kL) \cosh(kL)) \sin(kx)}{\sin(kL)^2 - \sinh(kL)^2 + \cos(kL)^2 + 2 \cos(kL) \cosh(kL) + \cosh(kL)^2} \\ & + \frac{(\cos(kL)^2 + \cos(kL) \cosh(kL) + \sin(kL)^2 + \sin(kL) \sinh(kL)) \cosh(kx)}{\sin(kL)^2 - \sinh(kL)^2 + \cos(kL)^2 + 2 \cos(kL) \cosh(kL) + \cosh(kL)^2} \\ & - \frac{(\cos(kL) \sinh(kL) + \sin(kL) \cosh(kL)) \sinh(kx)}{\sin(kL)^2 - \sinh(kL)^2 + \cos(kL)^2 + 2 \cos(kL) \cosh(kL) + \cosh(kL)^2} \end{aligned}$$

*simplify(Wx)*

$$\begin{aligned} & \frac{1}{2} \frac{1}{1 + \cos(kL) \cosh(kL)} (\cos(kx) + \cos(kx) \cos(kL) \cosh(kL) & (1.8) \\ & - \cos(kx) \sin(kL) \sinh(kL) + \sin(kx) \cos(kL) \sinh(kL) \\ & + \sin(kx) \sin(kL) \cosh(kL) + \cosh(kx) \cos(kL) \cosh(kL) + \cosh(kx) \\ & + \cosh(kx) \sin(kL) \sinh(kL) - \sinh(kx) \cos(kL) \sinh(kL) \\ & - \sinh(kx) \sin(kL) \cosh(kL)) \end{aligned}$$

definition of the physical and geometrical characteristics/parameters of the specimen

(actual youngs modulus is in the range of 190 - 210...), source "<http://www.steelss.com/Carbon-steel/s235.html>"

$$E := 190 \cdot 10^9 \qquad 190000000000 \qquad (1.9)$$

(actual density is in the range of 7.7 - 8.03...; calculated to 7700 !)

$$\rho := 7706 \qquad 7706 \qquad (1.10)$$

$$H := 0.003 \qquad 0.003 \qquad (1.11)$$

$$B := 0.050 \qquad 0.050 \qquad (1.12)$$

$$L := 0.250 \qquad 0.250 \qquad (1.13)$$

$$A := B \cdot H \qquad 0.000150 \qquad (1.14)$$

$$J := \frac{B \cdot H^3}{12} \qquad 1.125000000 \cdot 10^{-10} \qquad (1.15)$$

$$\omega := 2 \cdot \pi \cdot f \qquad 2 \pi f \qquad (1.16)$$

$$\# Ed := E \cdot (1 + 0.00001 \cdot i \cdot \omega)$$

$$k := \sqrt[4]{\frac{\rho \cdot A \cdot \omega^2}{E \cdot J}} \qquad 0.6819751231 (\pi^2 f^2)^{1/4} \qquad (1.17)$$

$$x := 0.225 \qquad 0.225 \qquad (1.18)$$

$$Freq := 1. + \cos(kL) \cosh(kL) \qquad 1. + \cos(0.1704937808 (\pi^2 f^2)^{1/4}) \cosh(0.1704937808 (\pi^2 f^2)^{1/4}) \qquad (1.19)$$

with(Student[Calculus1]) :

$$Roots(Freq, f=0 ..3500) \qquad [38.50204493, 241.2881968, 675.6139379, 1323.933672, 2188.557222, 3269.325526] \qquad (1.20)$$

$$kU \quad \# \text{ for } E = 190 \text{ Gpa} \qquad [-38.50204493, 38.50204493, 241.2881968, 675.6139379, 1323.933672, 2188.557222, 3269.325526, 4566.248083, 6079.324369] \qquad (1.21)$$

$$kL \quad \# \text{ for } E = 210 \text{ Gpa} \qquad [-40.47777607, 40.47777607, 253.6698926, 710.2830444, 1391.871283, 2300.862962, 3437.090855, 4800.564950, 6391.284695] \qquad (1.22)$$

FreqMass :=

#kUpperLimit

#kLowLimit

# plot(Wx, f=0 ..6400) :

# plot(abs(Wx), f=0 ..6400) :

# plot(argument(Wx), f=20 ..6400) :

## Determination of the amplitudes the fixed-free beam with defined excitation point and included influence of added mass

restart

**section 1  $0 < x < L_p$ , equation  $W_{xA}$ :**

$$W_{xA} := A1 \cdot \cos(k \cdot x) + A2 \cdot \sin(k \cdot x) + A3 \cdot \exp(-k \cdot x) + A4 \cdot \exp(-(L-x) \cdot k)$$

$$A1 \cos(kx) + A2 \sin(kx) + A3 e^{-kx} + A4 e^{-(L-x)k} \quad (1.1)$$

**section 2  $L_p < x < L$ , equation  $W_{xB}$ :**

$$W_{xB} := B1 \cdot \cos(k \cdot x) + B2 \cdot \sin(k \cdot x) + B3 \cdot \exp(-k \cdot x) + B4 \cdot \exp(-(L-x) \cdot k)$$

$$B1 \cos(kx) + B2 \sin(kx) + B3 e^{-kx} + B4 e^{-(L-x)k} \quad (1.2)$$

equations set-up:

for the clamped end, at  $x = 0$ :

**displacement at  $x = 0$ ,  $W_{xA} = 0$**

$$eq1 := eval(W_{xA}, x=0) = 0$$

$$A1 + A3 + A4 e^{-Lk} = 0 \quad (1.3)$$

**slope at  $x = 0$ ,  $W_{xA}' = 0$**

$$eq2 := eval(W_{xA}', x=0) = 0$$

$$A2 k - A3 k + A4 k e^{-Lk} = 0 \quad (1.4)$$

for the free end, at  $x = L$ , **section 2:**

**bending moment  $M = 0$**

$$eq3 := eval(E \cdot J \cdot W_{xB}'', x=L) = 0$$

$$E J (-B1 \cos(Lk) k^2 - B2 \sin(Lk) k^2 + B3 k^2 e^{-Lk} + B4 k^2) = 0 \quad (1.5)$$

**shear force  $Q = 0$**

$$eq4 := eval(E \cdot J \cdot W_{xB}''', x=L) = 0$$

$$E J (B1 \sin(Lk) k^3 - B2 \cos(Lk) k^3 - B3 k^3 e^{-Lk} + B4 k^3) = 0 \quad (1.6)$$

for the point of the force application, at  $x = L_p$ :

$$eq5 := eval(W_{xA}, x=L_p) = eval(W_{xB}, x=L_p)$$

$$A1 \cos(k L_p) + A2 \sin(k L_p) + A3 e^{-k L_p} + A4 e^{-(L-L_p)k} = B1 \cos(k L_p) + B2 \sin(k L_p) + B3 e^{-k L_p} + B4 e^{-(L-L_p)k} \quad (1.7)$$

$$eq6 := eval(W_{xA}', x=L_p) = eval(W_{xB}', x=L_p)$$

$$-A1 \sin(k L_p) k + A2 \cos(k L_p) k - A3 k e^{-k L_p} + A4 k e^{-(L-L_p)k} = -B1 \sin(k L_p) k \quad (1.8)$$

$$\begin{aligned}
 & + B2 \cos(k Lp) k - B3 k e^{-kLp} + B4 k e^{-(L-Lp)k} \\
 eq7 := & eval(E \cdot J \cdot WxA'', x = Lp) = eval(E \cdot J \cdot WxB'', x = Lp) \\
 EJ ( & -A1 \cos(k Lp) k^2 - A2 \sin(k Lp) k^2 + A3 k^2 e^{-kLp} + A4 k^2 e^{-(L-Lp)k} = EJ ( \quad (1.9) \\
 & -B1 \cos(k Lp) k^2 - B2 \sin(k Lp) k^2 + B3 k^2 e^{-kLp} + B4 k^2 e^{-(L-Lp)k}
 \end{aligned}$$

$$\begin{aligned}
 \#eq7 := & eval(E \cdot J \cdot WxA'', x = Lp) - eval(E \cdot J \cdot WxB'', x = Lp) - (Jmic \cdot \omega^2) \cdot eval(WxA', x = Lp) = 0 \\
 eq8 := & eval(E \cdot J \cdot WxA''', x = Lp) - eval(E \cdot J \cdot WxB''', x = Lp) = P - (m \cdot \omega^2) \cdot eval(WxA, x = Lp) \\
 EJ ( & A1 \sin(k Lp) k^3 - A2 \cos(k Lp) k^3 - A3 k^3 e^{-kLp} + A4 k^3 e^{-(L-Lp)k} \quad (1.10) \\
 - EJ ( & B1 \sin(k Lp) k^3 - B2 \cos(k Lp) k^3 - B3 k^3 e^{-kLp} + B4 k^3 e^{-(L-Lp)k} = P \\
 - m \omega^2 ( & A1 \cos(k Lp) + A2 \sin(k Lp) + A3 e^{-kLp} + A4 e^{-(L-Lp)k}
 \end{aligned}$$

calculation of constants Ai and Bi:

```

B := solve( {eq1, eq2, eq3, eq4, eq5, eq6, eq7, eq8}, [A1, A2, A3, A4, B1, B2, B3, B4]) [1]:
assign(B)

```

physical and geometrical characteristics/parameters of the specimen:

$$E := 195 \cdot 10^9 \quad 195000000000 \quad (1.11)$$

E=190\*10^9 gives fl=37.5 calculating for range f=35..45

#E:=195·10<sup>9</sup> gives fl=38.04

#E:=210·10<sup>9</sup> # gives fl=39.5

$$\rho := 7706 \quad 7706 \quad (1.12)$$

$$H := 0.003 \quad 0.003 \quad (1.13)$$

$$B := 0.050 \quad 0.050 \quad (1.14)$$

$$L := 0.250 \quad 0.250 \quad (1.15)$$

$$A := B \cdot H \quad 0.000150 \quad (1.16)$$

$$J := \frac{B \cdot H^3}{12} \quad 1.125000000 \cdot 10^{-10} \quad (1.17)$$

$$\omega := 2 \cdot \pi \cdot f \quad 2 \pi f \quad (1.18)$$

$$\#Ed := E \cdot (1 + 0.00001 \cdot i \cdot \omega)$$

$$k := \sqrt[4]{\frac{\rho \cdot A \cdot \omega^2}{E \cdot J}}$$

$$0.6775608128 (\pi^2 f^2)^{1/4} \quad (1.19)$$

$$Lp := 0.225$$

$$0.225 \quad (1.20)$$

$$\#x := 0.225$$

$$f := 208$$

$$208 \quad (1.21)$$

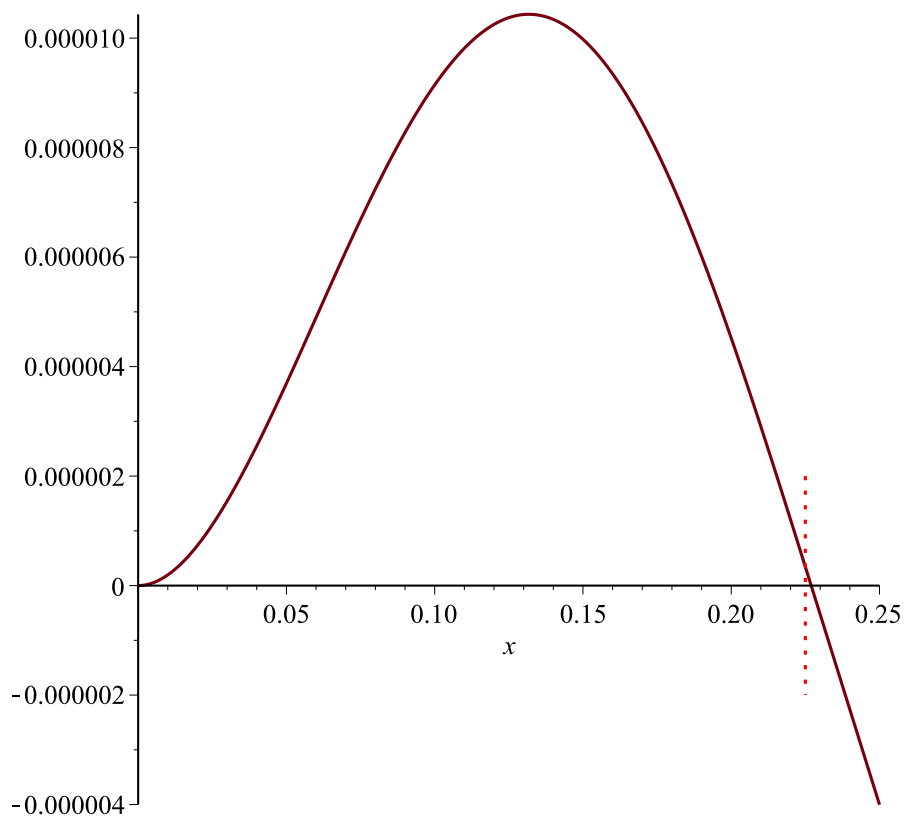
$$P := 1$$

$$1 \quad (1.22)$$

$$m := 0.005$$

with(plots) :

multiple(plot, [WxA, x=0..Lp], [WxB, x=Lp..L], [[Lp, Lp], [0.000002, -0.000002], color="Red", linestyle="dot"])



## Determination of the amplitudes the fixed-free beam with defined excitation point

restart

**section 1  $0 < x < L_p$ , equation  $W_{xA}$ :**

$$W_{xA} := A1 \cdot \cos(k \cdot x) + A2 \cdot \sin(k \cdot x) + A3 \cdot \exp(-k \cdot x) + A4 \cdot \exp(-(L - x) \cdot k)$$

$$A1 \cos(kx) + A2 \sin(kx) + A3 e^{-kx} + A4 e^{-(L-x)k} \quad (1.1)$$

**section 2  $L_p < x < L$ , equation  $W_{xB}$ :**

$$W_{xB} := B1 \cdot \cos(k \cdot x) + B2 \cdot \sin(k \cdot x) + B3 \cdot \exp(-k \cdot x) + B4 \cdot \exp(-(L - x) \cdot k)$$

$$B1 \cos(kx) + B2 \sin(kx) + B3 e^{-kx} + B4 e^{-(L-x)k} \quad (1.2)$$

equations set-up:

for the clamped end, at  $x = 0$ :

**displacement at  $x = 0$ ,  $W_{xA} = 0$**

$$eq1 := eval(W_{xA}, x=0) = 0$$

$$A1 + A3 + A4 e^{-Lk} = 0 \quad (1.3)$$

**slope at  $x = 0$ ,  $W_{xA}' = 0$**

$$eq2 := eval(W_{xA}', x=0) = 0$$

$$A2 k - A3 k + A4 k e^{-Lk} = 0 \quad (1.4)$$

for the free end, at  $x = L$ , **section 2:**

**bending moment  $M = 0$**

$$eq3 := eval(E \cdot J \cdot W_{xB}'', x=L) = 0$$

$$E J (-B1 \cos(Lk) k^2 - B2 \sin(Lk) k^2 + B3 k^2 e^{-Lk} + B4 k^2) = 0 \quad (1.5)$$

**shear force  $Q = 0$**

$$eq4 := eval(E \cdot J \cdot W_{xB}''', x=L) = 0$$

$$E J (B1 \sin(Lk) k^3 - B2 \cos(Lk) k^3 - B3 k^3 e^{-Lk} + B4 k^3) = 0 \quad (1.6)$$

for the point of the force application, at  $x = L_p$ :

$$eq5 := eval(W_{xA}, x=L_p) = eval(W_{xB}, x=L_p)$$

$$A1 \cos(k L_p) + A2 \sin(k L_p) + A3 e^{-k L_p} + A4 e^{-(L - L_p) k} = B1 \cos(k L_p) + B2 \sin(k L_p)$$

$$+ B3 e^{-k L_p} + B4 e^{-(L - L_p) k} \quad (1.7)$$

$$eq6 := eval(W_{xA}', x=L_p) = eval(W_{xB}', x=L_p)$$

$$-A1 \sin(k L_p) k + A2 \cos(k L_p) k - A3 k e^{-k L_p} + A4 k e^{-(L - L_p) k} = -B1 \sin(k L_p) k \quad (1.8)$$

$$\begin{aligned}
& + B2 \cos(k Lp) k - B3 k e^{-k Lp} + B4 k e^{-(L - Lp) k} \\
\#eq7 := & eval(E \cdot J \cdot WxA'', x = Lp) = eval(E \cdot J \cdot WxB'', x = Lp) \\
E J ( & -A1 \cos(k Lp) k^2 - A2 \sin(k Lp) k^2 + A3 k^2 e^{-k Lp} + A4 k^2 e^{-(L - Lp) k} = E J ( \quad (1.9) \\
& -B1 \cos(k Lp) k^2 - B2 \sin(k Lp) k^2 + B3 k^2 e^{-k Lp} + B4 k^2 e^{-(L - Lp) k}
\end{aligned}$$

$$\begin{aligned}
eq7 := & eval(E \cdot J \cdot WxA'', x = Lp) - eval(E \cdot J \cdot WxB'', x = Lp) - (Jmic \cdot \omega^2) \cdot eval(WxA', x = Lp) \\
& = 0 \\
& \# \text{ consideration of addition inertia of mic at point } Lp
\end{aligned}$$

$$\begin{aligned}
\#eq8 := & eval(E \cdot J \cdot WxA''', x = Lp) - eval(E \cdot J \cdot WxB''', x = Lp) = P \\
E J ( & A1 \sin(k Lp) k^3 - A2 \cos(k Lp) k^3 - A3 k^3 e^{-k Lp} + A4 k^3 e^{-(L - Lp) k} \quad (1.10) \\
& - E J ( B1 \sin(k Lp) k^3 - B2 \cos(k Lp) k^3 - B3 k^3 e^{-k Lp} + B4 k^3 e^{-(L - Lp) k} = P
\end{aligned}$$

*# consideration of addition mass at point Lp*

$$eq8 := eval(E \cdot J \cdot WxA''', x = Lp) - eval(E \cdot J \cdot WxB''', x = Lp) = P - (m \cdot \omega^2) \cdot eval(WxA, x = Lp)$$

calculation of constants Ai and Bi:

$$B := solve(\{eq1, eq2, eq3, eq4, eq5, eq6, eq7, eq8\}, [A1, A2, A3, A4, B1, B2, B3, B4])[1]:$$

*assign(B)*

physical and geometrical characteristics/parameters of the specimen:

$$\begin{aligned}
E := & 195 \cdot 10^9 & 195000000000 & (1.11)
\end{aligned}$$

$$\begin{aligned}
\rho := & 7706 & 7706 & (1.12)
\end{aligned}$$

$$\begin{aligned}
H := & 0.003 & 0.003 & (1.13)
\end{aligned}$$

$$\begin{aligned}
B := & 0.050 & 0.050 & (1.14)
\end{aligned}$$

$$\begin{aligned}
L := & 0.250 & 0.250 & (1.15)
\end{aligned}$$

$$\begin{aligned}
A := & B \cdot H & 0.000150 & (1.16)
\end{aligned}$$

$$\begin{aligned}
J := & \frac{B \cdot H^3}{12} & 1.125000000 \cdot 10^{-10} & (1.17)
\end{aligned}$$

$$\omega := 2 \cdot \pi \cdot f \quad 2 \pi f \quad (1.18)$$

$$Ed := E \cdot (1 + 0.000001 \cdot i \cdot \omega) \quad 195000000000 + 3.9000000000 \cdot 10^5 I \pi f \quad (1.19)$$

$$k := \sqrt[4]{\frac{\rho \cdot A \cdot \omega^2}{Ed \cdot J}} \quad 450.2533297 \left( \frac{\pi^2 f^2}{195000000000 + 3.9000000000 \cdot 10^5 I \pi f} \right)^{1/4} \quad (1.20)$$

$$Lp := 0.225 \quad 0.225 \quad (1.21)$$

$$x := 0.225 \quad 0.225 \quad (1.22)$$

$$P := 1 \quad 1 \quad (1.23)$$

$$m := 0.0295 \quad 0.0295 \quad (1.24)$$

$$Jmic := \frac{1}{3} \cdot Mmic \cdot Lmic^2 \quad \frac{1}{3} Mmic Lmic^2 \quad (1.25)$$

$$Mmic := 0.01 \quad 0.01 \quad (1.26)$$

$$Lmic := 0.035 \quad 0.035 \quad (1.27)$$

*WxA :*

*Smpl := simplify(WxA) :*

*eval(Smpl, f=20.)*

$-0.0002342243378 + 1.042435114 \cdot 10^{-8} I$

```
> Ds := Array(1..3481, 1..2)
```

$$Ds := \begin{bmatrix} 1..3481 \times 1..2 \text{ Array} \\ \text{Data Type: anything} \\ \text{Storage: rectangular} \\ \text{Order: Fortran\_order} \end{bmatrix} \quad (1.29)$$

```
> #for n from 1 to 3466 do
# Ds(n, 1) := 19. + n;
# Ds(n, 2) := eval(abs(Smpl), f=Ds(n, 1))
# end do:
```

---

(1.30)

*Ds*

*1..3481 x 1..2 Array*  
*Data Type: anything*  
*Storage: rectangular*  
*Order: Fortran\_order*

(1.31)

*Ds5 := convert(Ds, Matrix)*

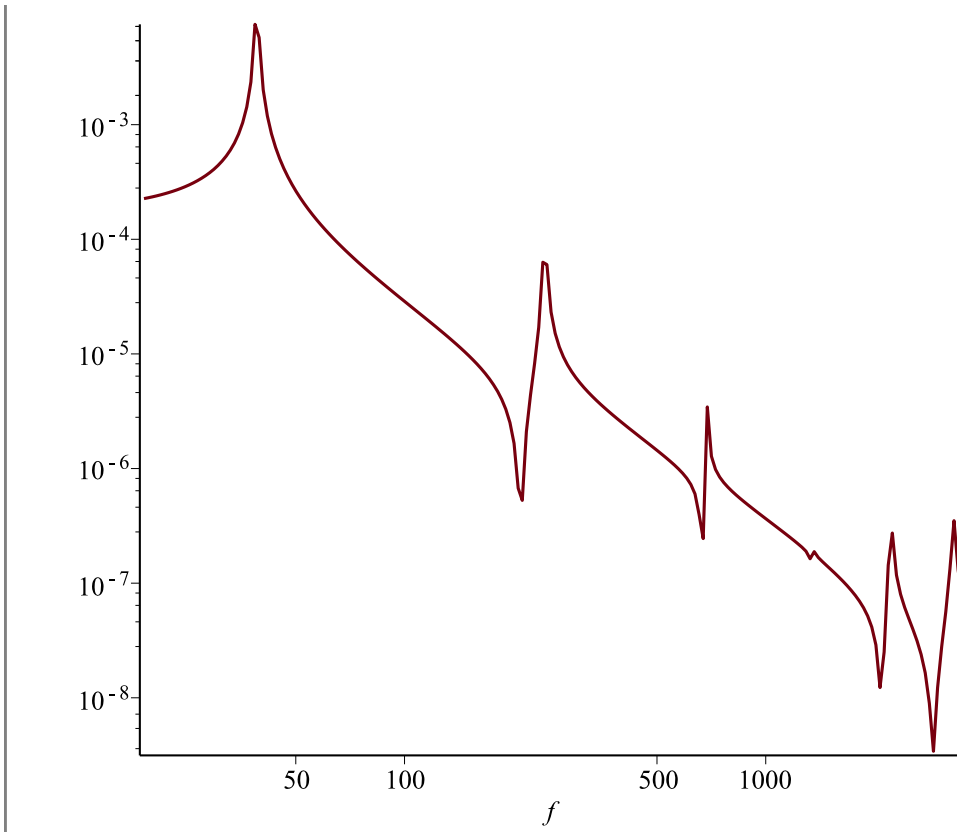
*3481 x 2 Matrix*  
*Data Type: anything*  
*Storage: rectangular*  
*Order: Fortran\_order*

(1.32)

(1.33)

*with(plots) :*

*loglogplot(abs(WxA), f= 19 ..3500)*



```
# plot(abs(Smpl), f= 20 ..250)
#plot( ( argument(WxA) * 180 / pi ), f= 35 ..3500 )
```

# Maple calculation for acoustic excitation set-up

---



In the following the maple documents where calculations of the impedance and transfer function for the devices used in acoustic excitation set-up are given.

## Transfer Function and Impedance.

restart

$$eqA := A + B = P \quad A + B = P \quad (1.1)$$

$$eqB := A \cdot \exp(I \cdot k \cdot L) + B \cdot \exp(-I \cdot k \cdot L) \quad A e^{1kL} + B e^{-1kL} \quad (1.2)$$

$$eqC := \frac{1}{\rho \cdot c} \cdot (A \cdot \exp(I \cdot k \cdot L) - B \cdot \exp(-I \cdot k \cdot L)) \quad \frac{A e^{1kL} - B e^{-1kL}}{\rho c} \quad (1.3)$$

$$Z := \frac{eqB}{eqC} = X \cdot \rho \cdot c \quad \frac{(A e^{1kL} + B e^{-1kL}) \rho c}{A e^{1kL} - B e^{-1kL}} = X \rho c \quad (1.4)$$

$$\text{solve}(\{eqA, Z\}, [A, B]) \quad \left[ \left[ A = \frac{P e^{-1kL} (1 + X)}{e^{-1kL} + X e^{1kL} - e^{1kL} + X e^{-1kL}}, B = \frac{e^{1kL} P (X - 1)}{e^{-1kL} + X e^{1kL} - e^{1kL} + X e^{-1kL}} \right] \right] \quad (1.5)$$

## Calculation of p(x,f).

$$pL := A \cdot \exp(I \cdot k \cdot x) + B \cdot \exp(-I \cdot k \cdot x) \quad A e^{1kx} + B e^{-1kx} \quad (2.1)$$

$$x := 0.012 \quad 0.012 \quad (2.2)$$

$$A := \frac{P e^{-1kL} (1 + X)}{e^{-1kL} + X e^{1kL} - e^{1kL} + X e^{-1kL}} \quad \frac{P e^{-1kL} (1 + X)}{e^{-1kL} + X e^{1kL} - e^{1kL} + X e^{-1kL}} \quad (2.3)$$

$$B := \frac{e^{1kL} P (X - 1)}{e^{-1kL} + X e^{1kL} - e^{1kL} + X e^{-1kL}} \quad \frac{e^{1kL} P (X - 1)}{e^{-1kL} + X e^{1kL} - e^{1kL} + X e^{-1kL}} \quad (2.4)$$

$$X := 1000 \quad 1000 \quad (2.5)$$

$$P := 1$$

$$k := \frac{2 \cdot \text{Pi} \cdot f}{343} \quad 1 \quad (2.6)$$

$$L := 0.012 \quad \frac{2}{343} \pi f \quad (2.7)$$

$$pL \quad 0.012 \quad (2.8)$$

$$\text{simplify}(pL) \quad \frac{2000 e^{-0.000069970845481\pi f} e^{0.000069970845481\pi f}}{1001 e^{-0.000069970845481\pi f} + 999 e^{0.000069970845481\pi f}} \quad (2.9)$$

$$\text{simplify}(pL) \quad \frac{2000.}{1001. e^{-0.0002198198942If} + 999. e^{0.0002198198942If}} \quad (2.10)$$

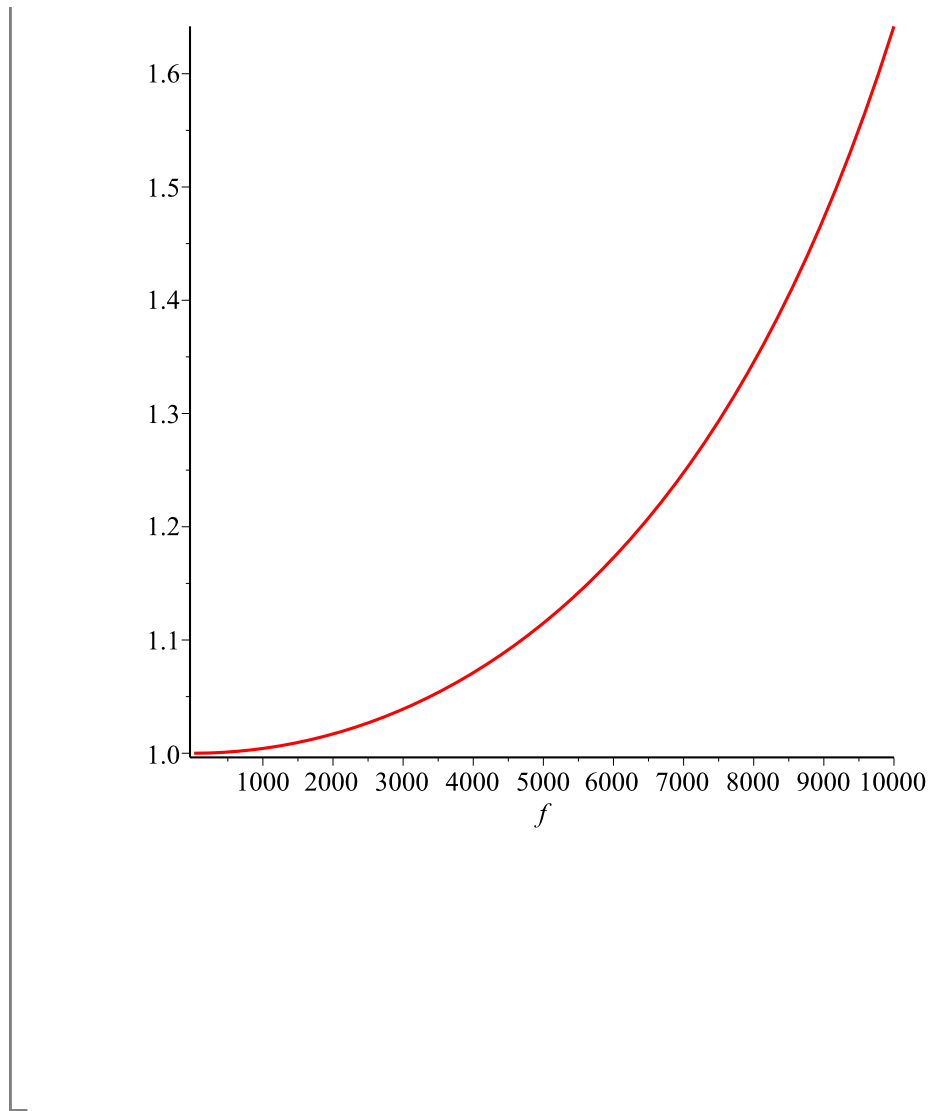
### ▼ Acoustic pressure vs frequency. Mic position $xM$ (xM).

$$xM := 0.007 \quad 0.007 \quad (3.1)$$

$$pM := A \cdot \exp(I \cdot k \cdot xM) + B \cdot \exp(-I \cdot k \cdot xM) : \\ \text{simplify}(pM) \quad \frac{1001. e^{-0.00009159162256If} + 999. e^{0.00009159162256If}}{1001. e^{-0.0002198198942If} + 999. e^{0.0002198198942If}} \quad (3.2)$$

$$H := \frac{pL}{pM} : \\ \text{simplify}(H) \quad \frac{2000.}{1001. e^{-0.00009159162256If} + 999. e^{0.00009159162256If}} \quad (3.3)$$

$\text{plot}(\text{abs}(H), f = 20 \dots 10000)$



## Plotting FRF for different cases

restart

$pL := A \cdot \exp(I \cdot k \cdot x) + B \cdot \exp(-I \cdot k \cdot x) :$

$$A := \frac{P e^{-1kL} (1 + X)}{e^{-1kL} + X e^{1kL} - e^{1kL} + X e^{-1kL}} :$$

$$B := \frac{e^{1kL} P (X - 1)}{e^{-1kL} + X e^{1kL} - e^{1kL} + X e^{-1kL}} :$$

$x := 0.041$

0.041

0.041

(1.2)

$X := 1 + 2 \cdot i$

1 + 2 I

(1.3)

#X:=1000

1000

(1.4)

$P := 1$

1

(1.5)

$k := \frac{2 \cdot \text{Pi} \cdot f}{343}$

$\frac{2}{343} \pi f$

(1.6)

$L := 0.041$

0.041

(1.7)

$pL :$

$\text{simplify}(pL)$

$$\frac{1. + 2. I}{e^{-0.0007510513051 I f} + 1. I e^{0.0007510513051 I f} + 1. I e^{-0.0007510513051 I f}}$$

(1.8)

$xM := 0.034$

0.034

(1.9)

$pM := A \cdot \exp(I \cdot k \cdot xM) + B \cdot \exp(-I \cdot k \cdot xM) :$

$\text{simplify}(pM) :$

$H := \frac{pL}{pM} :$

$H6i := \text{simplify}(H)$

$$\frac{1. + 2. I}{e^{-0.0001282282715 I f} + 1. I e^{-0.0001282282715 I f} + 1. I e^{0.0001282282715 I f}}$$

(1.10)

#####

$\text{unassign}('x', 'X', 'L', 'H', 'pL', 'pM')$

##### import data for M6

$$H6 = \frac{2000.}{1001. e^{-0.0001282282715 If} + 999. e^{0.0001282282715 If}} \quad (1.11)$$

$$H9 = \frac{2000.}{1001. e^{-0.0001831832451 If} + 999. e^{0.0001831832451 If}} \quad (1.12)$$

$$H1 = \frac{2000.}{1001. e^{-0.00009159162256 If} + 999. e^{0.00009159162256 If}} \quad (1.13)$$

$$H1i = \frac{(28. + 50. I) / (24. e^{-0.00009159162256 If} + 25. I e^{-0.00009159162256 If} + 4. e^{0.00009159162256 If} + 25. I e^{0.00009159162256 If})}{1} \quad (1.14)$$

$$H9i = \frac{14. + 36. I}{17. e^{-0.0001831832451 If} + 18. I e^{-0.0001831832451 If} - 3. e^{0.0001831832451 If} + 18. I e^{0.0001831832451 If}} \quad (1.15)$$

$$H6i = \frac{1. + 2. I}{e^{-0.0001282282715 If} + 1. I e^{-0.0001282282715 If} + 1. I e^{0.0001282282715 If}} \quad (1.16)$$

```
ImportData( )
ImportMatrix("C:\Users\timon.timon-
PC\Desktop\P_dms_4\rep_AcSetUp\set_4_mic_mic_TF\analytical_maple\DataMatlab\xM
6.mat", source = Matlab, datatype = float8)
xM6
```

$$xM6 = \left[ \begin{array}{l} \text{"xM6",} \\ \left[ \begin{array}{l} 1 \times 25 \text{ Matrix} \\ \text{Data Type: float}_8 \\ \text{Storage: rectangular} \\ \text{Order: Fortran\_order} \end{array} \right] \end{array} \right] \quad (1.18)$$

select entry 2 →

$$\left[ \begin{array}{l} 1 \times 25 \text{ Matrix} \\ \text{Data Type: float}_8 \\ \text{Storage: rectangular} \\ \text{Order: Fortran\_order} \end{array} \right] \quad (1.19)$$

to Vector →

$$\left[ \begin{array}{l} \text{"yMark11",} \\ \left[ \begin{array}{l} 1 \times 25 \text{ Matrix} \\ \text{Data Type: complex}_8 \\ \text{Storage: rectangular} \\ \text{Order: Fortran\_order} \end{array} \right] \end{array} \right] \quad (1.34)$$

select entry 2  
→

$$\left[ \begin{array}{l} 1 \times 25 \text{ Matrix} \\ \text{Data Type: complex}_8 \\ \text{Storage: rectangular} \\ \text{Order: Fortran\_order} \end{array} \right] \quad (1.35)$$

to Vector  
→

$$\left[ \begin{array}{l} 1 \dots 25 \text{ Vector}_{\text{column}} \\ \text{Data Type: complex}_8 \\ \text{Storage: rectangular} \\ \text{Order: Fortran\_order} \end{array} \right] \quad (1.36)$$

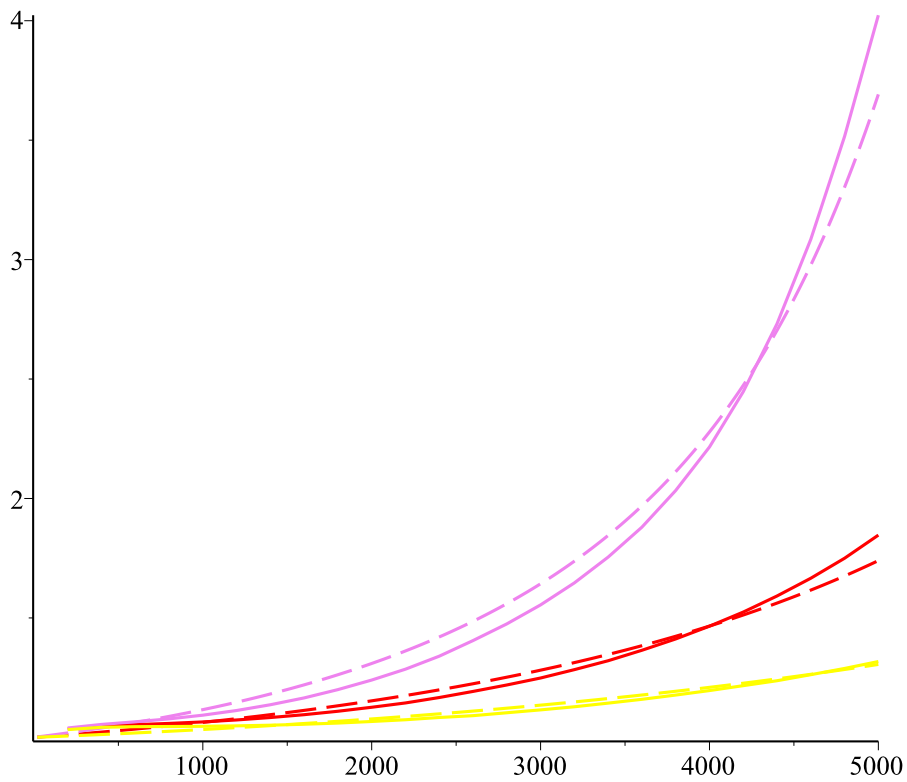
assign to a name  
→

$$hM1 \quad (1.37)$$

##### plotting the data

with(plots) :

```
multiple(plot, [abs(H6i), f=20..5000, color="Red", linestyle="dash"], [abs(H9i), f=20..5000,
color="Violet", linestyle="dash"], [abs(H1i), f=20..5000, color="Yellow", linestyle
="dash"], [fr, abs(hM6), color="Red", ], [fr, abs(hM9), color="Violet", ], [fr, abs(hM1),
color="Yellow"])
```



```
multiple(plot, [abs(H6), f=20 ..5000, color="Red", legend="M6 analytical", linestyle="dash"],
[abs(H9), f=20 ..5000, color="Violet", legend="M9 analytical", linestyle="dash"],
[abs(H1), f=20 ..5000, color="Yellow", legend="M1 analytical", linestyle="dash"], [fr,
abs(hM6), color="Red", legend="M6 experimental"], [fr, abs(hM9), color="Violet", legend
="M9 experimental"], [fr, abs(hM1), color="Yellow", legend="M1 experimental"],
legendstyle=[font=["HELVETICA", 9], location=right])
```